GROWING A SECOND SKIN:
TOWARDS SYNTHETIC BIOLOGY IN PRODUCT DESIGN

WILLIAM GRAHAM PATRICK
BACHELORS OF SCIENCE IN ENGINEERING, DUKE UNIVERSITY, 2010

Submitted to the Program in Media Arts and Sciences, School of Architecture and Planning, in partial fulfillment of the requirements for the degree of Master of Science in Media Arts and Sciences at the Massachusetts Institute of Technology, June 2015

WILLIAM GRAHAM PATRICK
PROGRAM IN MEDIA ARTS AND SCIENCES
MAY 8, 2015

CERTIFIED BY NERI OXMAN
ASSOCIATE PROFESSOR OF MEDIA ARTS AND SCIENCES
THESIS ADVISOR

ACCEPTED BY PATTIE MAES
ACADEMIC HEAD, PROGRAM IN MEDIA ARTS AND SCIENCES,

William Graham Patrick, MIT Media Lab, May 2015
Growing A Second Skin: *Towards Synthetic Biology in Product Design*

GROWING A SECOND SKIN:
TOWARDS SYNTHETIC BIOLOGY IN PRODUCT DESIGN

WILLIAM GRAHAM PATRICK

Submitted to the Program in Media Arts and Sciences, School of Architecture and Planning, on May 8, 2015 in partial fulfillment of the requirements for the degree of Master of Science in Media Arts and Sciences

ABSTRACT

Synthetic biology is a rapidly growing engineering discipline widely used in biotechnological applications. However, there are few examples of using synthetic biology in product design and there are even fewer — perhaps no — examples of incorporating fluids containing synthetic organisms and biomolecules into a product. The goals of this thesis are two-fold. First, the author investigates *how* to contain and control fluids in 3D printed fluid channels. 3D printing methods are characterized by their ability to create fluidic channels that are compatible with biochemistry and culturing microorganisms. Second, the author explores how to design the materiality and geometry of the fluid channels to affect biological function. These goals are pursued in two distinct projects: DNA assembly in 3D printed fluidics and *Mushtari*, a fluidic wearable designed to contain cyanobacteria and *E. coli* cultures. Contributions include (1) characterizing the resolution of three 3D printing methods for creating fluidic channels, (2) demonstrating compatibility of 3D printing methods with cell culture and DNA assembly biochemistry, (3) demonstrating the capability to print wearable-scale millifluidic networks up to 58 meters in length, and (4) developing approaches for fabricating geometrically complex fluidic systems.

Thesis advisor:
Neri Oxman
Associate Professor of Media Arts and Sciences

GROWING A SECOND SKIN:
TOWARDS SYNTHETIC BIOLOGY IN PRODUCT DESIGN

WILLIAM GRAHAM PATRICK

Submitted to the Program in Media Arts and Sciences in partial fulfillment of the requirements for the degree of Master of Science in Media Arts and Sciences

---

PAMELA SILVER
PROFESSOR OF SYSTEMS BIOLOGY
HARVARD MEDICAL SCHOOL
THESIS READER

William Graham Patrick, MIT Media Lab, May 2015
Growing A Second Skin: *Towards Synthetic Biology in Product Design*

GROWING A SECOND SKIN

TOWARDS SYNTHETIC BIOLOGY IN PRODUCT DESIGN

WILLIAM GRAHAM PATRICK

Submitted to the Program in Media Arts and Sciences in partial fulfillment of the requirements for the degree of Master of Science in Media Arts and Sciences

---

DAVID KONG
TECHNICAL STAFF
MIT LINCOLN LABORATORY
THESIS READER

William Graham Patrick, MIT Media Lab, May 2015
Growing A Second Skin: *Towards Synthetic Biology in Product Design*

GROWING A SECOND SKIN:
TOWARDS SYNTHETIC BIOLOGY IN PRODUCT DESIGN

WILLIAM GRAHAM PATRICK

Submitted to the Program in Media Arts and Sciences in partial fulfillment of the requirements for the degree of Master of Science in Media Arts and Sciences

---

EDWARD BOYDEN
ASSOCIATE PROFESSOR OF MEDIA ARTS AND SCIENCES
MASSACHUSETTS INSTITUTE OF TECHNOLOGY
THESIS READER

William Graham Patrick, MIT Media Lab, May 2015
Growing A Second Skin: *Towards Synthetic Biology in Product Design*

Dedicated to Margaret Graham Kemper

1950 – 2013

ACKNOWLEDGMENTS

I would like to first acknowledge my parents who have both served as providers, supporters, cheerleaders and role models. This thesis is dedicated to my mom, Margaret Graham Kemper, who passed away in December of 2013. My mom was uncommonly compassion, kind and loving. She believed that people are innately good and she treated each person with respect and compassion. Many people loved my Mom evidenced by the 17 people who asked to speak at her funeral. She worked for over 30 years as a counseling psychologist in Chapel Hill, NC, helping many clients, many of them graduate students. She counseled and advised me throughout life. For the six and a half years after her cancer diagnosis we spoke about living presently and appreciating moments even when life is uncertain. Although I can't speak to my Mom anymore, she still provides this daily inspiration. She's there with me when I'm stressed or frustrated, reminding me to breathe deeply, remember that I'm alive, and that life's little moments are curious, beautiful and worth appreciating.

If my Mom is my heart, then my Dad is my head. My dad subscribed to Scientific American and the New Yorker, put NOVA and Washington Week in Review on television, and got a computer and the Internet very early on. I realize now that all of these little privileges enabled and shaped my present worldviews and interests. My love for making and building comes from my Dad. He and mom designed our house by carefully selecting a piece of land that overlooks a forest and a creek. I spent my young years running outside around the house, climbing in a tree house that my Dad built, swinging in a swing set that my Dad built, walking down to the creek on a path that my Dad cleared. These experiences will continue to influence my life choices and interests. One day, I hope to build a family and home like he has.

My older sister, Susan, has always been my champion. She has always called me "Rockstar". Susan shows her love by taking action. I look up to her passion for social justice and serving her communities.

This thesis would have turned out differently without my girlfriend, Rachel Katz. She encouraged me to explore design and helped me think through the ideas that became synthetic symbiosis and Mushtari.

To Prof. Neri Oxman, you have been an advisor and friend. You enabled all of my work at MIT and helped me grow as an intellectual and designer. I now see my work as a means of asking questions and provoking ideas in addition to solving problems.

To my fellow Mediated Matter students, thank you for friendship and coaching. I have learned so much about design by working with you.

John Klein, thanks for encouraging me to develop an eye for graphical aesthetics.

Chikara Inamura, thanks for helping me through some rather basic CAD questions.

Markus Kayser, thanks for providing inspiring conversations about design and fabrication.

Steven Keating, I would not likely have pursued any of my thesis projects without you. Your inextinguishable curiosity encouraged me to learn about synthetic biology, two-photon polymerization, squid suckerin, cyanobacteria, tissue printing, stem cell differentiation and many, many more topics. Here's to many more years of friendship and crazy ideas.

Jorge, Laia, Kelly, Daniel, and the rest of the Mediated Matter crew: you all are all talented and rich individuals. I will particularly miss our nights dancing.

This work would not have been possible without my collaborators:

Alec Nielsen, thank you for the many late-night, lab bench conversations we shared while performing DNA assemblies. I look forward to many beers with you, hopefully in California.

Stephanie Hays, your spirit and attitude are infectious and you're a wicked good microbiologist. Thank you for introducing me to trillions of new small, green friends.

James Weaver, your curiosity is amazing! I have learned so much from you about marine organisms, materials, digital fabrication and microscopy. I'm looking forward to future visits to your office.

David Kong, thank you for introducing me to fluidics and synthetic biology! Where would I be without you and your IAP course? The communities you have built are thriving and reflect your energy. Thank you for being an advisor and friend.

Che-Wei Wang and Taylor Levy, I will always remember our session sketching the syringe pump. You showed me the focus and detail required for good design.

Christoph Bader and Dominik Kolb, you guys are supremely talented! Thanks for showing me a sneak peek of the future of computational design. I wish we had overlapped here in Cambridge.

To Boris Belocon and Daniel Dikovsky and the rest of the Stratasys team, your efforts made Mushtari possible. I hope to visit you some time in Israel.

Prof. Pam Silver and Prof. Ed Boyden, thank you for serving as thesis readers and providing advice and guidance!

Finally, I wouldn't be here at MIT without Astro Teller and Megan Smith. The two of you were my "Google parents" and remain as my biggest professional role models. Thanks for showing me how to think and act big and how to live life with ambition and humility.

CONTENTS

LIST OF FIGURES

LIST OF TABLES

LISTINGS

ACRONYMS

1 SYNTHETIC BIOLOGY IN PRODUCT DESIGN

> *Nature, in order to carry out the marvelous operations in animals and plants, has been pleased to construct their organized bodies with a very large number of machines, which are of necessity made up of extremely minute parts so shaped and situated, such as to form a marvelous organ*
>
> — Marcello Malpighi, 1697 [73]

The amazing feats of biology surround us everyday, so much so that they may seem mundane. Organisms replicate, regenerate, and respond to their immediate surroundings and adapt to evolutionary pressures over time. Cells self-assemble from nano-scale molecules [72] and then intelligently assemble into tissues depending on their environment [34]. It is not surprising then that designers, artists and engineers have taken inspiration from biology throughout history.

It bears repeating that the scale and complexity of biological systems dwarfs anything generated by humans. Consider a single HeLa cell, the oldest human cell line. A HeLa cell is approximately 20 microns in diameter and has been estimated to contain on the order of a billion to 10 billion protein molecules [69]. Each of these proteins is individually manufactured by a ribosome and serves a particular function for the cell. Integrated circuits (ICs) are arguably the most complex human built systems. The most complex, commercially available ICs today, such as Intel's 15-core Xeon IvyBridge, have on the order of a billion transistors in a package size of 50 mm by 50 mm. The HeLa cell and the Xeon IvyBridge have a similar number of parts but approximately a billion HeLa cells can fit inside an IvyBridge package. My interest is to bring some of biology's complexity and functionality into product design, not by using nanotechnology, but instead by using biology itself.

1.1 ADVANCES AND EXISTING APPLICATIONS OF SYNTHETIC BIOLOGY

Biology is composed of many small parts — DNA, RNA and proteins — that together form life. These molecules serve as hardware and software by storing information, computing, and physically performing operations. Biologists have researched the function and interoperation of these molecules for the past century, starting with the role of enzymes and later the structure and function of DNA and RNA. Geneticists started to create new biological functions by recombining or synthesizing DNA parts and then inserting them into organisms. In the past decade, the field of *synthetic biology* began standardizing these genetic parts and tools with the goal of creating an engineering science.

Synthetic biologists continue to develop powerful new tools for engineering organisms as evidenced by the recent discovery and widespread use of the CRISPR/Cas9 system for genome editing[50, 30, 66]. The price per base pair of sequenced and synthesized DNA have both dropped faster than Moore's Law[44], enabling much of this development. Today, synthetic biologists use these new techniques to create *microbial factories*. Synthetically designed organisms produce chemicals, therapeutics, fuels[53], biomaterials, such as spider silk[91] and squid suckerin[33], and dynamic, living materials that utilize embedded organisms to temporally manipulate material properties[24]. Synthetic organisms have also been designed to serve as highly sensitive biosensors of environmental signals (light, temperature) and chemical gradients[53].

As these industrial and medical applications have become mainstream, scientists, students, companies, artists and designers have started proposing methods for using synthetic biology in products. For example:

- Prof. George Church and Sriram Kosuri proposed using DNA for long-term data storage mechanism and demonstrated the concept by encoding the HTML version of Church's book, Regenesis, into DNA [29].
- Prof. George Church, Prof. Joi Ito, Prof. Neil Gershenfeld and Prof. Joe Jacobsen of the MIT Media Lab have discussed the possibility of using biological circuits (for example, neurons) instead silicon ones for performing logical operations due to their energy efficiency and density.
- Philips design studio developed the *Microbial Home Probe* which explored how engineered organisms could be used in household lighting, cooking and waste management appliances[71].
- Designers Michael Burton and Michiko Nitta designed a wearable algae suit. Microalgae in the suit photosynthesize and provide food for the wearer.
- IDEO designers have envisioned bacteria that morph into a physical cup when exposed to specific wavelength of light [49].

However, these ideas exist as concepts. There are, to my knowledge, no designed products that use synthetic DNA or engineered organisms. My thesis explores some first steps towards making these kinds of concepts and designs possible.

1.2 MANIPULATION OF BIOLOGY USING FLUIDICS

How might the means of synthetic biology — the design, synthesis, and assembly of synthetic DNA — or the ends — organisms with synthetically designed genomes — be incorporated into functional objects and products? Biomolecules used in synthetic biology,

such as proteins and nucleic acids, function in liquid. Common microorganisms engineered by synthetic biologists including *Escherichia coli*, *Saccharomyces cervisiae* (baker's yeast), cyanobacteria, and *Bacillus subtilis* all grow and function in liquid cultures. So the control of biomolecules and cell cultures in products necessitates the manipulation of liquids.

Fluidic systems could be used to control fluidics that contain biomolecules or microorganisms in a product. Fluidic systems — or fluidics — route liquids in small channels (from nano to millimeters) and include programmable elements that manipulate liquids using pressure. These systems contain simple fluidic elements, similar to circuit elements in electronics, to control and manipulate the liquid [43, 90].

What are the requirements for a product that incorporates fluidics to control cell cultures or biomolecules? The product's function would likely require fluidics with three-dimensional form, manufactured at product-scale. Using microbial cultures or aqueous biomolecules would require building the fluidics with compatible materials. Depending on the application, various methods of interfacing the biomolecules or organisms with digital systems, the surrounding air, or the user of the product would be required.

Consider a hypothetical example. Imagine a necklace that can produces the scent of Chanel No. 5 with a slight touch from the wearer. Synthetic microorganisms in the necklace are designed to create the ensemble of organic scents. An electronic system senses the touch of the wearer and then releases a chemical. The chemical induces the microorganism to produce the scents, which then emerge out of the necklace and into the surrounding air via a semi-permeable membrane. To make a product like this possible, a fluidic system would need to contain the engineered organisms and chemicals, integrate electronics than can release the chemical into organisms, and use a semi-permeable to allow the scent to pass into the air. Likely, even more fluidic elements would be required to make this product possible. How could something like this be built?

1.3 3D PRINTING FLUIDICS

Manufacturing microfluidics — fluidic systems with micron-scale features — has been an intense area of research for the past 25 years due to the disruptive potential to miniaturize fluidics and parallelize operations in diagnostics, chemical synthesis, and other biotechnological applications. These microfluidic, *lab on a chip* devices are typically manufactured in two and a half dimensions using molding. Plastic injection and soft replica molding, particularly of polydimethylsiloxane (PDMS), are both commonly used. However, these approaches cannot make three-dimensional devices (unless, several molded pieces are layerede) and they are typically used to make devices that are no bigger than several centimeters in x and y dimensions.

3D printing is a relatively new approach for fabricating fluidic systems. 3D printing could be used to build fluidic systems that are

(1) three-dimensional, (2) product scale, and (3) have channel dimensions between 100 microns and 1 cm. 3D printing has additional advantages over existing molding methods. 3D printing enables rapid prototyping of fluidics and multi-material 3D printers, such as the Connex3[4], could print fluidics with material property gradients of elasticity or transparency.

In the past two years, several 3D printed millifluidic and microfluidic *lab on a chip* devices have been demonstrated in literature. Channel sizes in these devices have ranged from two hundred microns [79] to millimeters. Most fluidic devices printed to date have been small, typically under 50 mm in any dimension. Two recent papers in the past twelve months have demonstrated the integration of several 3D printed parts to form larger fluidic system[19, 58]. Electronic components have also been integrated into these devices[19]. 3D printed fluidics have been manufactured using both single-material fuse deposition modeling [54], and stereolithography printing[12, 19] and have primarily been designed to perform chemical reactions[54, 55, 79, 83]. In the past 12 months, 3D printed fluidics have been used as biochemical reactionware for applications such as evaluating blood components [24] and diagnostics[58].

The systems published to date have not demonstrated (1) 3D printing of fluidic systems at a product scale (greater than 10 cm in dimension) and (2) compatibility with biomolecules such as DNA and RNA or microorganisms, such as *E.coli*, *S. cerevisiae*, *B. subtilis*, and cyanobacteria. All of the fluidic systems to date have been designed using single material 3D printing processes and have not leveraged the capabilities of multi-material fabrication.

1.4 THESIS STRUCTURE

The focus of this thesis is developing 3D printed fluidic systems that incorporate synthetic biology into products. I focused on two projects aimed at creating two very different types of products. The first project focused on 3D printing wet lab tools used to perform DNA assembly chemistry. DNA assembly is the foundational technology of synthetic biology and involves stiching together small segments of linear DNA into larger structures. The project aimed to broaden accessibility of microfluidic fabrication by using a single-step 3D printing process and to characterize the compatibility of the 3D printing material with DNA assembly chemistry[38]. My co-authors and I developed 3D printed microfluidic mixers that combined DNA segments and enzymes needed for Golden Gate assembly chemistry and a 3D printed pump to pull the reagents into the device. Our primary contributions were:

1. characterizing the fabrication of microfluidic devices using two methods, desktop stereolithography and on-demand 3D printing services

2. finding compatibility between the DNA assembly biochemistry and the 3D printing materials, and

3. demonstrating the collaborative design and fabrication of open lab ware, wet lab tools that can be downloaded from the web and fabricated using digital fabrication tools.

In the second project, my collaborators and I create a 3D printed fluidic wearable designed to co-culture photosynthetic cyanobacteria and *E. coli*. The project examines the *Material Ecology* [70] of a wearable that incorporates synthetic microorganisms. In particular, we design the material and geometric composition of the wearable to sustain and control the activity of embedded synthetic microorganisms. My collaborators and I focused on three research paths:

1. the computational generation of geometry and materiality of fluidic networks within the wearable,

2. printing wearable-scale, multimaterial fluidics using soluble and liquid supports, and

3. biological testing to examine the compatibility between 3D printing materials and cyanobacteria and *E. coli*.

The end product was *Mushtari*, a multimaterial wearable containing 58 meters of 3D printed fluid channels. We demonstrate computational approaches for growing channel geometry and printing multimaterial fluidics with channel diameters ranging from 1 mm to 2 cm. Initial biological results show compatibility between the 3D printing material and culturing microorganisms of interest.

Part I

DNA ASSEMBLY IN 3D PRINTED FLUIDICS

DNA assembly is a foundational technology for synthetic biology. Microfluidics present an attractive solution for miniaturizing assembly reagent volumes, enabling multiplexed reactions, and automating protocols by integrating multiple protocol steps. However, microfluidics fabrication and operation can be expensive and requires expertise, limiting access to the technology. With advances in commodity digital fabrication tools, it is now possible to directly print fluidic devices and supporting hardware. 3D printed micro and millifluidics are inexpensive, easy to make and quick to produce. We demonstrate Golden Gate DNA assembly in 3D printed fluidics with reaction volumes as small as 490 nL, channel widths as fine as 220 micrometers, and per unit part cost ranging from $0.61 to $5.71. A 3D-printed syringe pump with an accompanying programmable software interface was designed and fabricated to operate the devices. Quick turnaround and inexpensive material costs allowed for rapid exploration of device parameters, demonstrating a potentially disruptive manufacturing paradigm for design and fabricating hardware for synthetic biology.

Part I is adapted from a journal article, *DNA Assembly in 3D Printed Fluidics*, which will be submitted to *Lab on a Chip*.

Authors: William G Patrick, Alec A K Nielsen, Steven J Keating, Taylor Levy, Che-Wei Wang, Jaime J Rivera, Octavio Mondragón-Palomino, Peter A Carr, Christopher A Voigt, Neri Oxman, David S Kong

2 INTRODUCTION

2.1 DNA ASSEMBLY IN MICROFLUIDICS

Synthetic Biology is a rapidly advancing field that is being used to create novel biotechnology applications, next-generation therapeutics, and new methods of scientific inquiry[27, 53, 88]. The commercialization and rapid decline in price of DNA sequencing and synthesis technologies has enabled much of this development. Solid-phase DNA synthesis has declined in price, enabling researchers to routinely design and order synthetic DNA up to several kilobases in length. However, assembly of these sequences into larger constructs remains an essential technique. Indeed, DNA assembly is necessary to generate complex single-gene and multi-gene constructs[22, 87, 95], to create functionally-diverse part combinations (e.g., gene clusters with libraries of promoters [81]), to shuffle homologous proteins at specific recombination points (e.g., shuffling of three trypsinogen homologues[39]), and to explore higher-order effects of genetic architectures (e.g., the position and orientation of transcription units[81]). Recent advances in one-pot DNA assembly methods, such as Golden Gate assembly[38], have made assembling genetic constructs simpler.

Most practitioners perform DNA assembly reactions by pipette using traditional laboratory techniques. Microfluidics presents an opportunity to automate and parallelize DNA assembly reactions and reduce reagent volumes. Several researchers have demonstrated using microfluidics to synthesize genes in many parallel reactors (as small as 500 nL)[56, 48, 75]. These devices use polymerase chain amplification to assemble genes from pools of oligonucleotides, a process that requires in situ thermocycling. More recently, researchers have demonstrated one-pot and hierarchical DNA assembly in microfluidic devices to generate libraries of DNA constructs[62]. All devices used for gene synthesis and DNA assembly were manufactured using polydimethylsiloxane (PDMS) replica molding, a common approach for microfluidic device fabrication.

Design and fabrication of molded PDMS devices is time-consuming and expensive. A recent study estimates that the labor and material costs of a new single layer PDMS microfluidic costs is $215 and takes one day[15]. Microfluidics also require interfacing hardware, such as gravity pumps, compressor lines, and syringe pumps, to route liquids through the devices. The cost and complexity of fabricating and using PDMS microfluidic devices has slowed adoption even though the technology shows tremendous potential for the miniaturization and fine control of liquids. The duration, complexity and cost of the design, build, and test cycle for replica molded PDMS microfluidics makes rapid prototyping challenging and limits the accessibility of this technology for non-experts.

2.2 PRINTING FLUIDIC DEVICES

3D printing provides a potential one-step manufacturing approach for fabricating microfluidic devices to run DNA assembly reactions. Micro and millifluidics have been printed using fused-deposition modeling (FDM) of thermoplastics[54] and stereolithography and inkjet printing of photo-curable polymers[12, 40, 19, 59, 79, 25, 15, 57]. Devices have been built for less than $1 per device in only a few hours[54, 15]. Numerous desktop FDM and SLA printers are marketed between $300 to $6000[6, 9, 1]. On-demand 3D printing services, such as Shapeways, can print objects in a range of plastic polymers at a variable cost between $0.28-2.39 per cubic centimeter[3]. Internal channel diameters in 3D printed microfluidics have been reported as low as 100 microns[59]. However, DNA assembly has not been demonstrated in 3D printed fluidics. Moreover, the compatibility of 3D printed materials with nucleic acids has not been studied.

3D printing has another additional advantage for printing fluidics. 3D design files are easily shared on the web, allowing practitioners with access to a 3D printer to download and print fluidic devices and collaborate on new designs. There are many examples of other 3D printed labware, a centrifuge (DremelFuge[42]), optics equipment[94], syringe pumps[93, 80], a colorimeter[14], and a turbidostat[84]. Access to 3D printers has increased in the previous decade with the proliferation of desktop 3D printers and creation of online 3D printing services. Our ultimate goal is to allow synthetic biologists to download and 3D print devices that can be used to parallelize and automate DNA assembly reactions.

2.3 PROJECT OVERVIEW

In this work, we demonstrate Golden Gate DNA assembly in 3D printed fluidics (Figure 1). We printed the devices using two methods: a desktop stereolithography 3D printer (Form1+, Form Labs, Somerville, Massachusetts) and an on-demand 3D printing service (Shapeways, New York, New York). The smallest printed device had a channel width of 220 microns and reactor volume of 490 nL. We designed the micro and millifluidics to mix linear double stranded DNA with enzymes to assemble plasmids via Golden Gate biochemistry. The assembly reactions occurred at room temperature, eliminating the need for an incubator. We then transformed the assembled plasmids into *E. coli* and then compared the number of transformants to a tube control.

A bespoke, 3D printed syringe pump operated the fluidic devices (Appendix A Figure 5-11). The pump's mechanical components were 3D printed using a desktop fuse-deposition 3D printer (MakerBot Replicator 2, MakerBot Industries, Brooklyn, New York) (Appendix A, Figure 30) and the pump was controlled by a custom control board (Appendix A, Figure 34) fabricated using a desktop CNC mill (Roland Modela MDX-20 CNC mill, Roland DG Corporation, Hamamatsu,

Japan) running Arduino firmware. A user interface (Appendix A, Figure 35) enabled the user to control the pump via USB. We designed both the fluidic devices and syringe pump using rapid and collaborative design iterations, enabled by the use of desktop 3D printers and on-demand printing services. We tested and re-designed each fluidic device multiple times before arriving at the final forms (Appendix A, Figure 29).

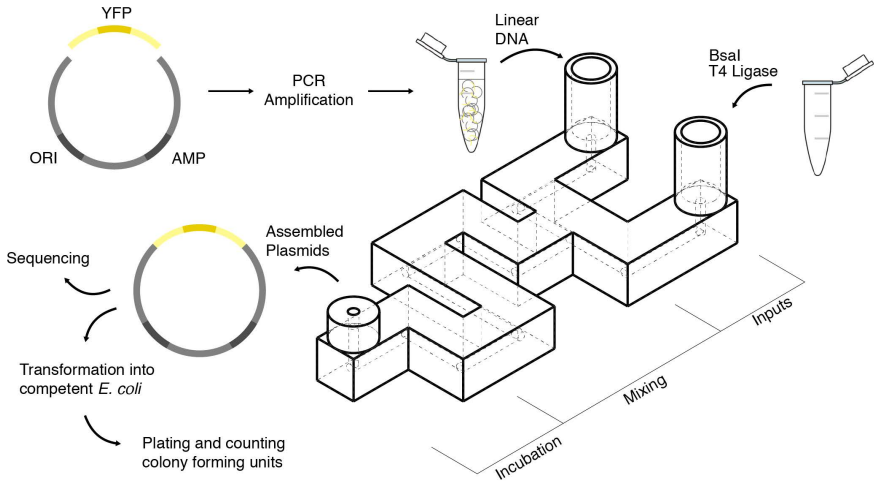

Figure 1: **DNA assembly in 3D printed fluidics**. Linear DNA was assembled into plasmids using the Golden Gate method inside of fluidics hardware. Two linear DNA segments were used, a constitutively expressed YFP reporter, and a backbone containing an ampicillin selection marker. Each linear segment was PCR amplified prior to assembly. The linear segments were inserted into one inlet of the fluidic device. Golden Gate reagent mix, BsaI, T4 Ligase, and T4 buffer, were inserted into the other. The two inputs were pulled into the device and mixed via co-laminar diffusion. After a 90-minute room-temperature incubation, the product was pulled off the device and then transformed into E. coli. This experiment was run on all three device designs (Figure 3). To control for device mixing efficacy, assemblies were also run in the devices in which the linear DNA segments and Golden Gate enzyme mix were mixed off-device prior to the experiment. Detailed visual protocols for running this experiment in the SW-FUD devices can be seen in Appendix A, Figure 26.

3

RESULTS

3.1 3D PRINTED MICRO AND MILLIFLUIDIC DEVICE DESIGN AND CHARACTERIZATION

Three fluidic devices were designed and fabricated to conduct DNA assemblies: a Co-Laminar Mixer printed on the Form 1+, (2) a 3D Micromixer printed on the Form 1+, and a Co-Laminar Mixer printed using Shapeways Frosted Ultra Detail material (SW-FUD) (Figure 2). Each printing method has advantages. The Form 1+ affords rapid and inexpensive design iterations and near optical clarity using the Clear Photoactive Resin. The build volume of the Form1+ is 125 x 125 x 165 mm (X x Y x Z) and the manufacturer claims a minimum lateral laser beam size of 10 microns and feature size of 300 microns[9]. The PreForm software package for the Form1+ offers four z-resolution steps for printing: 25, 50, 100 and 200 microns. We found no measurable difference in resolution between 25 and 50 microns; a 50-micron step size was used for all prints. For printing internal channels, no internal supports were required.

The highest resolution printing material offered by Shapeways is Frosted Ultra Detail (SW-FUD), a UV-cured acrylic polymer. The minimum embossed or engraved feature for SW-FUD is 100 microns. The printer accuracy is +/- 25 — 50 microns for every 2540 microns[3]. Frosted Ultra Detail is printed with wax support for external and internal features, which was removed using a hot water ultrasonic cleaning.

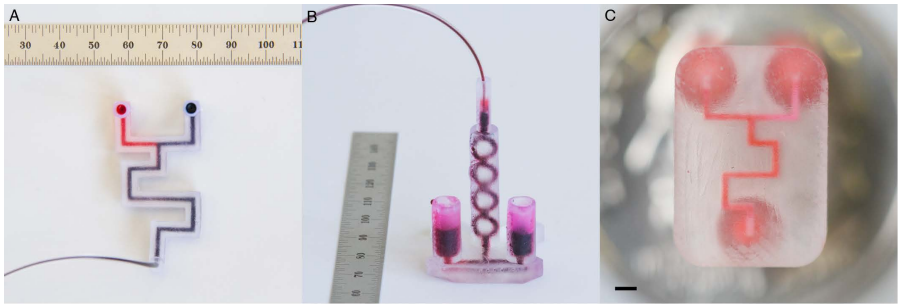

Figure 2: **Fluidics printed using the Form 1+ and Shapeways Frosted Ultra Detail**. DNA assembly efficacy was tested in three fluidic device designs: (**A**) the Form 1+ Co-Laminar Mixer, (**B**) the Form 1+ 3D Micromixer, and (**C**) the SW-FUD Co-Laminar Mixer. The Form 1+ devices were designed with 1.5 mm diameter circular channels and the SW-FUD device was designed with a 300-micron square channel.

3.1.1 *Minimum Channel Size On A Resolution Test Piece*

We designed and printed resolution test pieces on the Form1+ and using SW-FUD to characterize the fabrication accuracy for both methods and determine the minimum internal channel sizes (Appendix A, Figure 27). The resolution test piece was designed with 10 circular channels ranging in diameter from 1.9 to 0.1 mm and 12 square channels ranging in width from 1.15 to 0.05 mm. All channels were designed to be the length of the test piece, 40 mm. For the Form1+, the smallest diameter circular channel that cleared was 0.9 mm and the smallest square channel that cleared was 0.65 mm (in CAD). For SW-FUD, the smallest cleared circular channel was 0.3 mm and the smallest cleared square channel was 0.25 mm (Appendix A, Figure 27). These channel dimensions are similar to the minimum channel dimensions reported in previous studies that printed internal channels using SLA and inkjet printing[58, 79]. Actual channel dimensions were measured on the exterior of the resolution test piece using optical microscopy (Supereyes USB Digital Microscope, Shenzhen D&F, Shenzhen, China). For the Form 1+, the measured channel dimension was on average 20 microns greater than the expected dimension (range: 110 to -40 microns). For the SW-FUD, the measured channel dimensions were on average 40 microns smaller then the expected dimension (range: 30 to -90 microns) (Appendix A, Table 4).

3.1.2 *Channel Cross Sections*

In order to measure the geometry of the internal channels, four sample cross sections of each device were cut and measured (Appendix A, Figure 28). The Form 1+ devices (Figure 2 A-B) featured internal channels that were designed to be 1.5mm in circular diameter and measured to be 1.30 (stdev: 0.09) mm (Appendix A, Table 5). These devices took 3-4 hours to print and the cost per device was approximately $1. The SW-FUD Co-Laminar device (Figure 2 C) was designed to have a 300-micron square channel and a reactor volume of 910 nL. The average side length of the cross sections (Appendix A, Figure 28 I-L) was 220 microns (stnd. dev. of 30) (Appendix A, Table 5). Given this average side length, the average reactor volume of the printed SW-FUD devices was 490 nLs (stnd. dev. of 70). The devices cost $5.71 each on Shapeways with a delivery time ranging from 2-10 days.

3.1.3 *Scanning Electron Microscopy of Shapeways and Form 1+ Test Pieces*

To investigate the surface roughness of each printing method, scanning electron microscope images (SEMs) were taken of two test pieces printed using both fabrication methods. The two test pieces featured open channels designed to be 300 and 1500 microns wide. The open channels printed using SW-FUD (Figure 3 B & D) were less deformed and showed less surface roughness than parts printed on the Form1+

(Figure 3 A & C). Striations were clearly visible in all test pieces and their orientation appears to effect surface roughness. SW-FUD parts also featured additional roughness on some, but not all, walls for an unknown reason (the southeast facing walls in Figure 3 B & D).

3.1.4 *Rapid Prototyping and Iterative Development of Fluidics*

Devices were designed to mix the reagents via co-laminar diffusion and 3D micromixing. The syringe pump pulled the reagents from the two inlet chambers and into the device. The two reagents in the Form1+ and SW-FUD Co-Laminar devices mixed while being pulled through the long channel and during incubation. The design of the Form1+ 3D Micromixer was inspired by previous 3D passive micromixers that have been designed and fabricated using multiple layers of 2D substrates [61]. Mixing was visually confirmed in the Form1+ 3D Micromixer by pulling dyed inputs through the device at a flow rate of 5 micro liters per second and observing a mixed solution at the outlet.

Iterative design and printing were used to improve user interfacing and debug practical problems, such as leaks and trapped bubbles. Thirteen versions of the Form 1+ 3D Micromixer, five versions of the Form 1+ Co-Laminar Mixer, and three versions of the SW-FUD Co-Laminar Mixer were designed, fabricated, and tested (Appendix A, Figure 29). Figure 4 shows five versions of the Form1+ 3D Micromixer.

The usability and performance of the fluidic devices were improved through these many design iterations. Originally, reagents were pushed through device inlets (Figure 4 A-B), which required carefully aligning the reagents such that they entered the device at the same time. Devices were redesigned to pull reagents from the equidistant inlet channels to the T-junction and then to the outlet. To interface tubing (0.060 in OD, Tygon Microbore, Saint-Gobain, Courbevoie, France) with the fluidic hardware, a press-fit interface (1.5 mm hole with 0.15 mm diameter, 98 degree chamfer) was designed. This interface worked reliably for the Form1+ printed parts; however, leaks occasionally occurred in SW-FUD devices, likely due to the higher pressure required to push fluid through the smaller channel. Other studies have 3D printed standard Luer fittings[79, 15, 12, 25, 40] into the devices, which prevent leaks but adds dead volume. A press fit interface was also designed for a 23-gauge dispensing needle inside of the inlets and outlets of the SW-FUD device. This interface was used to clear wax out of the channels by aspirating the melted wax and hot water through the device.

3.2 DESIGN AND TESTING OF A 3D PRINTED SYRINGE PUMP

We operated the microfluidic devices using an open-source, 3D printed syringe pump (Appendix A, Figures 5-11). The syringe pump has three components: the mechanical components (Appendix A, Figures

7-8), a control circuit board (Appendix A, Figure 34), and a user interface which operates the pump (Appendix A, Figure 35). The mechanical components consist of a stepper motor, threaded rod, and 3D printed parts. The 3D printed parts were designed in SolidWorks and printed using the Makerbot Replicator 2X. The printed parts are modular. New parts were printed for different syringe sizes (Appendix A, Figure 33). The parts designed for this experiment were printed to operate a 1 mL syringe. The material cost of the printed parts was $10.11. The electronics were custom designed in EagleCAD and the circuit board was milled using a Roland Modela MDX-20 desktop CNC mill. Surface mounted components, including an Atmel ATMega328P microcontroller and Allegro A3909 stepper motor driver, were soldered onto the milled circuit board (Appendix A, Figure 34). Custom Arduino-based firmware was written to take commands from a computer via USB and then control the stepper motor (Appendix A Figure 6). A user interface was written in Processing to command the pump (Appendix A, Figure 35). In the interface, the user specified the volumetric flow rate and desired flow volume and commanded the syringe pump to either pull or push fluid. The total bill of materials cost of the pump was $56.63 and the full bill of materials is in Appendix A, Table 6. To characterize the performance of the pump, the pump flow rate was measured at 1 and 5 microliters per second. The measured flow rate was 1.2 and 3.4% lower than expected (Appendix A, Figure 36).

Unlike other open-source syringe pumps[93, 80], the mechanical components of our syringe pump can be 3D printed and assembled without using any fasteners (washers, screws, bearings, rods, etc). This makes the pump assembly far simpler; 3D printed parts are assembled with press and screw fits. This feature along with the custom PCB board makes the overall bill of materials cost 37-63% less than the bill of materials cost of previously published open-source syringe pumps[93].

Performance and usability improvements were also made to the syringe pump through many design iterations. All of the mechanical components in the pump (threaded rod, motor, base, mid, top sections, syringes) are fastened using press and screw fits. Each of these fits was designed using multiple rounds of prototyping. The end result, a design without traditional fasteners such as screws, bolts or nails, makes assembly simple (all parts of the pump can be seen in Appendix A, Figure 32) and enables the tool to be customized using modular elements. Several versions of the syringe pump were created for different syringes sizes by printing modular elements (Appendix A, Figure 33).

3.3 GOLDEN GATE DNA ASSEMBLY IN 3D PRINTED FLUIDICS

For each of the three fluidic designs, we tested the efficacy of Golden Gate DNA assembly to construct a bacterial plasmid from two pieces of linear double stranded DNA. One piece encodes a plasmid back-

bone with a p15A medium-copy number origin of replication and ampicillin resistance marker and the second piece encodes a constitutive promoter driving the expression of a yellow fluorescent protein (YFP).

Each fluidic device was used to mix two volumes: a solution containing both pieces of DNA in ligase buffer and a solution containing BsaI restriction enzyme and T4 DNA ligase in ligase buffer (Figure 2). Using our 3D printed syringe pump, the two solutions were drawn into each microfluidic device, mixed, and then allowed to incubate within the device for 90 minutes at room temperature. We determined the efficiency of in device Golden Gate assembly by transforming unpurified assembly reaction into *E. coli*, plating serial dilutions on agar media with antibiotics for plasmid selection, and then counting the number of colony forming units (CFUs) for each assembly reaction (CFUs, Table 1). For all devices, negative controls without enzyme addition yielded no CFUs. Positive controls — in which the components were mixed together by pipette and incubated in a PCR tube — yielded an average of 1.60 x 10^5 CFUs. In addition, for each device we incubated reactions that were pre-mixed by pipette to ascertain whether the 3D printed photopolymer material inhibited the assembly. For both the Form 1+ and SW-FUD devices, there was no significant difference in the number of CFUs from these experiments compared to the in-tube positive controls.

We counted the number of CFUs from the assembly reactions mixed within the microfluidic devices. For both of the Form 1+ devices, there was no significant difference in the number of CFUs compared to the in-tube positive control. The SW-FUD devices that mixed the DNA and enzymes yielded an average of 2.53 x 10^5 CFUs (Table 1). We grew five colonies from the Form1+ device assembly, purified plasmid from the cultures, and sequenced the assembly junctions and YFP insert. All five assembled plasmids were correct.

The reaction volumes for the SW-FUD devices were smaller (490 nL) than the reaction volumes for both Form1+ devices and the tube control (5 micro liters) yet the number of CFUs was similar in all cases. This observation can be attributed to a saturating quantity of DNA in the transformation reaction.

Device	Assembly Reaction	No. of Samples	Mean CFU (x 10^5)	S[a] (x 10^5)
In-tube reaction				
	No enzyme	4	0.00	0.00
	Enzyme & DNA	7	1.60	0.80
Form1+ co-laminar				
	No enzyme	1	0.00	0.00
	Off device mix[b]	6	1.42	0.83
	On device mix[c]	5	1.30	1.20
Form1+ micromixer				
	No enzyme	1	0.00	0.00
	Off device mix[b]	5	1.74	1.42
	On device mix[c]	7	1.71	1.54
Shapeways co-laminar				
	No enzyme	1	0.00	0.00
	Off device mix[b]	5	1.79	1.67
	On device mix[c]	7	2.53	0.52

a. standard deviation
b. Golden Gate enzymes and DNA mixed off device and incubated on device
c. Golden Gate enzymes and DNA mixed on device and incubated on device

Table 1: **Colony Forming Units (CFU) of *E. coli* transformed with Golden Gate products**.

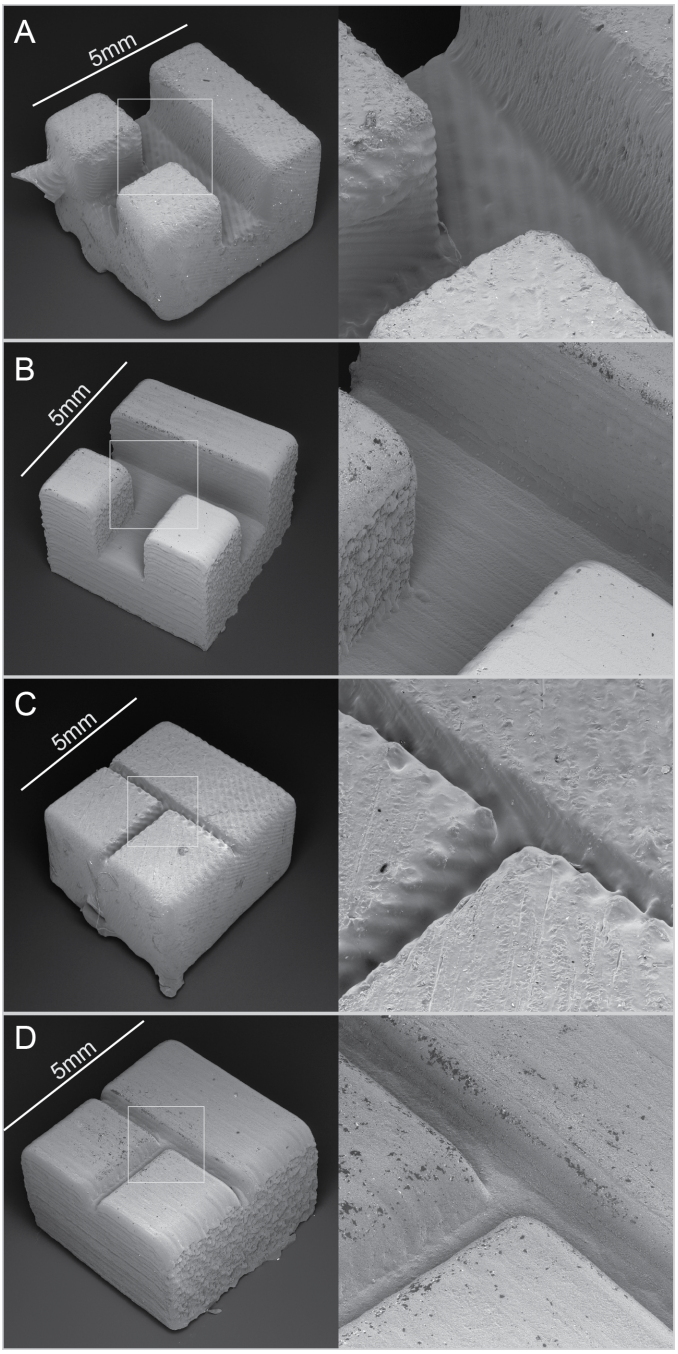

Figure 3: **Scanning Electron Microscope Images of Open Channels Printed Using The Form1+ and Shapeways Frosted Ultra Detail**. Print orientation in these test parts was not controlled. Opens channels in A & B and C & D were designed to be 1500 and 300 microns wide respectively.

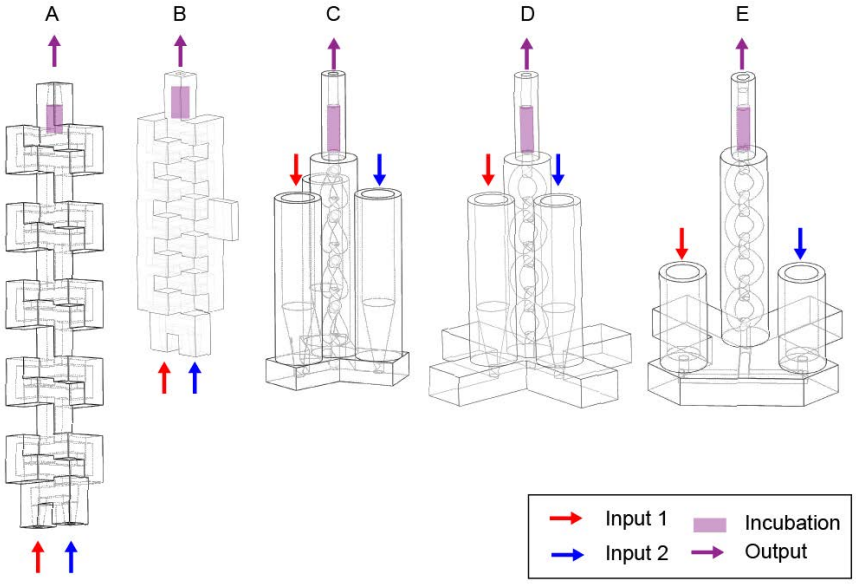

Figure 4: **Design Evolution of the 3D Micromixer**. Many designs were created and tested for each of the three fluidic devices (Figure 2) used in the DNA assembly experiments. 5 (A-E) of 13 iterations of the Form 1+ 3D Micromixer can be seen above. Several design changes can be seen A-E: The design of the 3D micromixer was changed from a recti-linear channels with square channels (A-B) similar to previous 3d micromixer designs[61, 79, 21], to a micromixer design using channels with a circular cross-section and smooth curves (C-E). A mount held the initial designs (A-B); later versions (C-E) stood freely on a base. All 13 iterations are in Appendix A Figure 4

4

DISCUSSION

This work accomplished three goals: (1) demonstrate iterative development of 3D printed fluidic devices; (2) characterize the performance of two types of 3D printing, the Form1+ SLA Desktop printer and Shapeways Frosted Ultra Detail, for creating micro and millifluidics; and (3) validate the efficacy of 3D printed fluidic devices for performing Golden Gate DNA assembly.

4.1 ITERATIVE DEVELOPMENT OF 3D PRINTED FLUIDIC DEVICES

Over the course of this project, we demonstrated that the speed, simplicity, and low expense of 3D printing enabled the iterative development of 3D printed fluidics and syringe pump hardware. Each fluidic design costs less than $6 to print and fluidics printed on the Form1+ typically required a few hours to print. As a result, many iterations of each fluidic device were designed, fabricated and tested. Some design iterations of the 3D Micromixer, fabricated on the Form 1+, can be seen in Figure 4 (all design iterations are in Appendix A, Figure 29). To develop the syringe pump, numerous versions of the mechanical components and PCB board (Appendix A, Figure 34) were fabricated using 3D printing and CNC milling.

This project is also an example of the development process for open lab ware [17]. The design, fabrication, and implementation of the 3D printed fluidic hardware began in an MIT course in January 2014, and then continued as collaboration between three different MIT labs (Lincoln Laboratory, Synthetic Biology Center, Media Lab). These laboratories each had common 3D printing infrastructure, enabling the exchange of digital design files and local printing & testing. As adoption of digital fabrication tools, particularly 3D printers, grows, co-development and sharing of open biology tools become more achievable.

Other than the necessary 3D printing infrastructure, other barriers remain for the co-development of 3D printed open lab ware. First, CAD remains a barrier for many potential designers. Fluidic devices, in particular, are challenging to design because they require complex 3D forms. The authors of this study had multiple years of experience working with SolidWorks. Many biologists interested in designing fluidics will likely not have similar experience. To overcome this barrier, microfluidic-specific 3D CAD tools could be created to make fluidic design more accessible. A tool that uses a library of microfluidic parts that can be dragged and dropped in a visual user interface may be particularly helpful. Secondly, open lab ware that require multiple fabrication machines, such as the syringe pump created for this project, are more challenging to fabricate and require additional skills to build. Creating hardware kits that can be purchased, assembled,

and modified may promote the dissemination of these types of tools. The OpenPCR [2] is a successful implementation of this strategy.

4.2 PERFORMANCE OF FORM1+ AND SHAPEWAYS-FROSTED ULTRA DETAIL FOR PRINTING MICRO AND MILLIFLUIDICS

The second aim of this work was to characterize the performance of the Form1+ and Shapeways-FUD for printing micro and millifluidics. Overall, device performance was consistent with previously reported devices printed using stereolithography and inkjet printing. Two reports published during this study used digital light projection (DLP) stereolithography to print square fluidic channels as small as 200-300 microns wide[15, 79], smaller than the minimum square channel dimension, 650 microns, printed using the Form 1+. Instead of DLP, the Form 1+ uses galvanometers to steer laser light into the unpolymerized resin. This suggests that desktop DLP stereolithography machines, such as the MiiCraft[7] (MiiCraft, Taiwan), Titan 1[5] (Kudo3D, Pleasanton, CA), and ProJet 1200[8] (3D Systems, Rock Hill, South Carolina), may be more effective than the Form1+ for printing the smallest internal channel dimensions. However, the Form1+ has a larger build area than these desktop DLP printers and has begun marketing flexible resins, which could be used to print elastomeric fluidic devices. Although Shapeways does not publicly state the machines they use for their various materials, the SW-FUD material is likely printed using the 3D Systems ProJet HD 3000[77] (3D Systems, Rock Hill, South Carolina), a high-resolution inkjet printer. A previous study reported using this printer to make internal square channels between 100-1000 microns[58], consistent with our results.

For both the SW-FUD and Form1+ devices, the geometry of the internal channel cross sections varied from part to part (Appendix A, Figure 28). This finding was similar to reports from previous studies[15, 79]. One of these studies found that print orientation affects the geometry of the printed channels[15]. Print orientation was not controlled in the fabrication of the Form1+ devices and was unknown for the SW-FUD devices. Therefore, it is possible that print orientation was a contributing factor for part-to-part variability.

4.3 EFFICACY OF FORM1+ AND SW-FUD FLUIDIC DEVICES FOR PERFORMING GOLDEN GATE DNA ASSEMBLY

The assembly products from both the Form 1+ and SW-FUD fluidic devices yielded tens of thousands of transformants. The pre-mix controls and on-device mixes produced comparable or greater numbers of transformants as compared to the in-tube controls. The volume of enzyme used to assemble DNA in the SW-FUD device was less than one twentieth of the volume used in either the Form1+ devices or tube controls. The SW-FUD devices yielded higher colonies per microliter of assembly reaction, an observation that can be explained due to the presence of saturating amounts of assembled DNA, and lower

reaction volumes. These results suggest that the 3D printed devices adequately mixed the enzyme and DNA and that the Golden Gate biochemistry proceeds successfully in these materials with these geometries. In this work, only two pieces of DNA were assembled. However, Golden Gate biochemistry is extensible to larger assemblies and has been used to generate constructs with many pieces. Thus, these devices or similar ones could be used to assemble more complex genetic circuits using the same method. Finally, the assembly efficiency of these reactions indicates that as printing technology improves and resolution increases, smaller reaction volumes would still yield a significant number of transformants.

Although these devices effectively assembled DNA constructs using Golden Gate biochemistry, more development is necessary before 3D printed fluidic devices can be integrated into a synthetic biology workflow. Several steps are required before and after assembly, including PCR of linear DNA segments and transformation of DNA constructs into *E. coli*. The advantage of microfluidic-based DNA assembly is multistep automation and parallelizing reactions. This work demonstrates an initial step towards developing 3D printed devices that can perform these functions. The next steps include demonstrating 3D printed fluidic devices that can perform PCR and route reagents and reaction products using 3D printed valves. Three separate researchers have demonstrated 3D printed valves using stereolithography printing and multi-material inkjet printing[16, 51, 76].

4.4 CONSCLUSIONS & OUTLOOK

This project demonstrated that the Shapeways-Frosted Ultra Detail and Form1+ 3D printed devices are compatible with Golden Gate biochemistry. This finding is a step towards creating open, inexpensive and rapidly produced 3D printed microfluidic devices that can perform the necessary tasks — PCR of linear segments, Golden Gate DNA assembly, transformation — to engineer microorganisms. The project also demonstrates how 3D printing enables open, collaborative and rapid design of fluidics. As highlighted above, limitations currently exist with printing fluidics using desktop 3D printers and on-demand printing services, particularly print resolution and part-to-part variability. However, 3D printing technology is rapidly improving due to considerable academic and commercial interest and these limitations may be overcome as the technology develops.

5

METHODS

5.1 DESIGNING & 3D PRINTING FLUIDICS

We designed fluidic devices using SolidWorks (Dassault Systèmes SolidWorks Corp, Waltham, Massachusetts). Micro and millifluidic CAD designs were printed using two approaches: (1) desktop stereolithography printing using the Form1+ (Formlabs, Somerville, Massachusetts) and (2) on-demand printing using Shapeways (Shapeways, New York, New York) Frosted Ultra Detail (SW-FUD) material.

Fluidic devices were designed using SolidWorks. STL files were generated in Solidworks. For 3D printing on the Form1+, STL files were opened in Form Lab's PreForm software. The software was used to orient the devices and generate supports. All devices printed on the Form1+ were printed using Form Labs Clear Resin (formulation: FLGPCL02) with a z-resolution of 0.05 mm. For 3D printing using Shapeways, STLs were uploaded to www.shapeways.com and Frosted Ultra Detail material was selected. For printing, the "print it anyway" option was selected.

5.2 POST-PROCESSING PARTS TO CLEAR CHANNELS

To process parts printed on the Form1+ (Figure 3 A-B), devices were removed from the build tray and submerged in 70% isopropyl alcohol for 3-5 minutes. Compressed air was blown into each inlet and outlet for 10 seconds to remove alcohol and any uncured resin. Devices were then submerged in 70% isopropyl alcohol again for 1 minute. A syringe was used to wash each channel with isopropyl alcohol. Then, compressed air was blown into each inlet and outlet for 10 seconds. Finally, support material on each device was removed.

To clear wax support material, SW-FUD devices (Figure 3 C) were submerged in hot water in a Magnasonic ultrasonic cleaner. The devices were cleaned for several minutes. While in the ultrasonic cleaner, a 1 cc syringe (BD, Franklin Lakes, New Jersey) with a 23 gauge, one half inch dispensing needle was used to dispense hot water through the channels. After cleaning, channels were tested by hand using the same syringe and needle.

5.3 CHARACTERIZATION OF FORM1+ AND SHAPEWAYS FROSTED ULTRA DETAIL RESOLUTION TEST PIECE

A resolution test piece (Appendix A, Figure 27) was designed in SolidWorks. A single resolution test piece was printed on the Form 1+ using using Form Labs Clear Resin (formulation: FLGPCL02) and 0.05 mm z resolution and using SW-FUD. Parts were post-processed

following the protocol above. Resolution test pieces were measured using digital calipers. Water with green food coloring was dispensed into each channel using a 1cc syringe with a 23 gauge, one half inch dispensing needle to determine if the square and circular channels in the resolution test piece were clear. A USB optical microscope (SuperEyes B008, Shenzhen D&F, Shenzhen, China) was used to measure the diameter of the circular channels and the side length of the square channels. To determine the scale of each image, a known length on the image was measured using calipers. Three technical replicates were performed for each measurement.

5.4 MEASURING CROSS SECTIONAL GEOMETRY OF DEVICE CHANNELS

To determine the dimensions of the internal channels of the Form 1+ and SW-FUD devices, 4 cross sections were measured for each type of device using a USB optical microscope (SuperEyes B008, Shenzhen D&F, Shenzhen, China). The cross sections were made by taking printed and processed devices and cutting a cross section using high leverage handheld metal snips. The sections were then sanded into a perpendicular surface using a belt sander. Liquid was dispensed and compressed air was blown through the sectioned channel to remove any debris created from sanding. Three technical replicates were performed for each measurement.

5.5 MEASURING CROSS SECTIONAL GEOMETRY OF DEVICE CHANNELS

To examine the surface roughness of the two printing methods, two small test pieces were designed. The test pieces featured open channels of 300 and 1500 microns. For electron microscopy, representative samples of each printing method for each test piece were sputter coated with gold and examined with a Tescan Vega GMU Scanning Electron Microscope (SEM).

5.6 DESIGN, FABRICATION, TESTING & OPERATION OF THE SYRINGE PUMP

The syringe pump was designed in SolidWorks. A MakerBot Replicator 2 (Makerbot Industries, Brooklyn, New York) was used to print parts in polylactic acid (PLA). The pump used a NEMA 17 bipolar stepping motor with 200 steps per revolution (Evil Mad Scientist LLC, Sunnyvale, California), a 3/8 inch threaded rod with 1/12 inch pitch (McMaster-Carr, Elmhurst, Illinois) and a custom electronics board designed in Eagle (Cadsoft Computer GmbH, Pleiskirchen, Germany). To create the circuit board, 4 x 6 inch FR1 circuit board blanks (Inventables, Chicago, Illionis) were milled using a Roland Modela MDX-20 CNC mill (Roland DG Corporation, Hamamatsu, Japan). The electronic components were then soldered into place. The

circuit board was powered by a USB FTDI cable, connected to a MacBook Pro laptop. The Atmel Atmega328P microcontroller was bootloaded with Arduino firmware using a AVR in-system programmer. A full bill of materials of the pump is in Appendix A, Table 6. The circuit board was then programmed and powered via USB FTDI. A user interface for the pump was written in Processing.

To operate the syringe pump, the user connected and powered (5V) the pump to a laptop via USB. The desired flow rates & flow volume were then inputted into the pump. The precise operation of the pump can be seen in Appendix A, Figure 31.

The performance of the syringe pump was characterized by pumping water at 1 and 5 µl per second for a specific flow volume and measuring the time and actual flow volume. Time was measured using a handheld timer as the interval between pressing the *push* button on the user interface and when the pump stopped moving. Flow volume was measured by weighing the amount of liquid that was pushed out of a tube and onto a piece of parafilm, using a high-accuracy scale.

5.7 PREPARING FLUIDICS FOR BIOLOGICAL PROTOCOL

Devices printed on the Form1+ were additionally cured under a 15 watt fluorescent UV lamp for 24 hrs.

30 minutes prior to running the biological experiment, both devices were blocked with bovine serum albumin (BSA). BSA was added by hand into each device using a syringe. After 30 minutes, BSA was removed from the channels by using pressurized air.

5.8 WORLD-TO-DEVICE INTERFACING

Inlets of all fluidic devices were designed to allow pipetting reagents into inlet wells. Outlets were designed to press-fit with a Tygon Microbore tube (0.060 inch outer diameter). The press-fit outlet-tube connection was checked for leaks. In the case of a leaky fit, parafilm was used to create an airtight fit. The outlet tube (Tygon Microbore, 0.060 inch OD, 10-15 cm long) was connected to a 23-gauge, 1/2 inch dispensing needle tip & syringe (1 mL BD Luer Lok) and loaded into the syringe pump.

5.9 AMPLIFICATION AND PURIFICATION OF DNA PARTS

The plasmid backbone encoding an ampicillin-resistance cassette[82] and a p15A origin of replication[65] was PCR amplified using primers that comprised (from 5 prime to 3 prime): a BsaI restriction enzyme recognition site, a 4bp assembly scar, and a backbone-annealing region. Forward primer: CGCGGGGGTCTCCAATGCCGTCTTCGCTTCCTCGCTC; reverse primer: GGTGCAGGTCTCGAAGCTGGTCTTCCAGTACAATCTGCTCTGATG.

The YFP cassette encoding the bacterial PTac promoter[64], ribozyme insulator RiboJ[64], ribosomal binding site Boo64[52], yellow fluores-

cent protein coding sequence[31], and transcriptional terminator L3S2P21[26] was amplified using primers that comprised a BsaI restriction enzyme recognition site, a 4bp assembly scar, and an insert-annealing region. Forward primer: CTAGCGGGTCTCAGCTTAACGATCGTTGGCTGTGTTGACAATTAATCATCGGC; reverse primer: TGCCCAGGTCTCTCATTGGACCAAAACGAAAAAAGGCCC.

PCR mixtures were set up that contained 25 µl KAPA HiFi HotStart ReadyMix (Kapa Biosystems, Wilmington, MA), 100 picomol of each DNA oligonucleotide primer (Integrated DNA Technologies, Coralville, IA), 23 µl of sterile water, and 0.1 nanograms of double-stranded DNA template. The reactions were thermocylced according to the following program: (1) 95°C for 3 min, (2) 98°C for 20 seconds, (3) 65°C for 15 seconds, (4) 72°C for 1 minute, (5) repeat steps 2-5 25 times, (6) 72°C for 2 min. PCR amplicons were electrophoresed on a 1% agarose gel, excised with a scalpel, and purified using a Zymoclean Gel DNA Recovery Kit (Zymo Research, Irvine, CA) and eluted in sterile water. The concentration of each purified PCR product was measured using a NanoDrop 1000 Spetrophotometer (NanoDrop, Wilmington, DE).

5.10 GOLDEN GATE ASSEMBLY SETUP

The Golden Gate assembly reaction was set up into two reaction halves: the first containing DNA in ligase buffer, and the second containing enzymes in ligase buffer. These reaction halves were mixed in subsequent steps. Enzymes and buffer were purchased from New England Biolabs, Ipswich, MA.

DNA solution composition (per reaction):
40 fmol linear plasmid backbone amplicon
40 fmol linear YFP insert
1 µl 10X T4 DNA ligase reaction buffer
Sterile H2O to 10 µl

Enzyme solution composition (per reaction):
1 µl BsaI
1 µl T4 DNA ligase
1 µl 10X T4 DNA ligase reaction buffer
7 µl sterile H2O

5.11 EXPERIMENTAL PROTOCOL FOR RUNNING DEVICES PRINTED USING THE FORM 1+

Before beginning experiments, devices were printed, processed, prepared for the biological protocol and interfaced with tubes to the syringe pump (see protocols above). 10 µl of DNA solution and 10 µl of enzyme solution were pipetted into separate inlets. 40 µl of mineral oil was pipetted on top of each solution. The reagents were then drawn through the device using the syringe pump at a rate of 5 µl per

second and allowed to incubate at the end of the device near the outlet. After incubation, the reaction product was drawn into the outlet tube with the syringe by hand and immediately pushed into a collection tube and heat inactivated at 80°C. The tube was then removed from the device and the product was pushed into a collection tube. For each device, we also tested pre-mixed reactions. 10 μl of DNA solution and 10 μl of enzyme solution were mixed using a pipette in a 1.5 mL Eppendorf tube. The pre-mix was then pipetted into one inlet. 80 μl of oil was pipetted on top of the mixed reagents. The other inlet was capped using parafilm. Pre-mixed reactions were similarly drawn through the device and into the incubation area and allowed to incubate for 90 minutes. A negative control was completed using the same protocol by substituting the 10 μl of enzyme solution with 10 μl of 1X ligase buffer.

5.12 EXPERIMENTAL PROTOCOL FOR SW-FUD DEVICESL

SW-FUD devices were cleared, prepared for biological protocol and interfaced with tubes to the syringe pump. 5 μl of DNA solution and 5 μl of enzyme solution were pipetted into separate inlets. 10 μl of mineral oil was pipetted on top of both solutions to minimize evaporative losses. Using the syringe pump, the two solutions were drawn through the device at a rate of 1 μl per second until liquid emerged from the outlet tube. To ensure that no reaction product from the outlet tube was collected, the outlet tube was removed & replaced with a new tube after incubation. Then, the reaction product in the device, remaining DNA and enzyme solutions and mineral oil in the inlets were drawn out of the device by hand using a syringe and immediately pushed into a collection tube and heat-inactivated at 80°C.

Pre-mix reactions and negative controls were also completed in the SW-FUD devices. For the pre-mix reactions, 5 μl of DNA solution and 5 μl of enzyme solution were mixed by micropipette and then the 10 μl mixture was pipetted into one inlet. The other inlet was covered. 10 μl of mineral oil was pipetted on top. The mixture was drawn into the device at 1 μl per second until it could be seen in the outlet tube. Post-incubation the outlet tube was replaced. The remaining pre-mix reaction and oil was removed from the inlet. 10 μl of de-ionized water was added to the inlet. The reaction product in the device and the DI water in the inlet were then drawn into the outlet, pushed into a collection tube and heat-inactivated at 80 C. A negative control was completed using the same protocol, except 5 μl of ligase buffer was substituted for the enzyme solution.

5.13 TRANSFORMATION AND CALCULATION OF ASSEMBLY EFFICIENCY

Heat-inactivated assembly mixtures were transformed into One Shot Mach1 T1 Phage-Resistant Competent Cells (*E. coli* genotype: F- φ80 (lacZ)ΔM15 ΔlacX74 hsdR(rK-mK+) ΔrecA1398 endA1 tonA; Life

Technologies, Carlsbad, CA). 0.6-5.0 µl of assembly mixture was added to 50 µl of thawed cells, incubated on ice for 35 minutes, incubated at 42°C for 30 seconds, placed back on ice for 2 minutes, and then 450 µl of SOC media was added to the cells. The cells were allowed to recover for 1 hour in a shaking incubator at 37°C. 50 µl of recovery outgrowth was diluted ten-fold into 450 µl SOC three times to obtain 1X, 10X, 100X and 1000X dilutions. 150 µl of each dilution was plated onto an LB agar plate with 100 micrograms per mL ampicillin and allowed to grow overnight at 37°C.

The following day, the number of colonies that grew on each agar plates corresponding to the 1000X dilution was tallied.

Part II

MUSHTARI

There are numerous applications of synthetic biology in industrial biotechnology but rarely has synthetic biology been used in product design. How could designers embed biological functionality into products? The second part of this thesis explores this question with *Mushtari*, a 3D printed, multimaterial wearable designed to host a coculture of photosynthetic cyanobacteria and *E. coli*.

Part II will be adapted into a journal article, which will be submitted for publication in the ensuing months.

Authors: William Patrick, Christoph Bader, Dominik Kolb, Steph Hays, Boris Belocon, Daniel Dikovsky, Sunanda Sharma, Steven Keating, Pamela Silver, Neri Oxman

6

INTRODUCTION: *SYNTHETIC SYMBIOSIS*

The second part of this thesis documents the design of a wearable that is part speculative design, part applied science. *Mushtari* is a 3D printed, multimaterial wearable designed to incorporate a coculture of E. coli and photosynthetic cyanobacteria. The piece is a part of *Wanderers*, a series of wearables designed to embed synthetic microorganisms. I led the project with my advisor, Neri Oxman, and Stratasys and collaborated with Christoph Bader and Dominik Kolb of Deskriptiv and Pamela Silver's Lab at Harvard Medical School. Our primary motivation was to investigate the *Material Ecology* of synthetic microorganisms within a wearable. How can embedded, synthetic microorganisms and the material properties and geometry of the wearable be designed to influence and ideally augment each other?

6.1 SYNTHETIC SYMBIOSIS: A DESIGN APPROACH FOR EMBEDDING LIVING ORGANISMS WITHIN A PRODUCT

How can synthetic organisms be incorporated as a component of a product? Biology provides inspiration. Endosymbiosis occurs when one organism lives within another one[68]. Many endosymbiotic relationships are mutually beneficial. These relationships can evolve over time such that the relationship becomes obligate, where each organism needs the other to survive. Endosymbionts — the organism that lives within another organism — in obligate relationships have evolved some of the smallest known genomes because they have eliminated genes that duplicate function provided by the host [89]. Several examples of endosymbiosis are particularly inspiring for designing organisms as components in products:

1. Giant tridacnid clams have evolved to protect single cell algae from photodamage. The geometry and material properties of the clam's mantle enable the even distribution of incoming sunlight deep into the clam, maximizing photosynthesis [46].

2. *Vibrio fischeri*, a marine bioluminescent bacterium, colonizes the light organ of Hawaiian bobtail squid, *Euprymna scolopes*, during development and produces bioluminescence throughout the squid's life[78].

3. The human microbiome comprises the 10-100 trillion bacterial cells that inhabit the human body [86]. Researchers are beginning to understand the complex interactions between human bacterial flora and their human hosts. Bacteria can be harmful to human health, particularly when organisms begin to dominate as a monoculture (for example, *Clostridium dificile*)[18]. However,

microflora have been demonstrated as integral elements of the digestive and immune systems[47]. Similar to gut microflora, could engineered bacteria function in a wearable to provide beneficial function to the wearer?

These biological case studies inspire the design of products that host endosymbionts. Similar to their biological counterparts, these products support the endosymbiont and the endosymbiont creates functional value. The design of the product-endosymbiont relationship can be thought of as a *synthetic symbiosis*. Design begins with the microorganism and the desired function it can provide to the product and user. Then the product host is designed to contain, nurture, and control the endosymbiont to perform that function.

We began the design process by investigating potential endosymbionts. The most commonly engineered microorganisms in synthetic biology are *Escherichia coli* (*E. coli*), *Saccharomyces cerevisiae* (*S. cerevisiae*), *Bacillus subtilis*, and cyanobacteria. Of these, cyanobacteria (Figure 5) stand out as a potential endosymbiont. Cyanobacteria function with minimal inputs — mainly water, light, carbon dioxide, a nitrogen source and salts — and tolerate marginal growth conditions[36]. This contrasts with *E. coli* and *S. cerevisiae*, which require a replenishing carbon source — typically a carbohydrate — to function. Cyanobacteria efficiently produce biomass from sunlight. The bacteria grow in minimal and inexpensive liquid media that contain salts and a nitrogen source and can produce many types of metabolites through photosynthesis.

Cyanobacteria and eukaryotic microalgae have been widely cultivated for at least the last 60 years in large-scale open ponds and closed photobioreactors to produce food and feedstocks[23, 32]. More recently, certain strains of cyanobacteria have been identified that produce antiviral, antibacterial and other bioactive compounds and polyhydroxyalkanoates (PHA), a polymer with similar material properties as common plastics such as a polypropylene[10]. Cyanobacteria have been metabolically engineered to increase production of natural occurring compounds and produce other high-value products, such as ethanol, fatty acids, butanol and hydrogen[13, 92]. Several start-up companies have begun commercializing modified cyanobacteria for the production of feed stocks and fuels and have built large-scale, enclosed photobioreactors[11, 28]. However, modified cyanobacteria have not been used to produce these high-value products at a small-scale within a household, personal or wearable product.

6.2 DESIGNING COCULTURES OF CYANOBACTERIA AND *e. coli*

Cyanobacteria have several advantages in comparison with other model organisms in synthetic biology for use within a product and they have been proven to produce high value products on a large scale[11, 28]. However, it is difficult to design complicated genetic circuits in cyanobacteria because few genetic parts (promoters, transcription factors, terminators) have been well characterized[20, 45]. This limitation

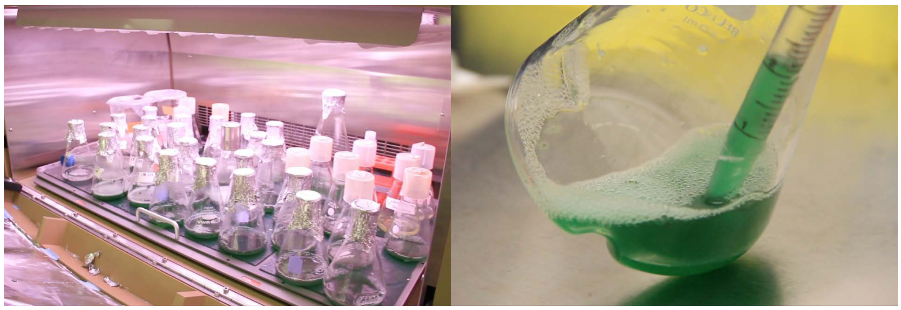

Figure 5: **Cyanobacteria culture**. Left: in a shaker incubator. Right: Extracting a sample. Photo credit: Will Patrick

makes complicated synthetic biology applications, such a cell-based therapeutics or cell-based logic, challenging to engineer in cyanobacteria.

One approach that could be used to overcome this challenge is to coculture cyanobacteria with *E. coli*, *S. cerevisiae*, and other microbes. In this approach, cyanobacteria photosynthesize and provide a carbon source for a heterotroph, which is engineered for a desired function. This approach is being pursued by the Pamela Silver laboratory at Harvard Medical School. Researchers at the Silver lab have engineered *Synechococcus elongatus* PCC 7942 (*S. elongatus*), a freshwater cyanobacterium, to photosynthesize, produce sucrose, and export it outside of its cell wall. The sucrose can then be consumed as the primary carbon source by heterotrophs, such as *E. coli*, *S. cerevisiae* and *B. subtilis* [37].

We decided to design *Mushtari* to coculture *S. elongatus* and *E. coli* (Figure 6). In the design, the modified *S. elongatus* convert light to sugar and *E. coli* convert sugar to useful functions for the wearer. E. coli are the workhorses of synthetic biology and have been engineered to produce many types of biological substances: color, drugs, food, fuel, and scents. These two bacteria form a platform for wearable microbial production. The wearer would be able to induce the engineered E. coli to begin producing a particular substance, for example a scent, a color pigment, or food.

6.3 DESIGN PROBLEM: DESIGNING A WEARABLE TO COCULTURE *e. coli* AND *s. elongatus*

We focused on the following questions:

1. How could we embed these two bacteria — *E. coli* and *S. elongatus* — within a wearable?

2. How could a coculture be utilized within a wearable design to generate aesthetic and functional value to the biology, users and natural environment?

3. How could the wearable mediate between the environment — sunlight, air and user — and the coculture to create a symbiotic relationship between user and bacteria?

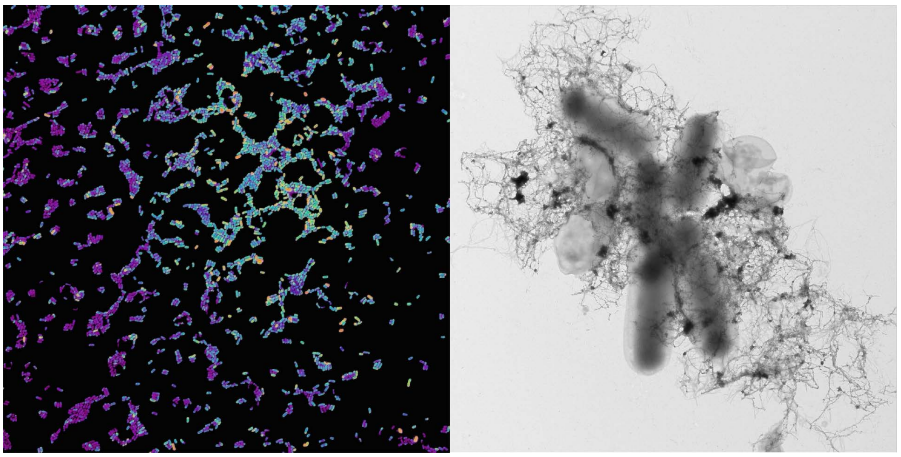

Figure 6: **Micrographs of *S. elongatus* and *E. coli***. Image credit: Steph Hays, Tom Ferrante, Will Patrick (left), Eleronore Tham, Sunanda Sharma, Will Patrick (right)

4. How could we alter the material properties and the geometry to affect the bacterial activity?
5. What fabrication method and material system could be used to create the wearable?
6. How could we design the fluidics, material properties, and geometry into the wearable?

6.4 DESIGN FORMULATION: FLUIDIC WEARABLE CONTAINING COCULTURE

There are several biological factors to incorporate into the design.

1. *S. elongatus* and *E. coli* both grow and function in liquid cell culture, so the containment and manipulation of liquid cultures is critical to the design of the wearable.
2. In coculture, the two bacteria are alternatively exposed to light and darkness to mimic natural lighting conditions.
3. *E. coli* and *S. elongatus* preferred culture temperatures are 37 and 30 degrees Celsius respectively.
4. Both organisms require gas exchange with ambient air.

Our initial concept for the wearable design (Figure 7) revolved around the design of a single long channel wrapped around the body. The material properties of the channel would vary from opaque to transparent; coculture pumped through the piece would experience alternating areas of light and darkness. Figure 8 demonstrates how spatially varying the transparency of the fluid channel could vary bacterial activity in those areas. In the initial concept, the geometry of photosynthetic regions was optimized for photosynthetic output and areas of *E. coli* function (opaque, dark areas) were situated closer to the body to collect additional heat. Various input and output locations

throughout the piece were designed to allow the user to trigger activity of the coculture or extract products generated by the organisms. We were not able to incorporate many these features into the design, however they would be exciting to explore in future research.

This design formulation requires the co-investigation of three areas: Computational form generation of fluidics, 3D printing of product-scale, multi-material fluidics, and biocompatibility testing between the 3D printed materials and the coculture micro-organisms.

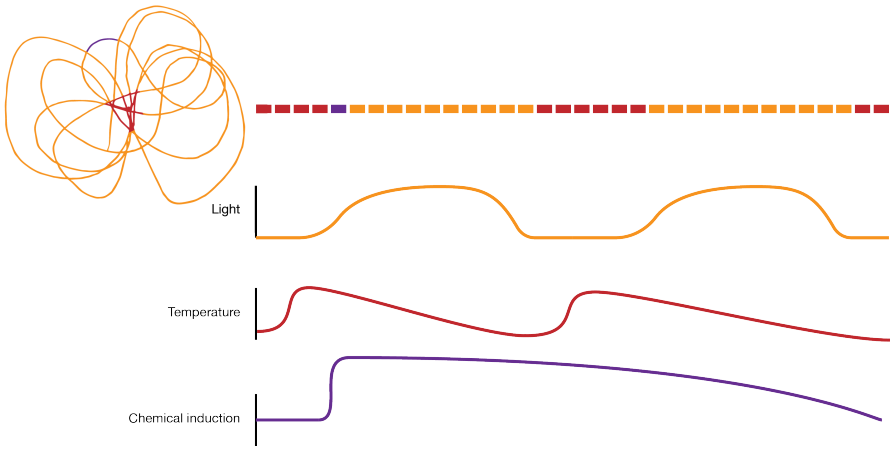

Figure 7: **Initial concept for *Mushtari***. Light, temperature, and chemical exposure are controlled in one long channel.

6.5 COMPUTATIONAL APPROACH: GROWING FLUIDICS IN WEARABLE FORMS

Previous 3D printed fluidic devices have been designed using conventional CAD based software packages, such as SolidWorks and AutoCAD. Scaling this approach to design a fluidic wearable with multi-material gradients is not possible, as these software packages are not designed to encode gradients of material properties within geometries. Instead we pursued generative approaches for creating form. We collaborated with Christoph Bader and Dominik Kolb of Deskriptiv who have developed computational approaches for growing form, a few of which can be seen in Figure 9. We developed several ways of generating inner fluidic structures within a wearable.

6.6 FABRICATION APPROACH: 3D PRINTING OF PRODUCT-SCALE, MULTI-MATERIAL FLUIDICS

3D printing can be used to manufacture wearable-scale products[35]. However, 3D printing has never been used to print a wearable with an inner fluidic network. 3D printed fluidic systems to date have been printed using a single material and each previously printed device is small (below 10 cm feature size) compared to a wearable. The Connex series of multi-material printers developed by Stratasys can print up to three model materials in a large gantry size (500 by 400 by 200

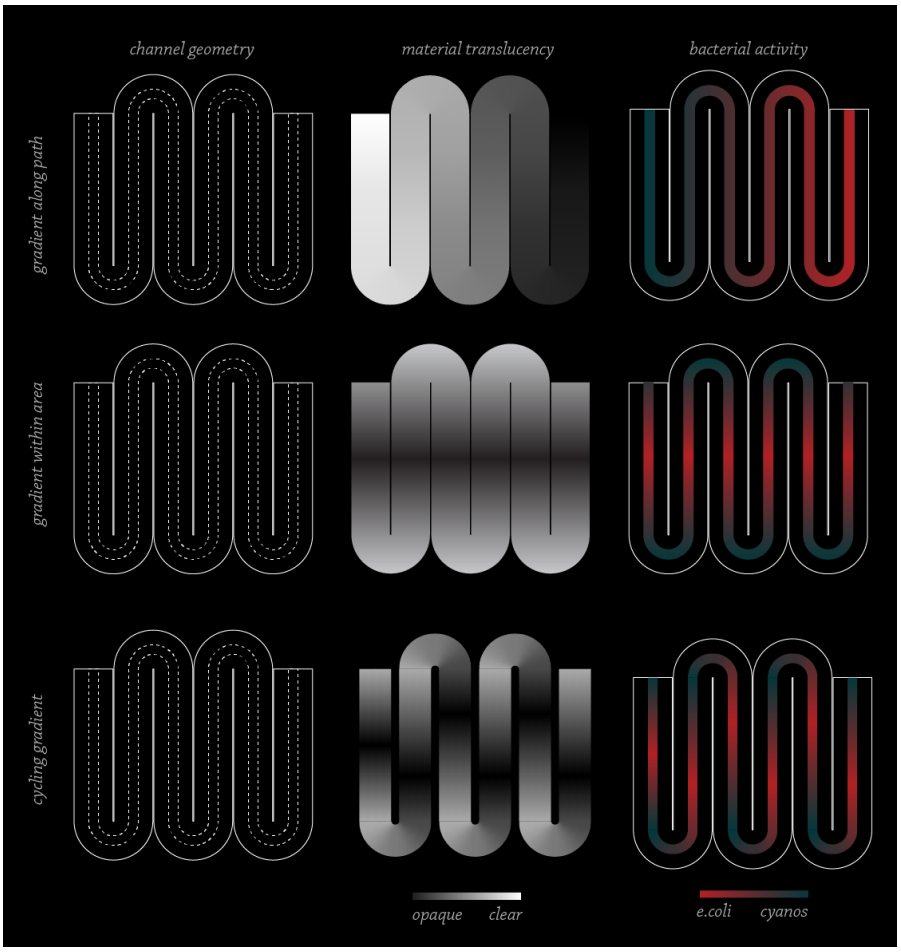

Figure 8: **The desired effect of material transparency on bacterial activity**. In translucent regions, the co-culture receives light, increasing cyanobacteria activity (right column). In opaque regions, the co-culture is dark, *E. coli* consume sucrose, and increase in activity. Transparency can be varied through the strand (center column), affecting the bacterial activity (right column).

mm). Commercially available photopolymers for the Connex printers vary in rigidity, opacity, and color. The bitmap printing workflow enables printing material property gradients (for example, stiff to flexible or transparent to opaque)[35]. Neri Oxman, in collaboration with Stratasys and Prof. W. Craig Carter, previously created a series of wearables with material property gradients in the series Imaginary Beings (Figure 10), which was on display at the Center Pompidou in Paris, France[70].

Although the Connex series printers have been demonstrated to produce wearables with material gradients, the printers use a support, which makes creating inner fluidic channels impossible. The printer adds the gel-like support in any internal structures, including fluid channels. This gel support must be removed abrasively and cannot be melted or dissolved. Therefore, the only fluidics that can be printed using the Connex series printers with gel support are simple cylindrical or square extrusions that can be cleared using a high-pressure water jet. To overcome this barrier, we explored soluble and liquid support methods in collaboration with Stratasys.

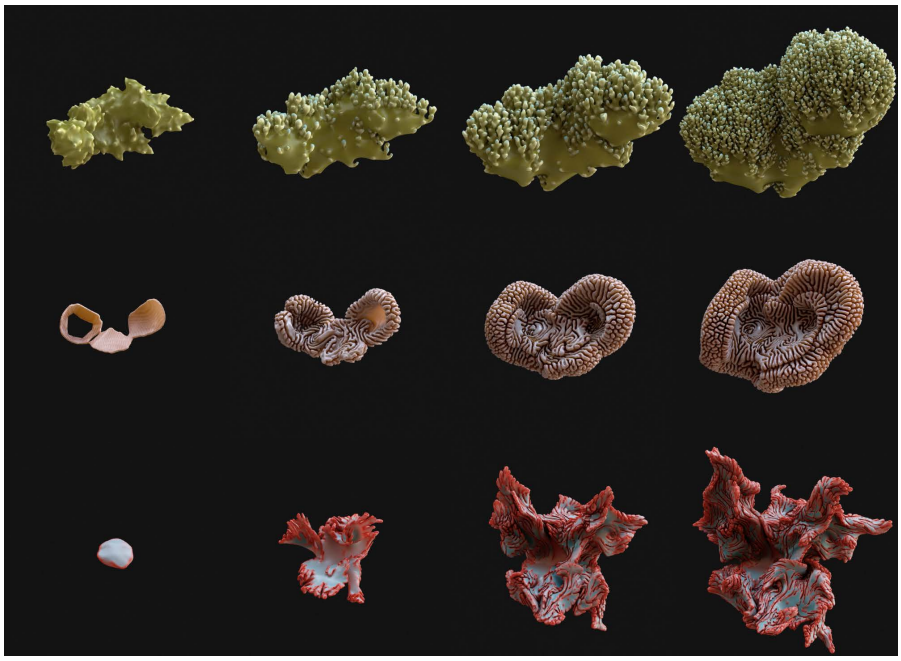

Figure 9: **Computationally grown structures**. Three growth variants created by Bader and Kolb.

Figure 10: **Multi-material, voxel-based 3D printing of a helmet**. A tissue micro-CT scan (left) informed the geometry and material deposition. From the Imaginary Beings series at the Centre Pompidou (Paris, France) by Neri Oxman in collaboration with Craig Carter, Stratasys, The Mathworks, and Turlif Vilbrandt. [35] 2012. Photo credit: Yoram Reshef.

6.7 BIOLOGICAL RESEARCH: 3D PRINTED MATERIAL BIOCOMPATIBLITY

The compatibility of the Connex PolyJet photopolymers with bacterial culture has not been tested. In fact, no data has been published to date on using 3D printed fluidic devices for bacterial cell culture. For this project, we collaborated with the Pamela Silver Lab at the Harvard Medical School to test the biocompatibility of the stiff, clear photopolymer (VeroClear) with *E. coli*, *S. elongatus* and a coculture of the two.

6.8 PROJECT GOALS

The project goals can be summarized as follows:

1. Develop computational approaches for generating fluidic channels in a wearable
2. Create a method for printing product-scale, multi-material fluidics in collaboration with Stratasys
3. Test the compatibility of Connex 3D printed materials with culturing *E. coli* and *S. elongatus*.

We focus on these specific goals to complete the project. However, there are several additional research directions we would like to pursue in future work:

1. Develop algorithms to optimize the geometry for photosynthesis or to pick up heat from the body.
2. Explore how the user would interface with the product including (1) using chemical induction to turn on or off bacterial activity and (2) collecting the end products generated from the bacteria.
3. Coculture *S. elongatus* with modified *E. coli* that generate functions such as (1) color changing, (2) scent generation, (3) therapeutic or drug production, or (4) fuel production.
4. Integrate functional 3D printed elements, such as proportional control valves.

7

METHODOLOGY

7.1 PREVIOUS WORK FROM COLLABORATORS

7.1.1 *Silver Lab: Modifying Cyanobacteria to Produce and Export Sucrose*

Our collaborators in the laboratory of Professor Pamela Silver at Harvard Medical School are currently designing cocultures between cyanobacteria and other microorgranisms. Their motivation is efficiently generating feedstock for large-scale microbial production of high value products[36]. Researchers in the lab have designed *Synechococcus elongatus* PCC 7942 (*S. elongatus*) to produce sucrose and export it from the cell. The researchers expressed a sucrose permease (cscB) into *S. elongatus*, which exports sucrose when the cell experiences osmotic pressure[37]. Researchers in the Silver lab (particularly graduate student Stephanie Hays) are currently investigating coculturing the modified *S. elongatus* with *E. coli*, *S. cerevisiae*, and *B. subtilis*. Their research is on going and the results will be published in an upcoming journal article. They have been able to coculture the modified *S. elongatus* with *E. coli* (W strain) (Figure 5) in a minimal media without an additional supplied carbon source for the *E. coli*. When the coculture is exposed to light, *S. elongatus* multiply and export sucrose to the media. The *E. coli* can then consume the sucrose and grow. To mimic natural conditions, the lighting conditions are cycled between light and dark regimes. *E. coli* modified to produce a small molecule were used in the initial experiments, however it should be possible to coculture *S. elongatus* with many previously modified *E. coli*, enabling the production of many types of high-value products and functions.

7.1.2 *Stratasys: Developing Alternative Support Methods for PolyJet Printing*

Stratasys has developed two alternative support methods to their normal support (Objet Support SUP705): soluble support and liquid support. Soluble support, Objet Support SUP707, is a polymer material, which can be dissolved in water and has a melting point of 120C. Soluble support can be substituted for the typical gel support in the Connex workflow and is currently commercially available for the Eden260VS printer. The liquid support method uses a model material with similar material properties as un-polymerized model material but cannot be polymerized by UV light. The liquid support is printed into inner channels by assigning a STL mesh or bitmap stack of the inner channel geometry to the liquid support material. Liquid is printed inside of the channel, accumulating and creating a liquid surface to print and polymerize model materials.

7.1.3 *Bader and Kolb: Computational Growth of Geometry and 3D Slicing for Voxel-Based 3D printing*

Bader and Kolb have developed two technologies, which were used to create Mushtari: computational growth algorithms and 3D slicing. Both technologies are unpublished and will be described in a follow-up publication. The growth algorithms developed by Bader and Kolb mimic natural growth systems to create organic forms. The process starts with an input geometry — for example a mesh or a line — which is then deformed by the algorithm and then re-meshed or re-sampled into a new geometry. The process repeats for many iterations and the deformations aggregate into the growth of a form. The algorithm deforms the local vertices using bulging, relaxation, and repulsion and the strength of these three parameters can be controlled, enabling many form variants. Bader and Kolb have also assigned material property information to each vertex, which can also be deformed and changed through iterations of the algorithm. These growth algorithms build on previous approaches, including Lindermayer-Systems (L-systems) [74], which have been used to generate branching structures and tropisms [60], and recent work on generating cellular forms using a simplified mass-spring model applied to cellular units within a mesh [63].

Secondly, Bader and Kolb created a 3D slicer to prepare grown geometries for multimaterial 3D printing on the Connex3. The software slices geometries into stacks of thousands of 2D bitmap layers. Each slice corresponds to a 30-micron layer in the z-dimension. The slicer generates three bitmap stacks per geometry, one for each of the Connex3's model materials. Each 2D bitmap image is an array of black and white pixels; white pixels signify material deposition. Input geometries have material property information at each vertex. The software converts this material information into sets of bitmap images that correspond to the desired material property. For example, in an area where 20% clear and 80% red is desired, the software would make 20% of the pixels in the clear bitmap stack white and 80% of the pixels in the red bitmap stack white.

7.2 METHODS & MATERIALS

7.2.1 *Design, fabrication and processing of test pieces used to characterize soluble and liquid support methods*

Test pieces were designed and printed to test soluble and liquid support methods. Test pieces were designed using Rhinoceros (Figure 11A). Test pieces were printed on the Connex3 using the Vero family of acrylic photopolymers. The pieces were printed using a standard STL workflow. Test pieces were printed in a horizontal orientation using a normal, soluble, and liquid support methods and vertically using liquid support. Several replicates were printed for each support type.

Each support method required separate processing:

Normal support — bulk external support was removed using a water jet cleaner (Powerblast High Pressure Water Cleaner, Balco UK). To remove all remaining external support, the pieces were then placed in a 2% NaOH bath for 1 hour, water jet cleaned again, placed again in the 2% NaOH bath for a hour, and finally water jet cleaned once more. To create cross sections, test pieces were cut using a band saw and the cross section face was sanded using a rotary belt sander. To remove the inner support, the pieces were water jet cleaned, and then soaked in a 2% NaOH bath for a hour and water jet cleaned in two successive rounds.

Liquid support — test pieces printed using the liquid support method are printed with normal gel support on the exterior. This external support was removed using the same method that was used for the normal support test pieces. After the final water jet cleaning, the pieces were then positioned to allow liquid support to drain out of the piece. Then, the pieces were sectioned using a band saw and the sectioned surface was sanded using a rotary band saw. To remove remaining liquid support in the channels, the pieces were water jet cleaned and water was forced through the channels.

Soluble support — pieces printed with soluble support had support material in the internal channels as well as on the external surface. To remove the soluble support on the external surface, the pieces were boiled at 100 C in water for an hour. Then the pieces were sectioned using a bandsaw and the cross sectioned surface was sanded using a rotary belt sander. The cross sections were boiled for approximately 2 hours until the remaining support dissolved into the boiling water. After the second boiling, the pieces were water jet cleaned.

7.2.2 *Characterizing test pieces using imaging*

Cross sections of test pieces were examined using optical and scanning electron microscopy. For optical microscopy, images were taken using the Vividia 2.0 MP handheld USB Digital Endoscope. Diameters in the images were measured in ImageJ. To determine the scale of each image, a known length on the image was measured using calipers. Three replicates were measured for each support type and three technical replicates were performed for each measurement. For electron microscopy, a representative sample for each support type was sputter coated with gold and examined with a Tescan Vega GMU Scanning Electron Microscope (SEM).

7.2.3 *Designing and printing small patches for testing soluble and liquid support*

We designed and printed larger patches using liquid and soluble support to investigate if the support could be removed from the inner channels. The patches were design in Solidworks (Figure 13) and using growth algorithms (Figure 14). Test patches were printed in Ve-

roClear material using the Connex3. After printing, patches printed with soluble material (as seen in Figure 13 and Figure 14) were submerged into a heated oil bath (120 C). Upon removing the pieces from the oil bath, dissolved support was cleared from the pieces by hand using a syringe. For patches printed using liquid support, external support was removed by water jet and then internal liquid drained out by gravity. Remaining internal liquid support was removed by hand using a syringe.

7.2.4 *Culture experiments with* E. coli

E. coli were grown in two types of culture tubes: a standard 14 mL polypropylene culture tube (Falcon, Corning) and a VeroClear culture tube with the same geometry. The support material was removed using the same method as the test pieces. The VeroClear tubes were then heat cured for 24 hours at 100C in an oven and then autoclaved.

5 colonies of W strain *E. coli* were picked into Luria broth (LB) and cultured overnight in an incubator with a temperature of 37C and shaking at 220 rpm. Three *E. coli* cultures were then diluted to 0.4 OD600 with LB media. Both the polypropylene and the VeroClear tubes were filled with 5 mL of each *E. coli* culture, creating 3 replicates. Each uncapped culture tube was then placed inside of a 50 mL polypropylene tube (Falcon Corning), which was then capped. To prepare the negative controls, 5 mL of LB media was added to 3 VeroClear and 3 polypropylene tubes. These tubes were also placed inside 50 mL BD Falcon polypropylene tubes.

All tubes were cultured in a 35 C incubator shaking at 150 rpm. Measurements were taken every 15 minutes until the cells appeared to hit stationary growth. OD600 measurements were taken using a 96 well plate reader. These measurements were then converted to OD600 cuvette measurements.

To calculate the doubling time, the log base 2 of each sample was calculated. The time series for each replicate was plotted in Excel with hours on the x-axis. For each condition, the initial and last data points were dropped and a line of best was added. Data points were dropped off the time series until the linear correlation (R^2) was >= 0.99. The average number of doublings per hour for each condition was determined from the slope of the line of best fit. To quantify the variation between the biological samples for each condition, we then found the doublings per hour for each biological sample and calculated the standard deviation.

7.2.5 *3D printing and post processing Mushtari*

Mushtari was printed using the Connex3 bitmap workflow. Three bitmap stacks were generated for each of Mushtari's five pieces. Two of the bitmap stacks corresponded to the modeling materials, VeroClear and Red. A third bitmap stack was generated for the inner channels which was used for printing the liquid support. Each piece

was printed using the matte setting. Pieces were post-processed in several steps. Pieces were water jet cleaned to remove the external support. Liquid support then drained from the pieces by gravity and the remaining liquid support was removed by hand using a syringe. The exterior of each piece was then sanded and lacquered.

7.2.6 *Filling printed with liquid*

Mushtari was filled with chemiluminescent liquid by hand using a syringe to visualize the internal channels. The piece was printed with many 1.5 mm diameter inlets throughout the channels. The inlets were used for removing any remaining liquid support material and filling the piece. A 22-gauge dispensing needle tip was press-fit into the inlets. After filling the piece, the inlets were filled with small plugs that were 3D printed on the Connex500. These plugs press-fit into the inlets to create a water tight seal.

8 RESULTS

8.1 CHARACTERIZING SUPPORT METHODS FOR MULTI-MATERIAL FLUIDICS

Soluble support and liquid support presented two potential options for creating internal liquid channels in the wearable. To characterize these two support methods, we designed a test piece that contained channels from 20 to 0.5 mm (Figure 11A). We printed the test piece using normal support, soluble support, and liquid support and imaged cross sections for comparison using both optical (Figure 12) and scanning electron microscopy (SEM) (Figure 11). The liquid support was printed in two orientations — horizontal and vertical — to investigates how orientation may effect build quality.

8.1.1 *Cleared channels*

The test pieces printed using liquid support in a horizontal orientation were the only test pieces that could be entirely cleared of support. Liquid could pass through all channels (A-G) for each of the three sample replicates. In test pieces printed using soluble and liquid support in a vertical orientation, channels greater or equal to 1 mm (B-G) could be cleared. In test pieces printed with normal gel support, only channels greater or equal to 3mm (E-G) could be cleared.

8.1.2 *Print accuracy, quality and channel shape*

Table 2 summarizes the expected and measured dimensions of the test piece cross sections.

For test pieces printed using soluble support, the channels were similar to the expected diameter for channels 2mm or greater. Channels designed with diameters of 0.5 and 1.0 mm were smaller than expected. The shape of these channels was oval-like and thinner in the z-direction of the printing (Figure 12).

The print accuracy of test pieces printed vertically or horizontally using liquid support varied greatly. The measured diameters of channels printed horizontally with liquid support were smaller than expected for both small channels (diameters 0.5 to 3.0 mm) and the 20 mm channel. The diameters of channels printed horizontally were also oval-like for channels with diameters 5 mm and smaller, but in the opposite direction as soluble support. 0.5 mm channels in these test pieces could all pass water through them and were measured to be 0.3 mm on average (standard deviation: 0.04).

The overall quality of test pieces printed using liquid horizontal support was lower than pieces printed using other support methods.

Mean and standard deviation (SD) of the diameters (A-G) (mm) on the test piece printed with various supports

Diameter	Expected Value	Normal	Soluble	Liquid - H	Liquid - V
A	0.5	0.46 (SD: 0.02)	0.41 (SD: 0.03)	0.3 (SD: 0.04)	0.36 (SD: 0.04)
B	1	0.97 (SD: 0.03)	0.88 (SD: 0.05)	0.73 (SD: 0.06)	0.90 (SD: 0.05)
C	2	2.02 (SD: 0.05)	1.96 (SD: 0.05)	1.76 (SD: 0.05)	1.92 (SD: 0.06)
D	3	3.10 (SD: 0.07)	2.96 (SD: 0.08)	2.82 (SD: 0.07)	3.0 (SD: 0.1)
E	5	5.2 (SD: 0.1)	5.0 (SD: 0.1)	4.9 (SD: 0.1)	5.0 (SD: 0.1)
F	10	10.0 (SD: 0.2)	9.9 (SD: 0.2)	9.8 (SD: 0.3)	9.8 (SD: 0.2)
G	20	20.0 (SD: 0.3)	19.9 (SD: 0.3)	19.0 (SD: 0.3)	19.8 (SD: 0.3)

The mean and standard deviation of each diameter for each support type were calculated using 3 replicates printed and measured for each support type. Diameters were measured in the dierection of the print orientation.
Normal, soluble and Liquid - H were all printed in the same horizontal orientation. Liquid - V was printed in a vertical orientation.

Table 2: **Measured vs expected diameters of the channels within the test piece for each of the support methods.**

SEM imaging revealed cracks and de-lamination between layers and distorted exterior channel geometry (Figure 11). The channel wall of the the largest channel was deformed for all test pieces printed as can be seen in Appendix B, Figure 37.

The measured diameters of test pieces printed using liquid support in a vertical orientation were similar to the measured diameters of test pieces printed using soluble support. In this printing orientation, channels with diameters 2mm and below were smaller than expected. The channel shape remained circle-like for all channels.

8.1.3 *Surface roughness in channels*

Surface roughness of the inner channel varied greatly between support methods as can be seen in both the SEM (Figure 11) and optical images (Figure 12).

Liquid support appears to create more surface roughness than other methods. Increased surface roughness is likely due to diffusive mixing between the liquid support and liquid model material during each printing layer.

Surface roughness of channels printed with soluble support appeared lower than channels printed with normal support as can be seen in the SEM and optical images.

In summary, we found that both soluble and liquid support can be used to fabricate fluid channels using the Connex3 printer. However, each had benefits and weaknesses. Liquid support can print smaller channels with diameters as small as 300 microns but creates additional surface roughness. Soluble support has higher print quality, is more accurate, and creates less surface roughness than liquid support, but the soluble support could not be cleared from the smallest channels in the test pieces.

8.2 TEST PATCHES PRINTED WITH LIQUID AND SOLUBLE SUPPORT

We continued to test the two potential support methods — soluble support and liquid support — with larger patches. We initially tested soluble support using a test patch (Figure 13) that featured 0.6 mm diameter, 15 cm long and 1.2 mm, 1.5 m long channels. We cleared the soluble support from all the channels in the piece and pumped colored with dye using a syringe.

We designed the second test piece (Figure 14) to reflect the geometry of the final wearable. The test piece featured five inlets and a channel diameter that ranged from 1.5 to 12 mm in diameter. First, the piece was printed with soluble support, which was unable to be cleared from the piece even after multiple attempts. We then printed the same patch using liquid support and the piece cleared successfully (Figure 14). We flowed liquid through this piece from inlet to outlet.

Even though the second test piece featured larger diameter channels than the first test piece and multiple inlets, the soluble support could not be cleared from the second piece. This suggests that the irregular geometry, including multiple branches, changing diameters, and small radii of curvature, factored into our ability to clear soluble support out of the channels. Based on these two test pieces, we used the liquid support for printing the wearable.

8.3 CULTURING *e. coli* AND CYANOBACTERIA IN PHOTOPOLYMER MATERIAL

Culturing experiments of *E. coli*, *S. elongatus* and cocultures of the two within the Connex photopolymer materials are ongoing. In preliminary experiments, we cultured *E. coli* (W strain) and *S. elongatus* in standard 14 mL polypropylene culture tubes (Falcon, Corning) and culture tubes of the same geometry printed on the Connex500 with VeroClear material. The difference between the doublings per hour of *E. coli* cultured in both tubes was statistically insignificant over one doubling (Table 3). We have anecdotal evidence that *S. elongatus* can persist in VeroClear tubes but have faced difficulties with growth experiments. We will continue to modify printing and pretreatment of VeroClear containers in hopes of finding conditions for robust cyanobacterial growth. Results will be published in a follow-up publication.

8.4 GENERATIVE GROWTH OF FLUIDIC NETWORKS

We created generative methods to grow inner channel structures in the wearable. Bader and Kolb developed several initial approaches to growing inner channel structures (Figure 15), including vein, hair, and bubble-like structures. The most applicable approach to our design used line-expansion to grow a channel structure upon a pre-

Condition	Doublings per hour	R^2	Standard Deviation	Doublings During Sampling
No Cells, Control	0.02	0.408	0.01	0.03
No Cells, VeroClear	-0.1	-0.653	0.1	-0.11
E. coli, Control	0.82	0.996	0.07	0.99
E. coli, VeroClear	0.84	0.998	0.06	1.03

The standard deviation shown above is calculated from 3 biological replicates.
One doubling was observed and a line of best fit with an R^2 greater than 0.99 was used to calculate the doublings per hour.
The control tube is a Falcon culture test tube. The VeroClear tube was printed with the same geometry as the control tube.

Table 3: **Doublings per hour of *E. coli* grown in culture tubes made of standard polypropylene and VeroClear material.**

defined surface. Four frames from a small-scale growth study using this approach can be seen in Figure 16. Initial parameters, such as channel diameter, material properties, length and shape, affect the geometry and material properties of the final form. However, these parameters to not determine the form; each run of the code yields a unique, emergent form.

We applied the line expansion approach to the human form to develop the form of the wearable. Figure 17 shows three potential approaches for assigning material properties to the structure: cycling transparency along the length of the channel (left), assigned transparency by channel diameter (middle) and regionally applying material properties (right).

8.5 DESIGN AND FABRICATION OF MUSHTARI

Figure 18 details the design of Mushtari. We assigned material properties regionally on the piece. Only two model materials were available, because we used the liquid support method. We used VeroClear and Red (stiff photopolymers) to create transparency gradients. The Red material was a specific color formulation created by Stratasys for Mushtari. We applied these two materials regionally to create opaque and transparent regions. We designed these two regions to affect the bacteria inhabiting them: in transparent regions the cyanobacteria would be able to photosynthesize and the *E. coli* would consume the sucrose and function in the opaque regions. The two materials were feathered to create smooth transparency gradients between regions

After growing and assigning material properties, we split the form into a five-piece assembly (Figure 18) such that each piece could fit in the build volume of the Connex3 printer. Each piece featured a single long channel. The five channels stretched 58 meters in total and ranged in diameter from 1 mm to 20 mm.

We designed each piece with a single channel with two inlets. However, for practical purposes, we added additional inlets along the channel to create multiple access points. Inlets were small tapered holes designed to press fit a 1.5 mm tube. These inlets can be plugged when they are not being used. In total, we added over 300 additional inlets to the five pieces, some of which can be seen in Figure 22.

To print the five pieces, we first sliced each geometry into three bitmap stacks, one for each material (VeroClear, Red and liquid support). One bitmap slice of the back right piece can be seen in Figure 19. Stratasys printed the pieces using these bitmap stacks (Figure 20). Print times ranged from 20 to 80 hours. Stratasys post-processed the pieces by removing external gel support, draining liquid support, and sanding and lacquering the final pieces. Images of the final, processed pieces can be seen in Figure 21.

8.6 FILLING MUSHTARI

We visualized the printed channels by filling Mushtari with chemiluminescent fluid (Figure 22 and 23). Nearly all channels in the five pieces were cleared. The only area that could not be cleared was a small section in the front piece (Figure 24, lower right). The channels in this section were designed to be 1 mm in diameter.

We found that we were not able to flow liquid from inlet to outlet in the pieces by hand. After a certain distance in each piece, the pressure required to move the liquid became too great to be applied by syringe. Figure 23 demonstrates filling one of the back pieces by syringe as far as possible. We were able to flow the liquid approximately 3.5 meters through a channel section with diameters that ranged from 1.4 to 11 mm. This suggests that the pressure losses due to the diameter, channel length, and channel curvature were higher than the pressure we were able to deliver by hand. Near the inlet of the piece, the liquid branched into two channels, suggesting that a wall section between two internal channels was breached. We filled one of the back pieces with cyanobacteria, demonstrated in Figure 25.

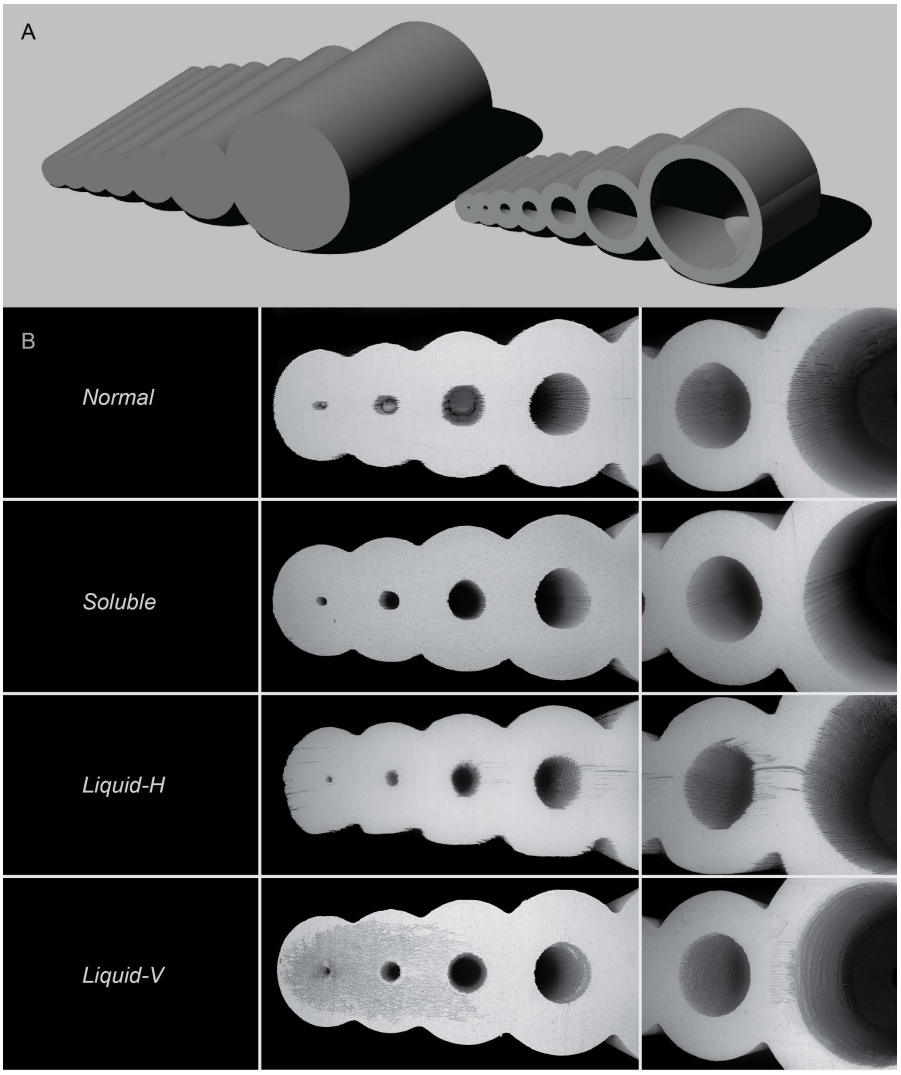

A. Test piece (left) and cross section (right). 7 diameters range from 0.5 to 20 mm. Diameters were labeled A to G smallest to largest.

B. SEM images of cross sections of the representative test piece printed with Normal, Soluble and Liquid support. Normal, Soluble and Liquid-H were all printed in a horizontal orientation, from top to bottom in the images. Liquid - V was printed in the direction of the camera.

Figure 11: **Support method characterization**. Characterizing a test piece (A) using scanning electron microscopy for three support methods, Normal, Soluble and Liquid. SEM images taken by James Weaver.

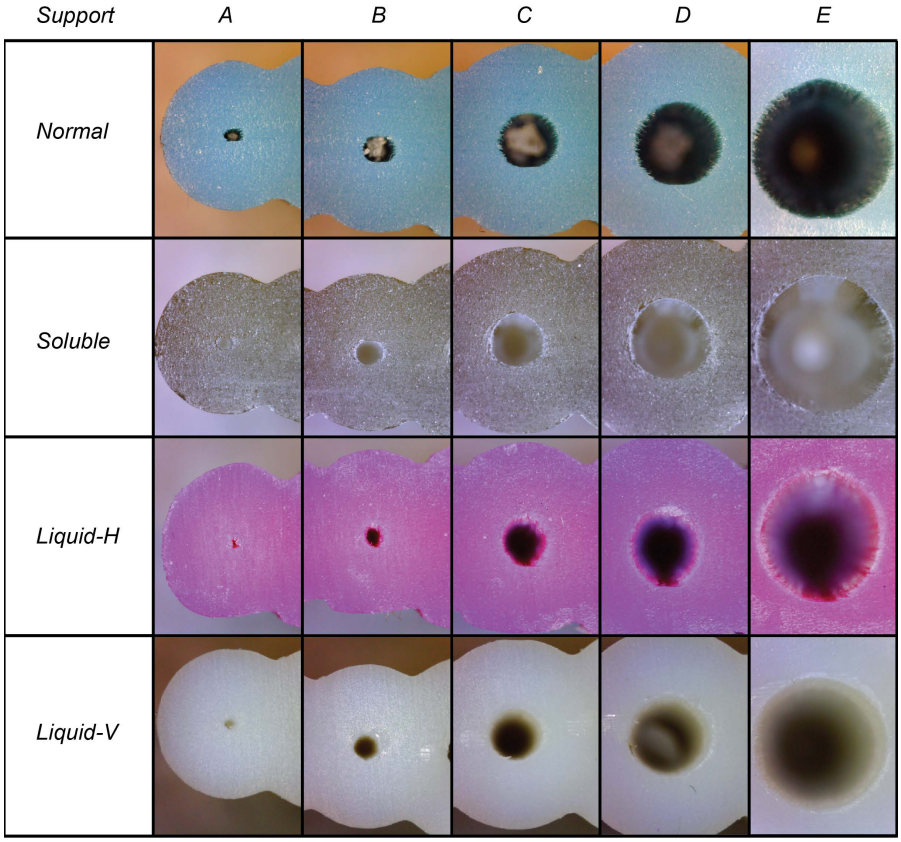

Optical images of diameters A-E from 1 of 3 test piece cross sections for each of the 4 conditions.

Figure 12: **Optical images of test piece cross-sections**. Representative optical images of test piece cross sections that were printed using the three support methods.

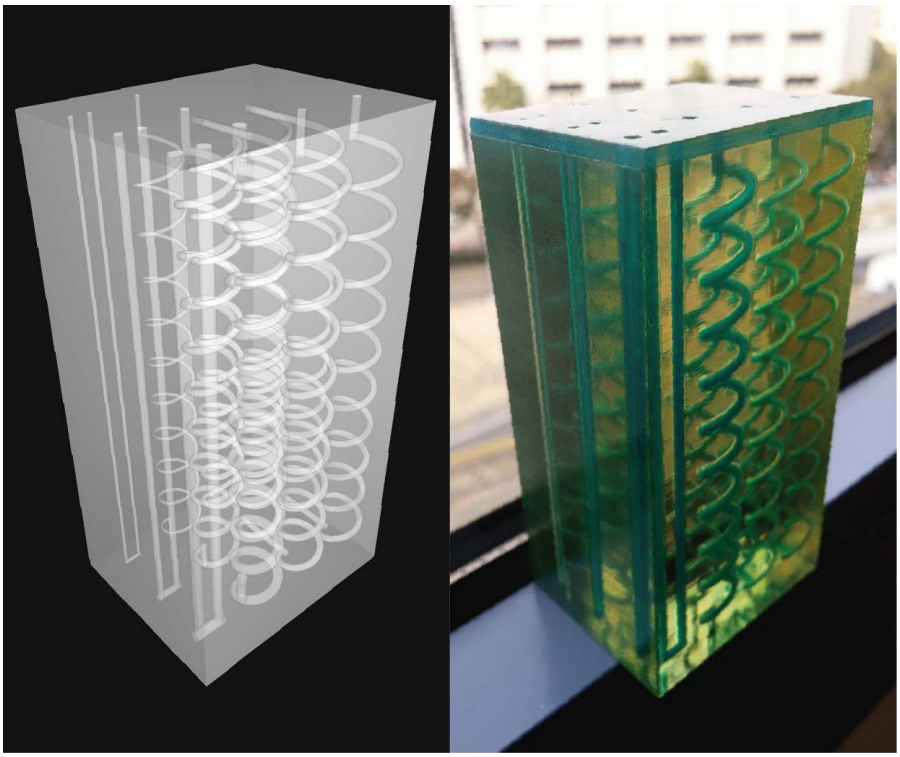

Figure 13: **Patch-scale support test.** Left: 3D geometry (80 by 33 by 40 mm), including a 15cm long 0.6 mm diameter channel and a 1.5m long 1.2 mm diameter channel. Right: Printed piece in VeroClear material and filled with green food coloring in all channels. The piece was printed with soluble support.

Figure 14: **Second small-scale support test.** Left: 3D test geometry. Center: Inner channel geometry (STL). Right: Testing model that was supported using liquid support. Image courtesy of Tal Ely & Daniel Divoksky of Stratasys.

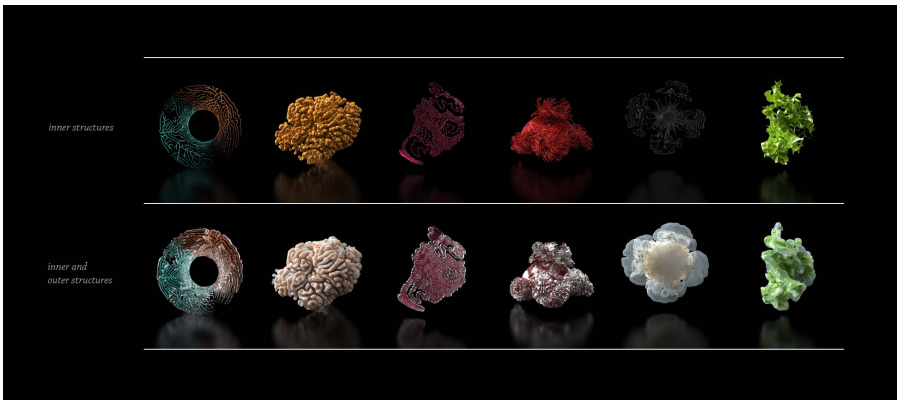

Figure 15: **A library of inner structure(top) and corresponding transparent outer structure (bottom).** The inner structures are colored. Renders courtesy of Christoph Bader and Dominik Kolb.

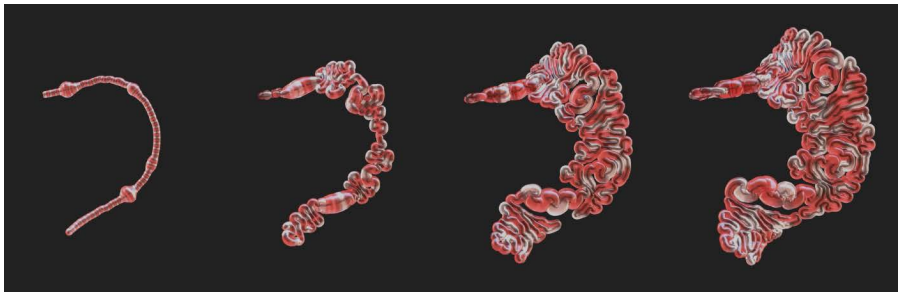

Figure 16: **Generative growth of fluid channels using line expansion.** 4 frames are pictured from one run of the algorithm. Renders courtesy of Christoph Bader and Dominik Kolb.

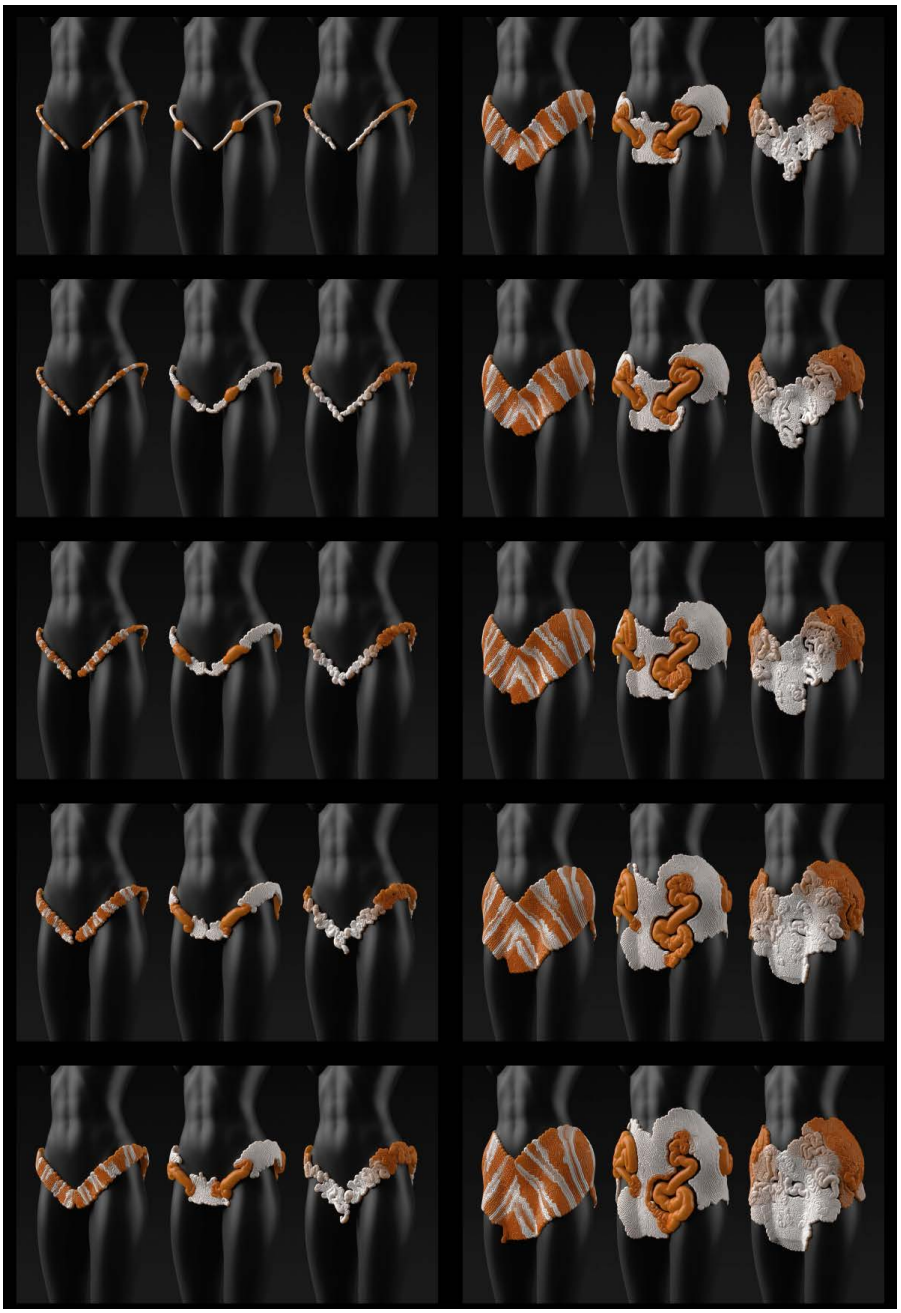

Figure 17: **A time lapse of three approaches growing geometry and material deposition.** White areas are translucent and orange areas are opaque. The left most approach (on each image) varies transparency by position in the length of the strand (cycling). The center approach varies transparency by the outer diameter of the tubing. In the right most approach, material properties are assigned by regions. Renders were created by Christopher Bader and Dominik Kolb.

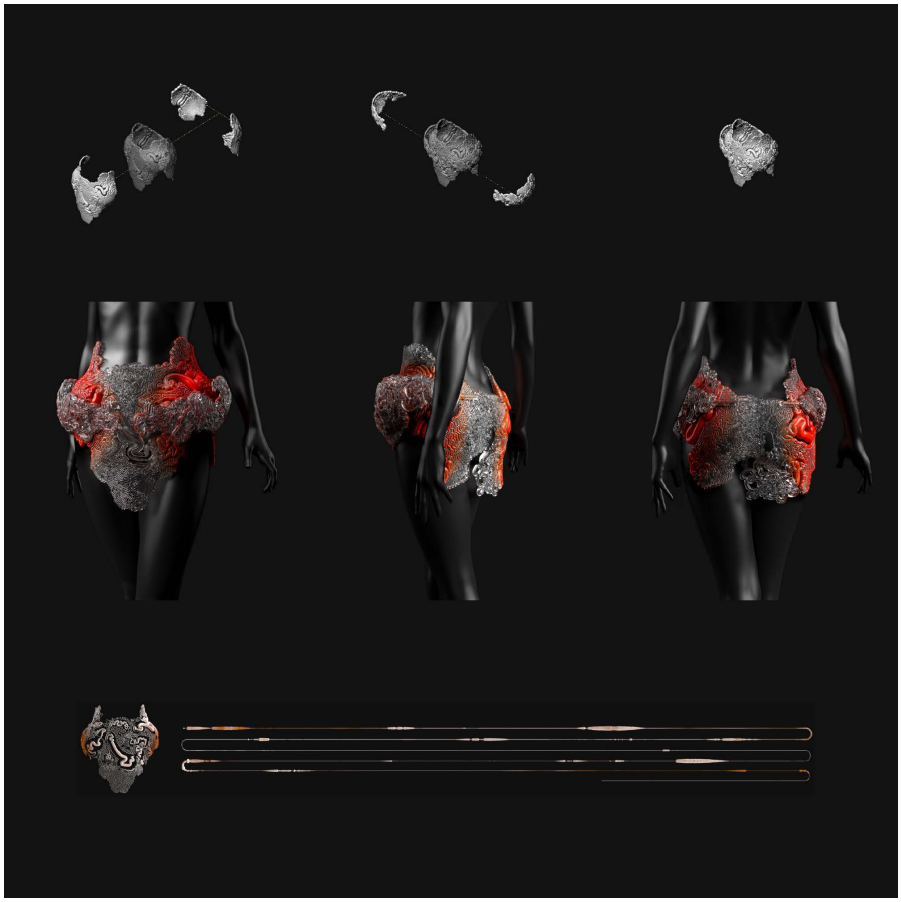

Figure 18: **The design of Mushtari**. 5 pieces form Mushtari (top): a front piece, two back pieces, and two mirrored outer pockets. Each piece contains a single long strand (bottom). The inner channel diameter of the strands ranges from 1 mm to 2.5 cm. The total length of the channels in Mushtari measures 58 meters. Two materials make up the piece: stiff red (Red) and stiff transparent (VeroClear) acylic polymers. The concentrations of these two materials vary throughout the piece, creating translucency gradients. Translucent areas enable photosynthetic activity and opaque areas are designed for *E. coli* activity. The author generated the assembly renders (top). Christoph Bader and Dominik Kolb generated the renders (center) and strand diagram (bottom).

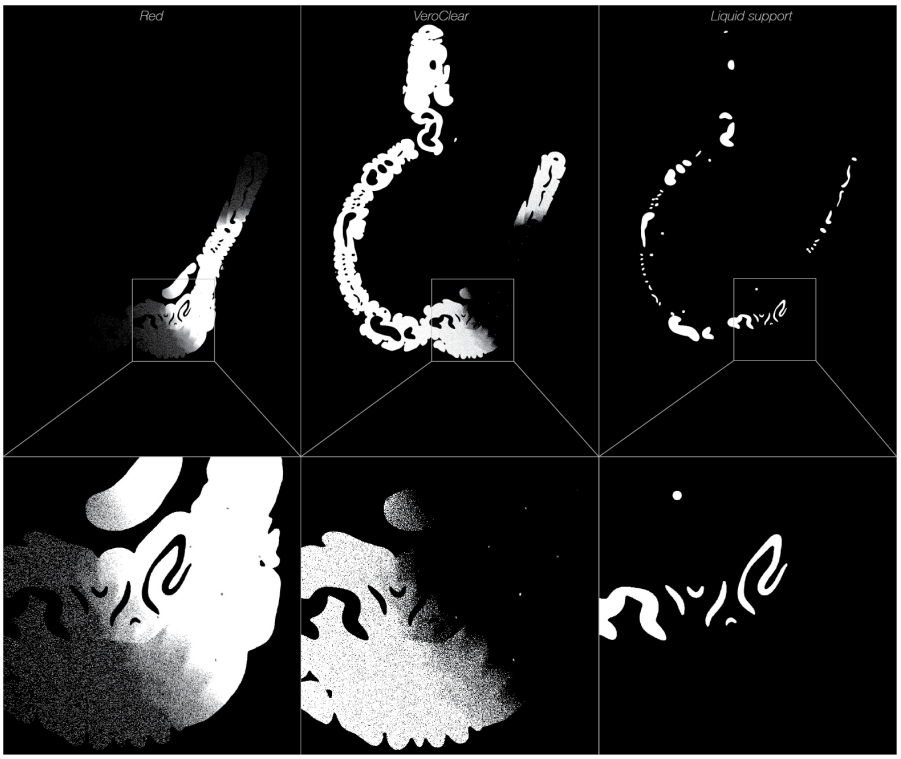

Figure 19: **One set of bitmap slices from Mushtari**. Each slice contains three bitmaps, corresponding to the two model materials and the liquid support. Inset images demonstrate a transparency gradient created by the VeroClear and Red materials (lower left and center). The inner channels were created using liquid support (lower right).

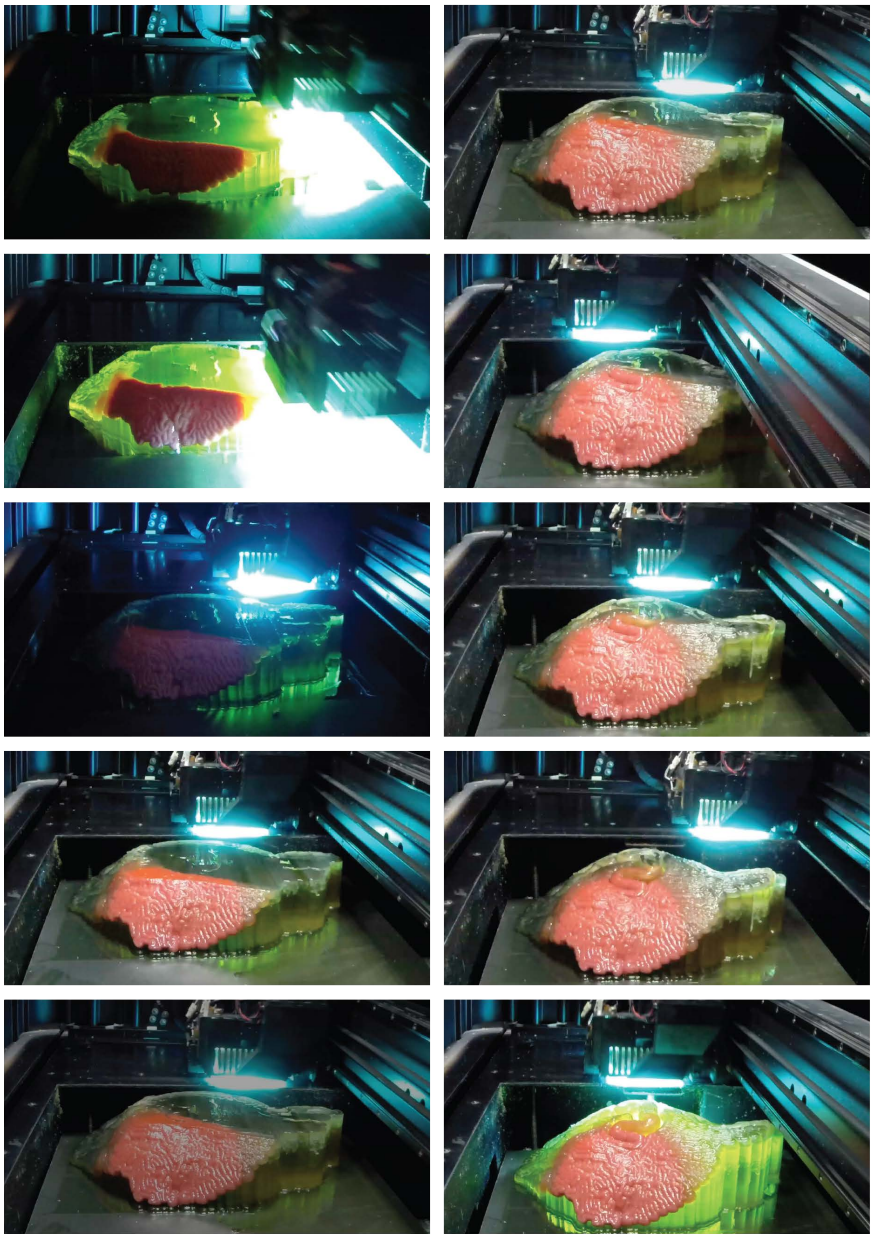

Figure 20: **3D printing Mushtari using liquid support**. The Connex3 printed the liquid support in the inner channels, allowing UV-curable model materials to be printed and polymerize in overhangs (for example, the top of a circular channel). After printing, the liquid support drained out of the piece, leaving cleared inner channels. The piece was printed by the Stratasys Objet R&D team. Photo credit: Boris Belocon.

Figure 21: **Printed, processed, assembled and unfilled pieces of Mushtari**. The transparency gradient between clear and opaque can be seen in the right images. Photo credit (left, top-right): Jonathan Williams. Photo credit (bottom-right): Will Patrick.

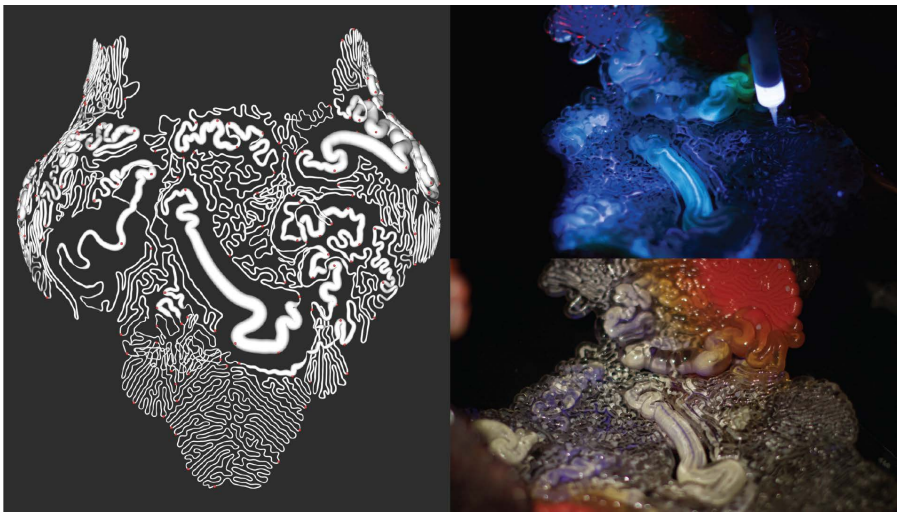

Figure 22: **Filling Mushtari**. Left: A rendering of the inner channel geometry. Red spheres signify inlet locations. Top-right: an image of filling the front piece with chemiluminescent fluid using a syringe in one of the inlet holes. Bottom-right: Mushtari while being filled (lights on). Photo credit: Steven Keating.

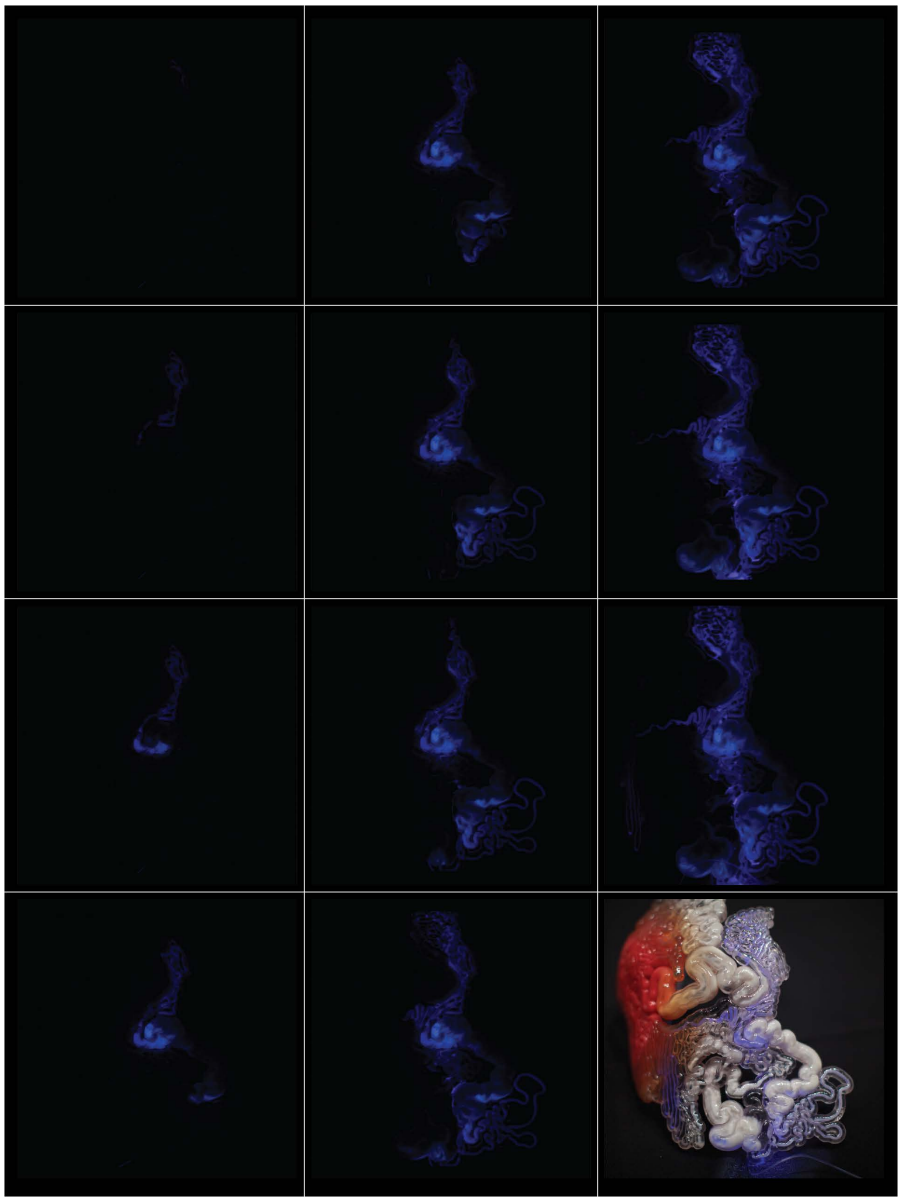

Figure 23: **Filling one of the back pieces**. We filled one of the left back pieces by hand with chemiluminescent fluid. We were unable to fill the piece any more than is pictured in the second to last image (right column, second from bottom). Photo credit: Jonathan Williams.

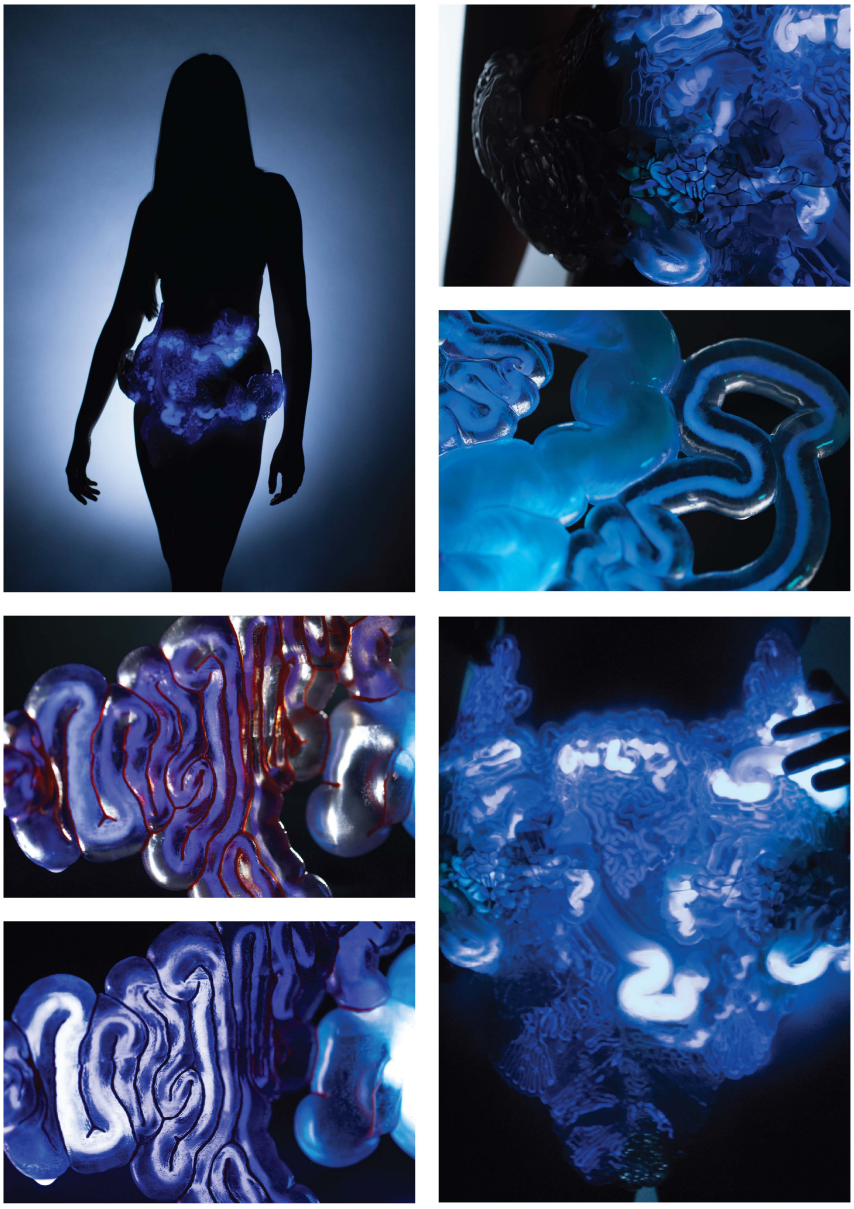

Figure 24: **Printed pieces filled with chemiluminescent fluid** We filled and assembled the front and pocket pieces (top left image). The chemiluminescent fluid glowed brightly in transparent areas and was not visible in opaque areas (top right). We filled nearly all of the channels in the assembled piece. One exception was the lower portion of the front piece (lower right image). We were not able to fill all of the channels in this region. Photo credit: Jonathan Williams and Steven Keating.

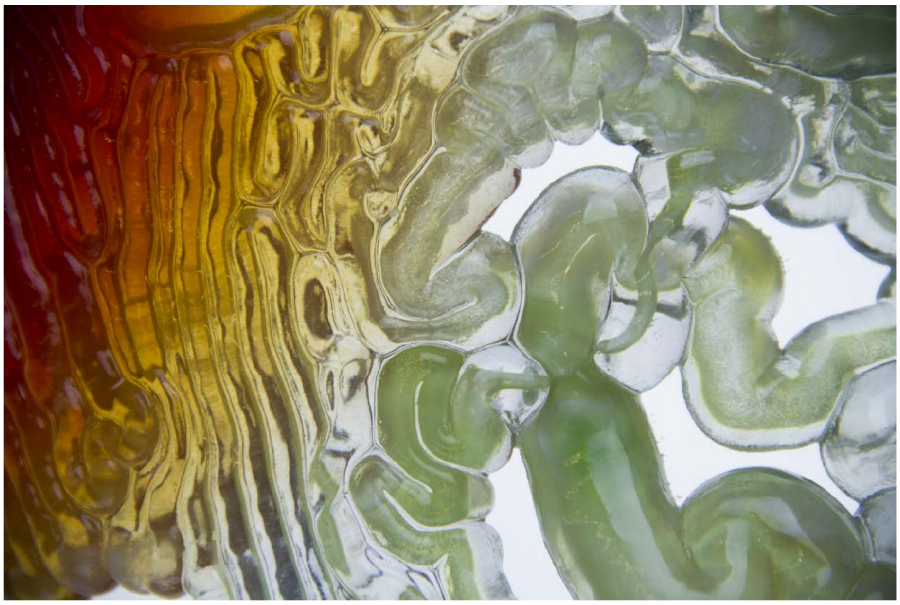

Figure 25: **Cyanobacteria in one of the back pieces**. Photo credit: Will Patrick.

9 DISCUSSION

This project accomplished three goals. We:

1. Developed computational approaches for generating product-scale fluidics within a multi-material wearable
2. Investigated and characterize support methods for creating product-scale fluidics
3. Tested the compatibility of the photopolymer 3D printed materials with culturing *S. elongatus* and *E. coli*.

9.1 COMPUTATIONAL GROWTH OF FLUIDIC CHANNELS

We developed an approach for growing fluidic networks within a product (Figure 15,16, and 17). The approach gave us top-down control over several important design elements, such as the geometry of the channels (inner and outer diameter, wall thickness) and material properties by region. However, the design process was not deterministic and the final form and material distribution emerged from the algorithm. We designed the wearable iteratively by changing initial parameters and observing new generated outputs. For example, Figure 17 shows three sets of initial parameters and their effect on material property distribution. The ability to alter initial parameters gave us some *top-down* design control. For example, we assigned transparency by region to create seperate regions of photosynthesis and *E. coli* activity. However, the actual material composition and geometry were still created *bottom-up* by the algorithm.

There are opportunities to build on this computational approach to embed greater intelligence in the growth algorithms. First, the model could incorporate functional optimization. For example, the model could optimize for maximize incident light exposure. Previous work has used L-systems to generate root systems. These models generated roots based on a distribution of nutrient concentration in the soil [60]. A similar approach could be applied to the line expansion model to respond to a light path diagram. Second, computational fluid dynamics (CFD) analysis could be incorporated into the algorithm. For example, we found in our experiments that we were unable to flow fluids more than 2-3 meters in the piece. The model could calculate pressure losses throughout the fluidic system and prevent geometries that create pressure losses greater than some threshold.

It is worth noting that this is the first example of using algorithms to computational grow geometry for micro or millifluidics based on an initial set of parameters. This method could be generally useful for other fluidics applications where local environmental conditions

should influence materiality or geometry of the fluidics. Generating geometries for printing tissue vasculature may be a particularly promising application for these computational methods.

9.2 FLUIDICS FABRICATION USING LIQUID AND SOLUBLE SUPPORT

The fluidics printed within Mushtari present advances over existing 3D printed fluidics. First, Mushtari contains 3D printed, multi-material fluidics. All published 3D printed fluidics to date have been printed using a single, bulk material. Members of the Oxman lab at MIT previously created multi-material proportional valves using the Connex500 printer [51]. However, the valves were printed using gel support, which limited geometries to small, straight channels. With soluble and liquid support, the Connex3 or Connex500 could print these valves within larger fluidic systems. Mushtari also features material property gradients using voxel-based bitmap printing. Stiffness, transparency and color gradients could be used to create new functional parts within fluidic systems. The fluidic system within Mushtari is also larger scale than any published 3D printed fluidic system. The liquid and soluble support methods enable the Connex printers to fabricate fluidics directly within larger products.

9.3 PRELIMINARY BIOLOGICAL COMPATIBILITY TESTING

Preliminary results demonstrated that the VeroClear material is compatible with culturing *E. coli*. The photopolymer material could be used to fabricate culture reactors for *E. coli*. Further testing is required to fully characterize the material compatibility with culturing *S. elongatus* and a coculture of the organisms. Needed experiments include:

1. Repeating the *E. coli* experiment for a period of two doubling times, the standard for OD600 *E. coli* growth characterization.
2. Growing *S. elongatus* in a container of VeroClear and standard polypropylene, controlling for light radiance.
3. Culturing *S. elongatus* and *E. coli* together in a VeroClear container and observing growth over time of both using fluorescence activated cell sorting.

In future work, our team plans to investigate the efficacy of the material design — light and dark regions created using transparency gradients — for coculturing *S. elongatus* and *E. coli* flowing through the reactor. Generally, the initial results suggest that the Connex3 could be used to rapidly prototype 3D culture reactors for E. coli and potentially other microorganisms.

9.4 CONCLUSIONS

The design approach pushed us to think about how engineered microorganisms could be incorporated into a wearable. Our work initially focused on investigating how material property gradients and geometry could affect bacterial activity. We then focused on how microorganisms could be contained using fluidic networks and developed new 3D printing support methods to enable the fabrication of wearable-scale 3D fluidics. We developed generative approaches to grow the geometry and material properties of the embedded fluidics. Finally, we designed, printed and tested a wearable, visualized the channels with chemiluminescent fluid and found initial evidence of compatibility between the wearable material and *E. coli*.

The fields of *Synthetic Biology* and 3D printing are both quickly developing. With Mushtari, we explored the intersection of these two fields and their application to product design. We designed fluidic wearables to mediate the function of two synthetic microorganisms and fabricated the design using multi material 3D printing. This project is both speculative and technical. We designed possible relationships between us, products, and synthetic microorganisms and we developed novel technical approaches: (1) computational generation of fluidic networks, (2) liquid and soluble support methods for printing multimaterial, wearable-scale fluidics, and (3) 3D printing bacterial reactors. The project advances the state of the art in all of these areas.

10

CONCLUDING THOUGHTS

10.1 LOOKING BACK: DESIGNING FLUIDICS TO INCORPORATE SYNTHETIC BIOLOGY IN PRODUCT DESIGN

My research at MIT began with a question. How can designers use synthetic biology in design? Particularly, I was interested in bringing biological capabilities — regeneration, self-assembly, photosynthesis, sensing — into the design of products. My attention focused on engineered microorganisms given their ubiquity in synthetic biology and industrial biotechnology and wondered how they could be incorporated into products. I initially probed the question as an engineer by investigating how to contain and control microbial cultures in 3D printed channels. The research led me to develop research relationships with several different labs at MIT and Harvard and collaborate with industrial partners. We made tremendous progress. We characterized three methods of 3D printing fluidics — desktop stereolithography printing, on-demand printing using Shapeways, and wearable-scale, multimaterial printing on the Connex3. We tested the compatibility of 3D printing materials with DNA assembly biochemistry and culturing microorganisms. And, we created computational approaches for generating fluidic networks. I hope these novel efforts push the field of 3D printed fluidics in new research directions.

As I grew at MIT, I departed from solely developing and characterizing methods and developing new technologies. My motivations changed from proving to provoking. With Mushtari, I probed the question, how should designers use synthetic biology in design? Endosymbiosis and particularly the giant tridacnid clam showed me the elegance of evolved relationships between microorganisms and organisms they inhabit. I became curious if we could design these relationships. With Mushtari, we attempted to do so by designing a relationship between the two bacteria and the transparency of a printed wearable. We thought of these two systems, the biological and the polymer material, as a part of a Material Ecology and aimed to design a synthetic symbiosis between the materiality of the biology — the DNA, RNA and proteins of the organisms — and the 3D printed wearable — gradients of transparency.

Mushtari never contained a coculture of cyanobacteria and *E. coli* and we do not know if the transparency gradient within the wearable would have influenced the activity of the contained cyanobacteria and *E. coli*. As an engineer, I am eager to continue the basic research associated with this project and determine the efficacy of our approach. As a designer, I am satisfied that these technical challenges didn't stop us from articulating our vision. We designed Mushtari as a speculative design project and one that would open new possibilities for designers and engineers operating at the intersection of 3D printing,

synthetic biology and microfluidics. We will have succeeded if the project sparks new ideas and questions about why and how synthetic biology should be used in the design of our products.

10.2 PRIMARY CONTRIBUTIONS

This thesis makes technical contributions to the fields of 3D printing and fluidics and design contributions to fashion, wearable, and biological based design.

1. Characterized the Form1+, Shapeways-Frosted Ultra Detail and Connex Polyjet 3D printing methods for creating micro and millifluidics.
2. Designed, fabricated, and open-sourced a 3D printed syringe pump.
3. Demonstrated compatibility of the Form1+ and Shapeways materials with Golden Gate biochemistry
4. Investigated and characterized soluble and liquid support techniques for creating micro and millifluidics using the Connex3 multimaterial printer.
5. Demonstrated multimaterial micro and millifluidic systems for the first time.
6. Designed, fabricated and tested the largest 3D printed fluidic system to date, which featured 58 meters of channels ranging from 1 to 20 mm in diameter.
7. Demonstrated compatibility of the Objet VeroClear material for culturing *E. coli*.
8. Used growth algorithms to generate micro and millifluidics. This had never been done before.
9. Conceptualized *Synthetic Symbiosis* as a design approach for embedding synthetic microorganisms in products.
10. Designed a method to use translucency gradients within a multimaterial wearable to control the activity of enclosed bacterial cultures.

10.3 FUTURE WORK: AREAS FOR EXPLORATION

I end this project with many new ideas, questions, and areas for exploration. Here are a few thoughts about where this research could go.

10.3.1 *From containers to valves: printing fluidics with functional parts*

The 3D printed devices in this thesis are all fairly simple in their function: containing fluids, mixing two fluid species, and differentially exposing fluids to light using a transparency gradient. Many microfluidic systems use proportional valves to achieve more complicated functions, including routing liquids, multiplexing reactions, and performing multiple reactions sequentially in a single reactor[85]. State of the art microfluidics integrate thousands of these valves into a single device to perform parallelized, multi-step reactions. These systems are typically manufactured using molded two-dimensional layers of PDMS stacked in layers.

Multimaterial 3D printing may enable the manufacturing of these systems in a single step. We've built a simple, multimaterial proportional valve using the Connex500 printer[51]. The valve is made of two stiff, transparent channels that are separated by a thin membrane of flexible material. When the flow channel is pressurized with air, the membrane deforms and slows or stops flow in the other channel. At the time that we were printing these valves, we were using the standard gel support on the Connex machine. All of the internal support was removed either by water blasting or by using a small metal rod. With soluble or liquid support, these valves may be able to be printed within larger microfluidic devices. This may enable on step printing of microfluidics with integrated valves. We initially wanted to integrate these valves into Mushtari in order to create a peristaltic pump to circulate the bacterial cultures through the channels.

10.3.2 *Biological-digital interoperability*

I am interested in how to design interoperability between biological and digital systems. How can digital systems communicate to engineered biological systems and vice versa? How could a software system communicate to a bacterial culture to "turn on or off"? One potential answer for information input is optogenetics, a field that studies gene regulatory elements that can be switched on or off when exposed to light. Several photoreceptors that change confirmation in the presence of light, including plant phytochromes and channel rhodopsin, have been expressed and characterized in bacteria, yeast and mammals to regulate gene expression[41, 67]. Optogenetic control could be used to trigger expression of an output of interest, for example the production of scent, drug or food, within a product.

10.3.3 *Biological-Human Interfaces*

What is the point of communication between humans and microorganisms? What might interfaces that control biological systems look and feel like? How would a user operate a product that includes cell cultures or other biological components? All of these questions beg exploration. While working on *Mushtari*, I was curious how a user

might refill needed media into the product or introduce a new designed organism into the coculture. I imagined using a station — a turbidostat that would contain fresh media and cell cultures — to *charge* the wearable. Perhaps some day soon, I will.

Part III

APPENDIX

A

SUPPLEMENTARY FIGURES FOR PART I

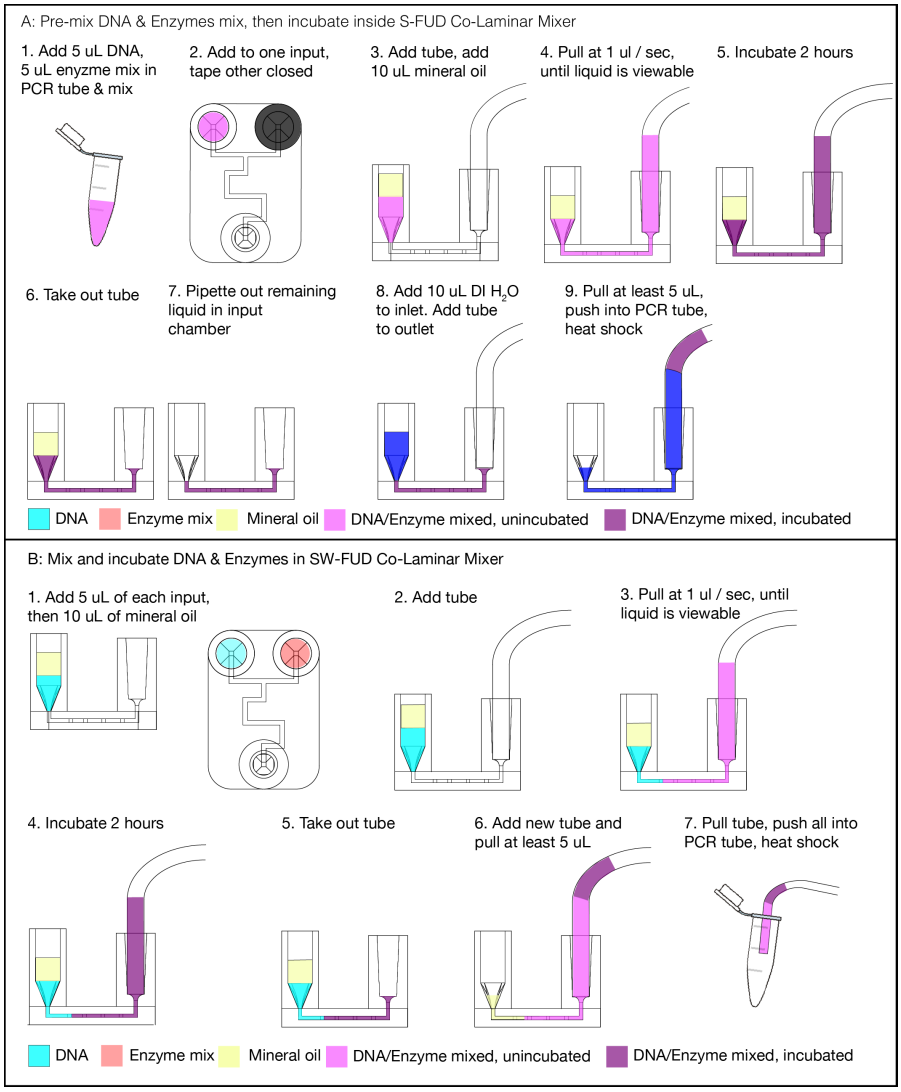

Figure 26: **Visual protocol for running pre-mix and on chip mix for the SW-FUD device.**

		Form 1+		SW-FUD	
	Expected (mm)	D (mm)	Sta. Dev. (mm)	Side (mm)	Sta. Dev. (mm)
C1	1.9	2.01	0.05	1.88	0.02
C2	1.7	1.73	0.05	1.62	0.03
C3	1.5	1.51	0.02	1.45	0.02
C4	1.3	1.29	0.03	1.23	0.06
C5	1.1	1.11	0.03	1.02	0.04
C6	0.9	0.86	0.03	0.87	0.01
C7	0.7	0.71*	0.02	0.63	0.01
C8	0.5	0.46*	0.03	0.43	0.03
C9	0.3	CNM*		CNM	
C10	0.1	CNM*		CNM*	
S1	1.15	1.22	0.05	1.09	0.03
S2	1.05	1.09	0.09	0.98	0.03
S3	0.95	0.97	0.03	0.90	0.01
S4	0.85	0.87	0.01	0.82	0.03
S5	0.75	0.81	0.02	0.70	0.03
S6	0.65	0.69	0.04	0.56	0.02
S7	0.55	0.58*	0.06	0.50	0.02
S8	0.45	CNM*		0.48	0.01
S9	0.35	CNM*		0.38	0.01
S10	0.25	CNM*		0.27	0.02
S11	0.15	CNM*		CNM*	
S12	0.05	CNM*		CNM*	

Table 4: **Dimensions for the circular (C1-10) and square (S1-12) channels of the Form 1+ and SW-FUD resolution test pieces**. The circular dimension was the diameter and was measured 3 times for each circle. The square dimension was the side length and was measured 6 total times per square (3 in each direction). CNM = could not be measured. * = channels that could not be cleared with liquid. All measurements were taken using ImageJ.

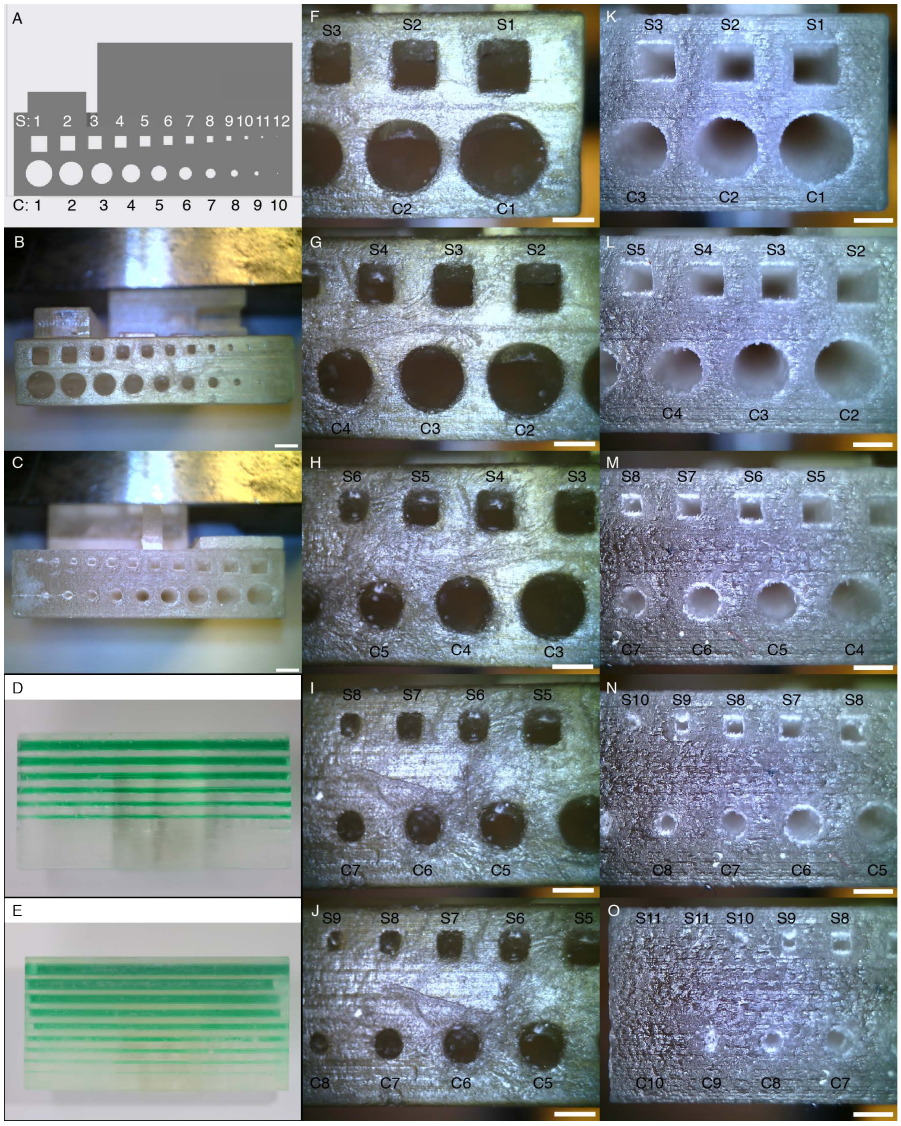

Figure 27: **Form 1+ and SW-FUD resolution test piece: design, microscopy and dimensions**. (**A**) Expected dimensions of the channels (S1-12 & C1-10) are in Appendix A, Table 4. Side views of printed Form 1+ (**B**) and SW-FUD (**C**) resolution test pieces. Visualization of cleared circular fluid channels in the Form 1+ (**D**) and SW-FUD (**E**) resolution test pieces. Close-in images of a resolution test piece printed on the Form 1+ (**F-J**) and SW-FUD (**K-O**). Scale bar: 1 mm. All images except **D** & **E** were taken using a SuperEyes B008 USB Microscope (Shenzhen D&F Co, Ltd, Shenzhen, China). **D** & **E** were taken using a Canon EOS 7D Digital SLR camera. Measurements of the channel dimension (diameter for the circle & side length for the square channel) can be found in Appendix A, Table 4.

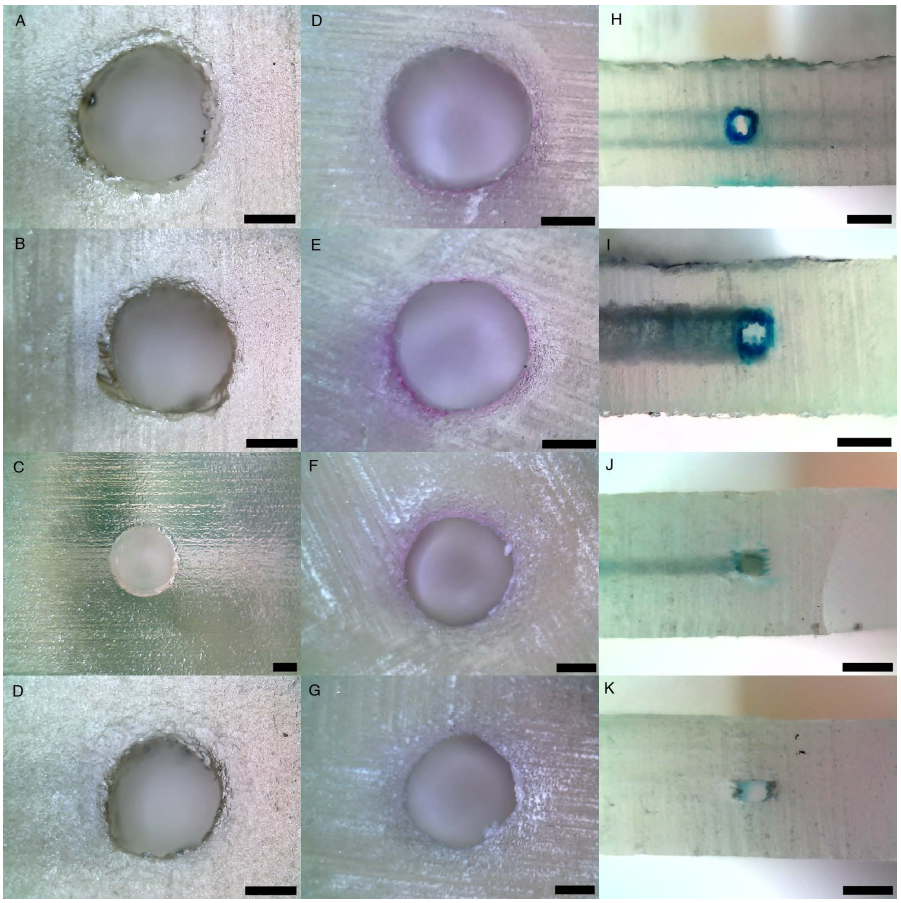

Figure 28: **Cross sections & channel dimensions of fluidic devices**. Cross-sections were taken of the Form1+ Co-Laminar Mixer devices (**A-D**), Form 1+ 3D Micromixer devices (**D-H**), and SW-FUD Co-Laminar Mixer device (**I-L**). Scale bar: 0.5 mm. All images were taken using a SuperEyes B008 USB Microscope (Shenzhen D&F Co, Ltd, Shenzhen, China). Measurements of the channel dimension (diameter for the circle & side length for the square channel) can be found in Appendix A, Table 5.

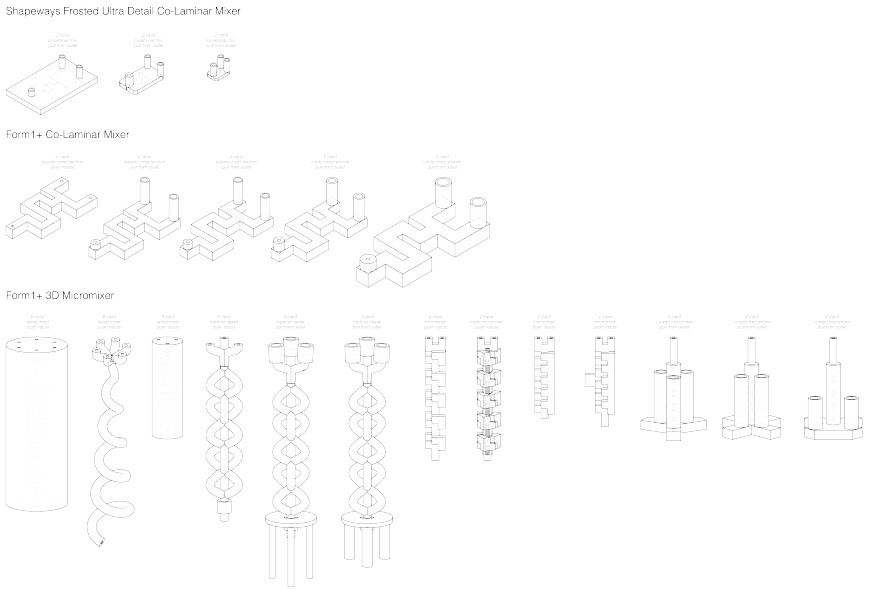

Figure 29: **Design iterations of each fluidic device**. SW-FUD Co-Laminar Mixer (Top), Form 1+ Co-Laminar Mixer (Middle), and Form 1+ 3D Micromixer (Bottom). The rightmost iteration of each design were used for DNA assembly. All CAD designs were produced using Solidworks.

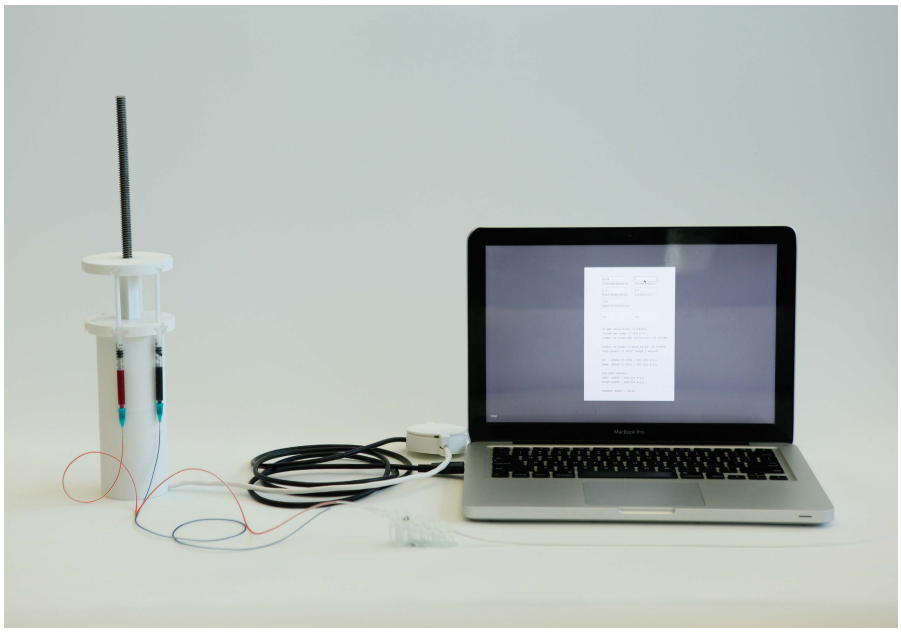

Figure 30: **Operation of the syringe pump**. A bespoke syringe pump and user interface designed and fabricated for this experiment. The syringe pump was used to pull the two inputs through the device at 1 and 5 micro liters per second. The syringe pump is composed of several parts (Appendix A, Figure 32, including 3D printed mechanical pieces, a custom designed and fabricated circuit board (Appendix A, Figure 34), and a software user interface (Appendix A, Figure 35). The CAD designs and software for the syringe pump have been made openly available. The total cost of the pump was $56.33 (Appendix A, Table 6) and the 3D printed components can each be printed in less than 3 hours. Photo credit: Taylor Levy and Che-Wei Wang

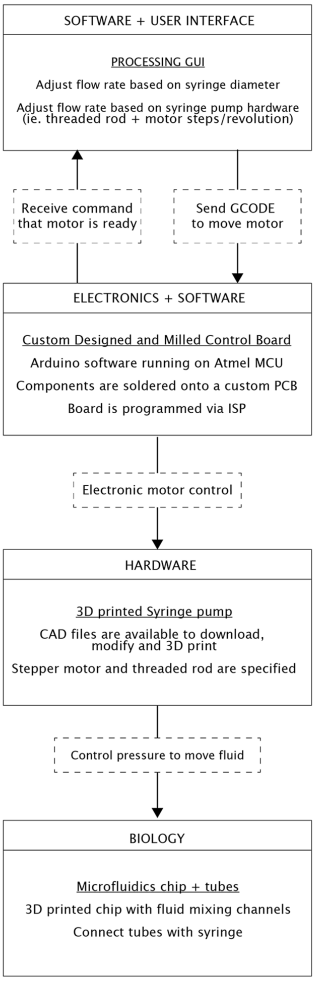

Figure 31: **Operation of the syringe pump**. From Top to Bottom: A user interface (UI) (Appendix A, Figure 34) was designed in Processing and enabled the user to control the syringe pump. Depending on the desired pumping direction, flow rate & volume and the hardware settings (syringe ID, thread dimension, steps per revolution of the motor), the UI sent a G CODE command to the electronics firmware with the desired motor rotation direction, speed and number of steps. The circuit board (Appendix A, Figure 33) received the G Code command and translated it into electronic motor controls that moved the stepper a number of steps at the desired speed and in the desired direction. Each motor step moved the syringe a small distance, pushing a small amount of fluid in or out of the dispensing needle top. Figure created by Taylor Levy.

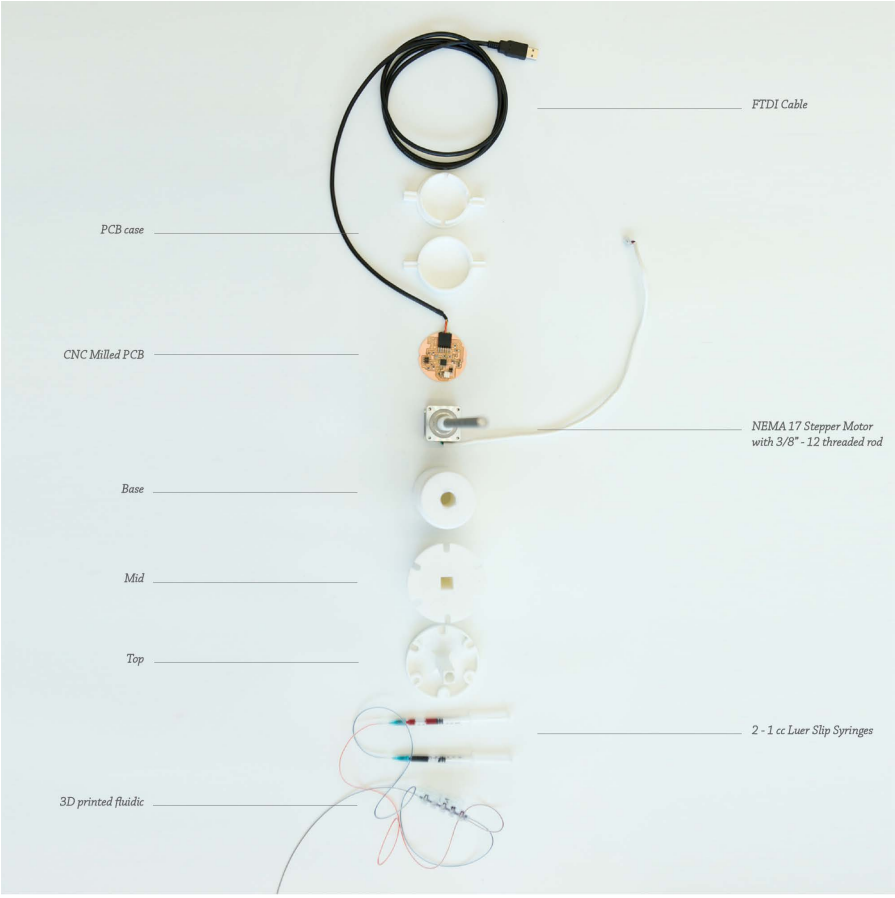

Figure 32: **Syringe pump components**. From top to bottom: USB-FTDI cable; 3D printed circuit board case top and bottom (optional); Milled electronic control board; Bi-polar stepper motor, threaded rod & 3D printed adapter; 3D printed base; 3D printed mid-section; 3D printed top; 2-1cc syringes with 23 gauge luer lock 1/2 inch dispensing needles connected to 3D printed fluidic device using 0.060 in OD Tygon Microbore tubing. Photo credit: Che-Wei Wang & Taylor Levy

Figure 33: **Modular 3D printed components of the syringe pump**. (**A**) The base of the pump which includes the Nema 17 stepper motor, a 3D printed connector, and the 3D printed base. The motor press fits into the 3D printed base. (**B**) The components for a 1cc syringe pump, the pump used to run the gene assemblies. The Mid piece, above the base components, screws into the base. The Top piece is threaded and is moved vertically by the threaded rod. (**C**) The Mid & Top pieces were modified to accommodate 10cc syringes. (**D**) The Mid & Top pieces were modified to accommodate 100cc syringes. Photo credit (top images): Che-Wei Wang and Taylor Levy

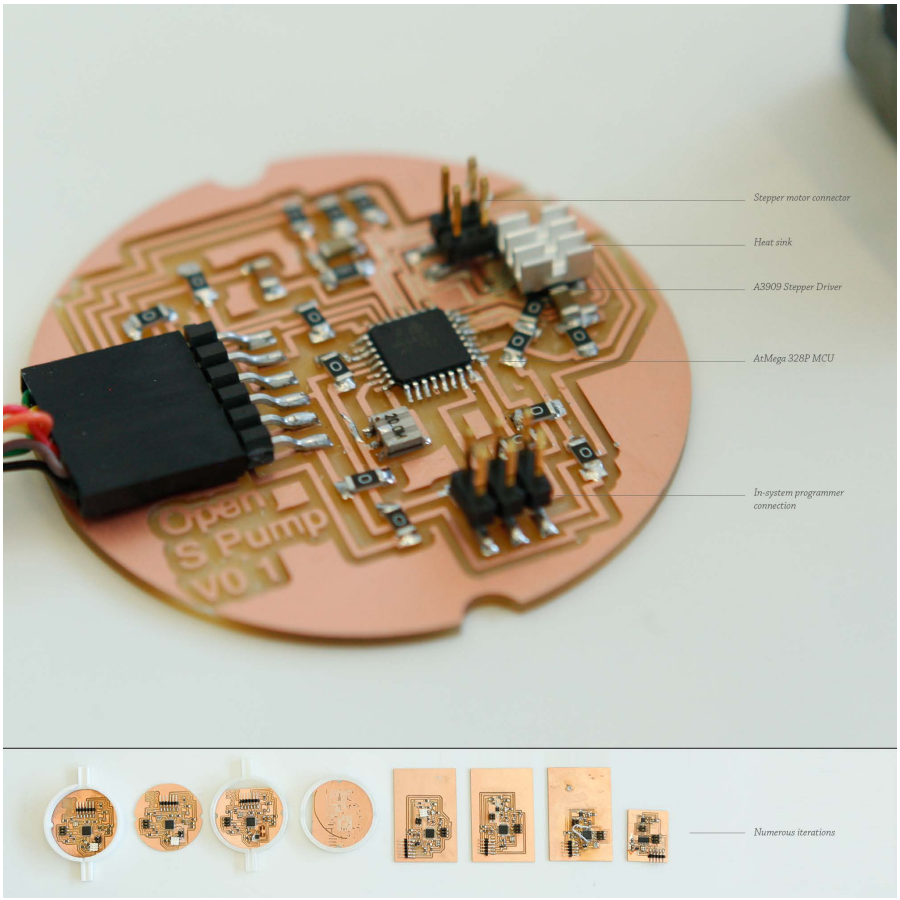

Figure 34: **Syringe pump control board**. The circuit board traces were milled using a Roland Modela MDX2-20 CNC mill. Serial commands from the Processing UI and 5V DC were transmitted to the circuit board via FTDI USB TTL Serial. The board used a ATMega 328P (Atmel, San Jose, California) microcontroller that was programmed via an AVRISP. The ATMega 328P was bootloaded with Arduino and used the AccelStepper library to send commands to an Allegro A3909 Dual Stepping Motor driver. A heat sink was attached to the top of the A3909 driver. Photo credit: Che-Wei Wang & Taylor Levy

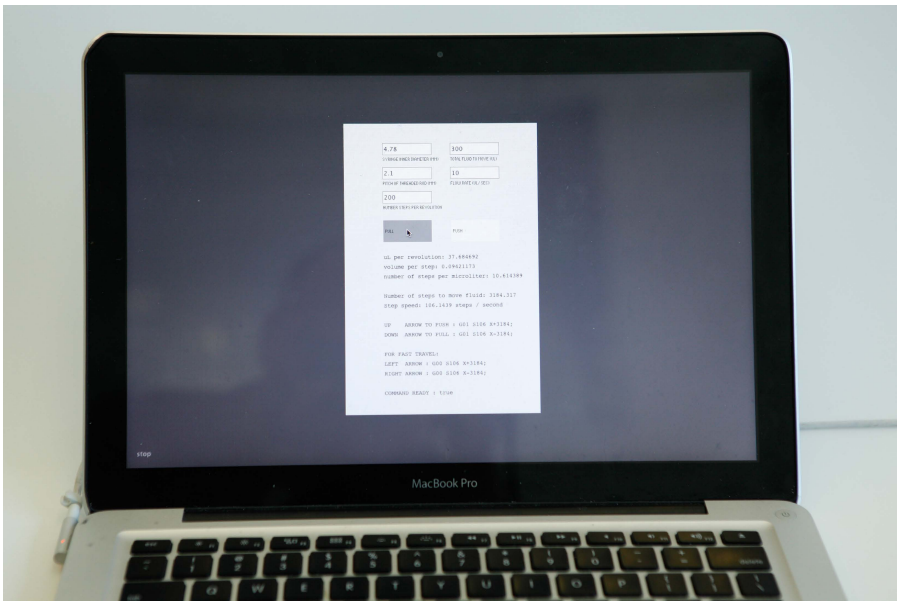

Figure 35: **Syringe pump user interface**. The interface was written using Processing and communicated to the circuit board (Appendix A, Figure 33) via USB TTL Serial commands. In the interface, the user specified parameters of the syringe pump: thread size, steps per revolution of the motor, and the inner diameter of the syringe. These values were used to compute a volume moved per step. To control the pump, the user inputted a desired flow rate & flow volume and then clicked "Pull" or "Push" to move the pump accordingly. Photo credit: Che-Wei Wang & Taylor Levy

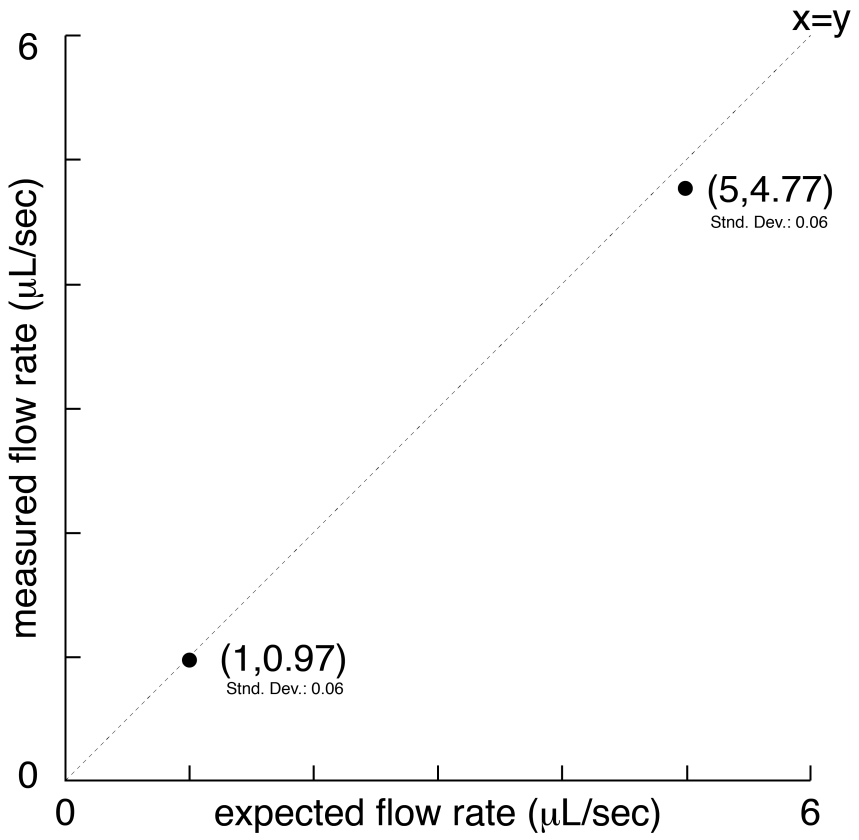

Figure 36: **Measured versus expected flow rate of the syringe pump.** The pump was characterized at the two flow rates used in the experiments: 1 microliters and 5 microliters per second. The measured flow rate at 1 microliters per second was 0.97 microliters per second with a standard deviation of 0.06 microliters per second. The measured flow rate at 5 microliters/sec was 4.77 micro liters per second with a standard deviation of 0.06 microliters per second. Error bars were not plotted because they could not be seen. The dotted line is x=y, the expected value for these measurements.

Manufacturing	D (mm)	Sta. Dev. (mm)
Form1+		
Expected	1.5	
A	1.31	0.01
B	1.26	0.04
C	1.40	0.02
D	1.14	0.02
E	1.37	0.01
F	1.28	0.02
G	1.36	0.04
H	1.40	0.06
Total	1.30	0.09
SW-FUD		
Expected	0.3	
I	0.19	0.01
J	0.20	0.01
K	0.23	0.03
L	0.26	0.04
Total	0.22	0.03

Table 5: **Dimensions of SW-FUD and Form 1+ cross sections**. For the circular channels (FL1+, CL1-4 & FL1+, MM1-4), D is the circular diameter. Each diameter was measured 3 times. For the square cannels (SW1-4), D is the square side length. Each square side length was measured 6 times (3 in each direction). All measurements were taken using ImageJ.

3D Printed Parts	
Syringe Pump Mid-section	$3.19
Syringe Pump Top	$1.19
Syringe Pump Base	$5.06
Syringe Pump threaded rod adapter	$0.67
	$10.11
Mechanical parts	
1cc BD Luer Lock Syringe - 2	$0.77
23 gauge 1/2" dispensing needle - 1	$0.18
Tygon Microbore Tubing, 0.060" OD - 6"	$0.41
Bi-polar Nema 17 stepper motor	$14.00
6" Threaded rod - 3/8" - 12	$3.34
	$18.70
Electronics	
PCB board	$1.00
A3909 Dual Stepper Driver	$1.66
ATMega328P	$3.61
FTDI cable	$17.95
0 Ohm - 15	$0.07
10K SMD resistor	$0.01
1 uF ceramic SMD capacitor	$0.07
0.1 uF ceramic SMD capacitor	$0.12
10 uF ceramic SMD capacitor	$0.19
20 Mhz resonator	$0.43
FTDI header	$0.55
2x2 Bergstik pin header	$0.65
2x3 pin header	$0.72
Aluminum heat sink - 1	$0.03
2x2 IDC ribbon cable connector	$0.48
	$27.52
Total:	$56.33

Table 6: **Syringe pump bill of materials**.

B

SUPPLEMENTARY FIGURES FOR PART II

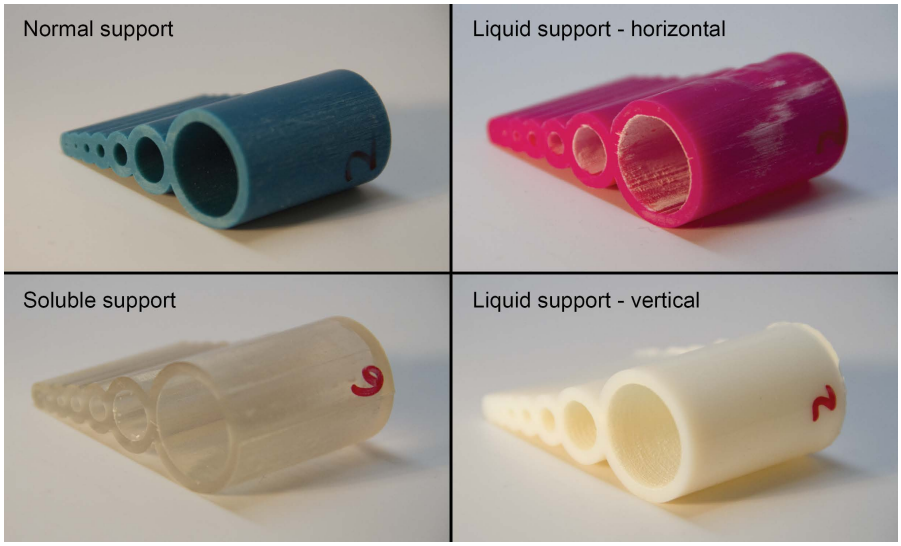

Figure 37: **Macroscopic optical images of test pieces printed to evaluate support methods.**

BIBLIOGRAPHY

[1] Spark | Ember 3D Printer, 2014. URL http://spark.autodesk.com/ember#about-explorer.

[2] OpenPCR, 2014. URL http://openpcr.org/.

[3] Shapeways, 2014. URL http://www.shapeways.com.

[4] Objet Connex 3D Printers, 2015. URL http://www.stratasys.com/3d-printers/design-series/connex-systems.

[5] Kudo3D, 2015. URL http://www.kudo3d.com/.

[6] The Micro: The First Truly Consumer 3D Printer by M3D LLC, 2015. URL https://www.kickstarter.com/projects/m3d/the-micro-the-first-truly-consumer-3d-printer.

[7] MiiCraft, 2015. URL http://www.miicraft.com/.

[8] ProJet® 1200 | www.3dsystems.com, 2015. URL http://www.3dsystems.com/es/projet1200.

[9] Formlabs, 2015. URL www.formlabs.com.

[10] R. M M Abed, S. Dobretsov, and K. Sudesh. Applications of cyanobacteria in biotechnology. *Journal of Applied Microbiology*, 106(1):1–12, 2009. ISSN 13645072. doi: 10.1111/j.1365-2672.2008.03918.x.

[11] John Aikens and Robert J Turner. Transgenic photosynthetic microorganisms and photobioreactor for disaccharide production., 2012.

[12] Kari B. Anderson, Sarah Y. Lockwood, R. Scott Martin, and Dana M. Spence. A 3D printed fluidic device that enables integrated features. *Analytical Chemistry*, 85(12):5622–5626, 2013.

[13] S. Andreas Angermayr, Klaas J. Hellingwerf, Peter Lindblad, and M. Joost Teixeira de. Energy biotechnology with cyanobacteria. *Current Opinion in Biotechnology*, 20(3):257–263, 2009. ISSN 09581669. doi: 10.1016/j.copbio.2009.05.011.

[14] Gerald C Anzalone, Alexandra G Glover, and Joshua M Pearce. Open-source colorimeter. *Sensors (Basel, Switzerland)*, 13(4):5338–46, January 2013. ISSN 1424-8220. doi: 10.3390/s130405338. URL http://www.pubmedcentral.nih.gov/articlerender.fcgi?artid=3673140&tool=pmcentrez&rendertype=abstract.

[15] Anthony K Au, Wonjae Lee, and Albert Folch. Mail-order microfluidics: evaluation of stereolithography for the production of microfluidic devices. *Lab on a chip*, 14(7):1294–301, April 2014. ISSN 1473-0189. doi: 10.1039/c3lc51360b. URL http://www.ncbi.nlm.nih.gov/pubmed/24510161.

[16] Anthony K Au, Nirveek Bhattacharjee, Lisa F Horowitz, Tim C Chang, and Albert Folch. 3D-printed microfluidic automation. *Lab on a chip*, 15(8):1934–1941, 2015. doi: 10.1039/c5lc00126a. 3D-Printed.

[17] Tom Baden, Andre Maia Chagas, Greg Gage, Timothy Marzullo, Lucia L. Prieto-Godino, and Thomas Euler. Open Labware: 3-D Printing Your Own Lab Equipment. *PLOS Biology*, 13(3): e1002086, 2015. ISSN 1545-7885. doi: 10.1371/journal.pbio.1002086. URL http://dx.plos.org/10.1371/journal.pbio.1002086.

[18] Johan S. Bakken, Thomas Borody, Lawrence J. Brandt, Joel V. Brill, Daniel C. Demarco, Marc Alaric Franzos, Colleen Kelly, Alexander Khoruts, Thomas Louie, Lawrence P. Martinelli, Thomas a. Moore, George Russell, and Christina Surawicz. Treating clostridium difficile infection with fecal microbiota transplantation. *Clinical Gastroenterology and Hepatology*, 9(12):1044–1049, 2011. ISSN 15423565. doi: 10.1016/j.cgh.2011.08.014. URL http://dx.doi.org/10.1016/j.cgh.2011.08.014.

[19] K. C. Bhargava, B. Thompson, and N. Malmstadt. Discrete elements for 3D microfluidics. *Proceedings of the National Academy of Sciences*, 111(42):15013–15018, September 2014. ISSN 0027-8424. doi: 10.1073/pnas.1414764111. URL http://www.pnas.org/cgi/doi/10.1073/pnas.1414764111.

[20] Daniel Camsund and Peter Lindblad. Engineered Transcriptional Systems for Cyanobacterial Biotechnology. *Frontiers in Bioengineering and Biotechnology*, 2(October):1–9, 2014. ISSN 2296-4185. doi: 10.3389/fbioe.2014.00040. URL http://journal.frontiersin.org/journal/10.3389/fbioe.2014.00040/full.

[21] Philippe Carriere. On a three-dimensional implementation of the baker's transformation. *Physics of Fluids*, 19 (11):118110, 2007. ISSN 10706631. doi: 10.1063/1.2804959. URL http://scitation.aip.org/content/aip/journal/pof2/19/11/10.1063/1.2804959.

[22] Tomas Cermak, Erin L Doyle, Michelle Christian, Li Wang, Yong Zhang, Clarice Schmidt, Joshua a Baller, Nikunj V Somia, Adam J Bogdanove, and Daniel F Voytas. Efficient design and assembly of custom TALEN and other TAL effector-based constructs for DNA targeting. *Nucleic acids research*, 39(12):e82, July 2011. ISSN 1362-4962. doi: 10.1093/nar/gkr218. URL http://www.pubmedcentral.nih.gov/articlerender.fcgi?artid=3130291&tool=pmcentrez&rendertype=abstract.

[23] Daniel Chaumont. Biotechnology of algal biomass production: a review of systems for outdoor mass culture, 1993. ISSN 0921-8971.

[24] Allen Y Chen, Zhengtao Deng, Amanda N Billings, Urartu O S Seker, Michelle Y Lu, Robert J Citorik, Bijan Zakeri, and Timothy K Lu. Synthesis and patterning of tunable multiscale materials with engineered cells. *Nature materials*, 13(5):515–23, May 2014. ISSN 1476-1122. doi: 10.1038/nmat3912. URL http://www.pubmedcentral.nih.gov/articlerender.fcgi?artid=4063449&tool=pmcentrez&rendertype=abstract.

[25] Chengpeng Chen, Yimeng Wang, Sarah Y Lockwood, and Dana M Spence. 3D-printed fluidic devices enable quantitative evaluation of blood components in modified storage solutions for use in transfusion medicine. *The Analyst*, 139(13):3219–26, July 2014. ISSN 1364-5528. doi: 10.1039/c3an02357e. URL http://www.ncbi.nlm.nih.gov/pubmed/24660218.

[26] Ying-Ja Chen, Peng Liu, Alec a K Nielsen, Jennifer a N Brophy, Kevin Clancy, Todd Peterson, and Christopher a Voigt. Characterization of 582 natural and synthetic terminators and quantification of their design constraints. *Nature methods*, 10(7):659–64, 2013. ISSN 1548-7105. doi: 10.1038/nmeth.2515. URL http://www.ncbi.nlm.nih.gov/pubmed/23727987.

[27] Allen a. Cheng and Timothy K. Lu. Synthetic Biology: An Emerging Engineering Discipline. *Annual Review of Biomedical Engineering*, 14(1):155–178, August 2012. ISSN 1523-9829. doi: 10.1146/annurev-bioeng-071811-150118.

[28] Yusuf Chisti. Constraints to commercialization of algal fuels, 2013. ISSN 01681656.

[29] George M Church and Ed Regis. *Regenesis: How Synthetic Biology Will Reinvent Nature and Ourselves*. Basic Books, 2014.

[30] Le Cong, F Ann Ran, David Cox, Shuailiang Lin, Robert Barretto, Naomi Habib, Patrick D Hsu, Xuebing Wu, Wenyan Jiang, Luciano a Marraffini, and Feng Zhang. Multiplex genome engineering using CRISPR/Cas systems. *Science (New York, N.Y.)*, 339(6121):819–23, February 2013. ISSN 1095-9203. doi: 10.1126/science.1231143. URL http://www.pubmedcentral.nih.gov/articlerender.fcgi?artid=3795411&tool=pmcentrez&rendertype=abstract.

[31] B P Cormack, R H Valdivia, and S Falkow. FACS-optimized mutants of the green fluorescent protein (GFP). *Gene*, 173(1 Spec No):33–38, 1996. ISSN 0378-1119. doi: 10.1016/0378-1119(95)00685-0.

[32] J de la Noue and N de Pauw. The potential of microalgal biotechnology: a review of production and uses of microalgae. *Biotechnology advances*, 6(4):725–770, 1988. ISSN 07349750. doi: 10.1016/0734-9750(88)91921-0.

[33] Dawei Ding, Paul a Guerette, Shawn Hoon, Kiat Whye Kong, Tobias Cornvik, Martina Nilsson, Akshita Kumar, Julien Lescar,

and Ali Miserez. Biomimetic production of silk-like recombinant squid sucker ring teeth proteins. *Biomacromolecules*, 15(9):3278–89, September 2014. ISSN 1526-4602. doi: 10.1021/bm500670r. URL http://www.ncbi.nlm.nih.gov/pubmed/25068184.

[34] Dennis E Discher, Paul Janmey, and Yu-Li Wang. Tissue cells feel and respond to the stiffness of their substrate. *Science (New York, N.Y.)*, 310(5751):1139–1143, 2005. ISSN 0036-8075. doi: 10.1126/science.1116995.

[35] E.L. Doubrovski, E.Y. Tsai, D. Dikovsky, J.M.P. Geraedts, H. Herr, and N. Oxman. Voxel-based fabrication through material property mapping: A design method for bitmap printing. *Computer-Aided Design*, 60:3–13, 2014. ISSN 00104485. doi: 10.1016/j.cad.2014.05.010. URL http://www.sciencedirect.com/science/article/pii/S0010448514001067.

[36] Daniel C Ducat, Jeffrey C Way, and Pamela a Silver. Engineering cyanobacteria to generate high-value products. *Trends in biotechnology*, 29(2):95–103, February 2011. ISSN 1879-3096. doi: 10.1016/j.tibtech.2010.12.003. URL http://www.ncbi.nlm.nih.gov/pubmed/21211860.

[37] Daniel C. Ducat, J. Abraham Avelar-Rivas, Jeffrey C. Way, and Pamela A. Silvera. Rerouting carbon flux to enhance photosynthetic productivity. *Applied and Environmental Microbiology*, 78(8):2660–2668, 2012. ISSN 00992240. doi: 10.1128/AEM.07901-11.

[38] Carola Engler, Romy Kandzia, and Sylvestre Marillonnet. A one pot, one step, precision cloning method with high throughput capability. *PloS one*, 3(11):e3647, January 2008. ISSN 1932-6203. doi: 10.1371/journal.pone.0003647. URL http://www.pubmedcentral.nih.gov/articlerender.fcgi?artid=2574415&tool=pmcentrez&rendertype=abstract.

[39] Carola Engler, Ramona Gruetzner, Romy Kandzia, and Sylvestre Marillonnet. Golden gate shuffling: A one-pot DNA shuffling method based on type ils restriction enzymes. *PLoS ONE*, 4, 2009. ISSN 19326203. doi: 10.1371/journal.pone.0005553.

[40] Jayda L Erkal, Asmira Selimovic, Bethany C Gross, Sarah Y Lockwood, Eric L Walton, Stephen McNamara, R Scott Martin, and Dana M Spence. 3D printed microfluidic devices with integrated versatile and reusable electrodes. *Lab on a chip*, 14(12):2023–32, June 2014. ISSN 1473-0189. doi: 10.1039/c4lc00171k. URL http://www.ncbi.nlm.nih.gov/pubmed/24763966.

[41] Lief Fenno, Ofer Yizhar, and Karl Deisseroth. The development and application of optogenetics. *Annual review of neuroscience*, 34:389–412, 2011. ISSN 0147-006X. doi: 10.1146/annurev-neuro-061010-113817.

[42] Cathal Garvey. DremelFuge - A One-Piece Centrifuge for Rotary Tools by cathalgarvey - Thingiverse, 2009. URL http://www.thingiverse.com/thing:1483.

[43] Peter Gravesen, Jens Branebjerg, and Ole Sondergard Jensen. Microfluidics-a review. *Journal of Micromechanics and Microengineering*, 168(3), 1993.

[44] Erika Hayden. The $1,000 genome. *Nature*, 507:294–295, 2014.

[45] Thorsten Heidorn, Daniel Camsund, Hsin-Ho Huang, Pia Lindberg, Paulo Oliveira, Karin Stensjö, and Peter Lindblad. Synthetic biology in cyanobacteria: Engineering and analyzing novel functions. *Method Enzymol*, 497:539–79, 2011. ISSN 1557-7988. doi: 10.1016/B978-0-12-385075-1.00024-X. URL http://www.sciencedirect.com/science/article/pii/B978012385075100024X.

[46] Amanda L Holt, Sanaz Vahidinia, Yakir Luc Gagnon, Daniel E Morse, and Alison M Sweeney. Photosymbiotic giant clams are transformers of solar flux. *Journal of the Royal Society, Interface / the Royal Society*, 11(October), 2014.

[47] L V Hooper and J I Gordon. Commensal host-bacterial relationships in the gut. *Science (New York, N.Y.)*, 292(5519):1115–1118, 2001. ISSN 00368075. doi: 10.1126/science.1058709.

[48] Mo Chao Huang, Hongye Ye, Yoke Kong Kuan, Mo-Huang Li, and Jackie Y Ying. Integrated two-step gene synthesis in a microfluidic device. *Lab on a chip*, 9(2):276–85, January 2009. ISSN 1473-0197. doi: 10.1039/b807688j. URL http://www.ncbi.nlm.nih.gov/pubmed/19107285.

[49] IDEO. Future Visions of Synthetic Biology for University of California San Francisco Lim Lab, 2011. URL http://www.ideo.com/work/future-visions-of-synthetic-biology.

[50] M. Jinek, K. Chylinski, I. Fonfara, M. Hauer, J. A. Doudna, and E. Charpentier. A Programmable Dual-RNA-Guided DNA Endonuclease in Adaptive Bacterial Immunity, 2012. ISSN 0036-8075.

[51] Steven Keating. Beyond 3D Printing : The New Dimensions of Additive Fabrication. In Jonathan Follett, editor, *Designing for Emerging Technologies: UX for Genomics, Robotics, and the Internet of Things*, pages 379–405. O'Reilly Media, 2015. ISBN 0636920030676.

[52] Jason Kelly. Part:BBa_B0064, 2008. URL http://parts.igem.org/Part:BBa_B0064.

[53] Ahmad S Khalil and James J Collins. Synthetic biology: applications come of age. *Nature reviews. Genetics*, 11(5):367–79, May 2010. ISSN 1471-0064. doi: 10.1038/nrg2775. URL

http://www.pubmedcentral.nih.gov/articlerender.fcgi?artid=2896386&tool=pmcentrez&rendertype=abstract.

[54] Philip J Kitson, Mali H Rosnes, Victor Sans, Vincenza Dragone, and Leroy Cronin. Configurable 3D-Printed millifluidic and microfluidic 'lab on a chip' reactionware devices. *Lab on a chip*, 12(18):3267–71, September 2012. ISSN 1473-0189. doi: 10.1039/c2lc40761b. URL http://www.ncbi.nlm.nih.gov/pubmed/22875258.

[55] Philip J Kitson, Ross J Marshall, Deliang Long, Ross S Forgan, and Leroy Cronin. 3D Printed High-Throughput Hydrothermal Reactionware for Discovery, Optimization, and Scale-Up. *Angewandte Chemie (International ed. in English)*, pages 1–7, July 2014. ISSN 1521-3773. doi: 10.1002/anie.201402654. URL http://www.ncbi.nlm.nih.gov/pubmed/25079230.

[56] David S Kong, Peter a Carr, Lu Chen, Shuguang Zhang, and Joseph M Jacobson. Parallel gene synthesis in a microfluidic device. *Nucleic acids research*, 35(8):e61, January 2007. ISSN 1362-4962. doi: 10.1093/nar/gkm121. URL http://www.pubmedcentral.nih.gov/articlerender.fcgi?artid=1885655&tool=pmcentrez&rendertype=abstract.

[57] Ludmila Krejcova, Lukas Nejdl, Miguel Angel Merlos Rodrigo, Michal Zurek, Miroslav Matousek, David Hynek, Ondrej Zitka, Pavel Kopel, Vojtech Adam, and Rene Kizek. 3D printed chip for electrochemical detection of influenza virus labeled with CdS quantum dots. *Biosensors & bioelectronics*, 54:421–7, April 2014. ISSN 1873-4235. doi: 10.1016/j.bios.2013.10.031. URL http://www.ncbi.nlm.nih.gov/pubmed/24296063.

[58] Jongho Lee, Tahar Laoui, and Rohit Karnik. Nanofluidic transport governed by the liquid/vapour interface. *Nature nanotechnology*, 9(4):317–23, April 2014. ISSN 1748-3395. doi: 10.1038/nnano.2014.28. URL http://www.ncbi.nlm.nih.gov/pubmed/24633525.

[59] Kyoung G. Lee, Kyun Joo Park, Seunghwan Seok, Sujeong Shin, Do Hyun Kim, Jung Youn Park, Yun Seok Heo, Seok Jae Lee, and Tae Jae Lee. 3D printed modules for integrated microfluidic devices. *RSC Advances*, 4(62):32876, July 2014. ISSN 2046-2069. doi: 10.1039/C4RA05072J. URL http://xlink.rsc.org/?DOI=C4RA05072J.

[60] Daniel Leitner, Sabine Klepsch, Gernot Bodner, and Andrea Schnepf. A dynamic root system growth model based on L-Systems. *Plant and Soil*, 332(1):177–192, 2010. ISSN 0032079X. doi: 10.1007/s11104-010-0284-7.

[61] Yang Liao, Jiangxin Song, En Li, Yong Luo, Yinglong Shen, Danping Chen, Ya Cheng, Zhizhan Xu, Koji Sugioka, and Katsumi Midorikawa. Rapid prototyping of three-dimensional microfluidic mixers in glass by femtosecond laser direct writing. *Lab*

on a chip, 12(4):746–9, February 2012. ISSN 1473-0189. doi: 10.1039/c2lc21015k. URL http://www.ncbi.nlm.nih.gov/pubmed/22231027.

[62] Gregory Linshiz, Nina Stawski, Garima Goyal, Changhao Bi, Sean Poust, Monica Sharma, Vivek Mutalik, Jay D. Keasling, and Nathan J. Hillson. PR-PR: Cross-platform laboratory automation system. *ACS Synthetic Biology*, 3(8):515–524, 2014. ISSN 21615063. doi: 10.1021/sb4001728.

[63] Andy Lomas. Cellular Forms : an Artistic Exploration of Morphogenesis. In *SIGGRAPH*, New York, New York, 2014. ACM. ISBN 9781450329774. doi: 10.1145/2619195.2656282. URL http://www.andylomas.com/.

[64] Chunbo Lou, Brynne Stanton, Ying-Ja Chen, Brian Munsky, and Christopher A Voigt. Ribozyme-based insulator parts buffer synthetic circuits from genetic context, 2012. ISSN 1087-0156.

[65] Rolf Lutz and Hermann Bujard. Independent and tight regulation of transcriptional units in escherichia coli via the LacR/O, the TetR/O and AraC/I1-I2 regulatory elements. *Nucleic Acids Research*, 25(6):1203–1210, 1997. ISSN 03051048. doi: 10.1093/nar/25.6.1203.

[66] Prashant Mali, Luhan Yang, Kevin M Esvelt, John Aach, Marc Guell, James E DiCarlo, Julie E Norville, and George M Church. RNA-guided human genome engineering via Cas9. *Science (New York, N.Y.)*, 339(6121):823–6, February 2013. ISSN 1095-9203. doi: 10.1126/science.1232033. URL http://www.pubmedcentral.nih.gov/articlerender.fcgi?artid=3712628&tool=pmcentrez&rendertype=abstract.

[67] Andreas Möglich and Keith Moffat. Engineered photoreceptors as novel optogenetic tools. *Photochemical & photobiological sciences : Official journal of the European Photochemistry Association and the European Society for Photobiology*, 9(10):1286–1300, 2010. ISSN 1474-905X. doi: 10.1039/c0pp00167h.

[68] Nancy a. Moran and Paul Baumann. Bacterial endosymbionts in animals. *Current Opinion in Microbiology*, 3(3):270–275, 2000. ISSN 13695274. doi: 10.1016/S1369-5274(00)00088-6.

[69] Nagarjuna Nagaraj, Jacek R Wisniewski, Tamar Geiger, Juergen Cox, Martin Kircher, Janet Kelso, Svante Pääbo, and Matthias Mann. Deep proteome and transcriptome mapping of a human cancer cell line. *Molecular systems biology*, 7(548):548, January 2011. ISSN 1744-4292. doi: 10.1038/msb.2011.81. URL http://www.pubmedcentral.nih.gov/articlerender.fcgi?artid=3261714&tool=pmcentrez&rendertype=abstract.

[70] Neri Oxman, Christine Ortiz, Fabio Gramazio, and Matthias Kohler. Material ecology. *CAD Computer Aided Design*, 2014. ISSN 00104485. doi: 10.1016/j.cad.2014.05.009.

[71] Philips. Microbial Home concepts. Technical report, Philips, 2011. URL http://www.design.philips.com/shared/assets/design_assets/pdf/news/annex_microbial_home_concepts.pdf.

[72] Douglas Philp and J Fraser Stoddart. Self-Assembly in Natural and Unnatural Systems. *Angew. Chem. In Ed. Engl.*, 35:1154–1196, 1996. ISSN 0570-0833. doi: 10.1002/anie.199611541. URL http://onlinelibrary.wiley.com/doi/10.1002/anie.199611541/references.

[73] Marco Piccolino. Biological machines : from mills to molecules. *Nature reviews. Molecular cell biology*, 1(November), 2000.

[74] Przemyslaw Prusinkiewicz. Graphical Applications of L-Systems. *Graphics Interface*, pages 247—-253, 1986. ISSN 07135424. URL http://citeseerx.ist.psu.edu/viewdoc/download?doi=10.1.1.105.4242&rep=rep1&type=pdf.

[75] Jiayuan Quan, Ishtiaq Saaem, Nicholas Tang, Siying Ma, Nicolas Negre, Hui Gong, Kevin P White, and Jingdong Tian. Parallel on-chip gene synthesis and application to optimization of protein expression. *Nature biotechnology*, 29(5):449–52, May 2011. ISSN 1546-1696. doi: 10.1038/nbt.1847. URL http://www.ncbi.nlm.nih.gov/pubmed/21516083.

[76] Chad I Rogers, Kamran Qaderi, Adam T Woolley, and Gregory P Nordfin. 3D printed microfluidic devices with integrated valves. *Biomicrofluidics*, 016501:1–10, 2015.

[77] Jessica Rosenkrantz. A visit to Shapeways NY factory! | Nervous System blog, 2013. URL http://n-e-r-v-o-u-s.com/blog/?p=3937.

[78] Edward G Ruby. The Vibrio fischeri â Euprymna scolopes Light Organ Symbiosis. *Annual Review of Microbiology*, 50:591–624, 1996.

[79] Aliaa I Shallan, Petr Smejkal, Monika Corban, Rosanne M Guijt, and Michael C Breadmore. Cost-Effective Three-Dimensional Printing of Visibly Transparent Microchips within Minutes. *Analytical Chemistry*, 2014.

[80] Siderits. Syringe pump 0.3 ml intradermal, 2013. URL http://www.thingiverse.com/thing:210756.

[81] Michael J Smanski, Swapnil Bhatia, Dehua Zhao, YongJin Park, Lauren B A Woodruff, Georgia Giannoukos, Dawn Ciulla, Michele Busby, Johnathan Calderon, Robert Nicol, D Benjamin Gordon, Douglas Densmore, and Christopher a Voigt. Functional optimization of gene clusters by combinatorial design and assembly. *Nature Biotechnology*, 32(12), November 2014. ISSN 1087-0156. doi: 10.1038/nbt.3063. URL http://www.nature.com/doifinder/10.1038/nbt.3063.

[82] J G Sutcliffe. Nucleotide sequence of the ampicillin resistance gene of Escherichia coli plasmid pBR322. *Proceedings of the National Academy of Sciences of the United States of America*, 75(8): 3737–3741, 1978. ISSN 0027-8424. doi: 10.1073/pnas.75.8.3737.

[83] Mark D Symes, Philip J Kitson, Jun Yan, Craig J Richmond, Geoffrey J T Cooper, Richard W Bowman, Turlif Vilbrandt, and Leroy Cronin. Integrated 3D-printed reactionware for chemical synthesis and analysis. *Nature chemistry*, 4(5):349–54, May 2012. ISSN 1755-4349. doi: 10.1038/nchem.1313. URL http://www.ncbi.nlm.nih.gov/pubmed/22522253.

[84] Chris N Takahashi, Aaron W Miller, Felix Ekness, Maitreya J Dunham, and Eric Klavins. A Low Cost, Customizable Turbidostat for Use in Synthetic Circuit Characterization. *ACS Synthetic Biology*, 4:32–38, 2015.

[85] Todd Thorsen, Sebastian J Maerkl, and Stephen R Quake. Microfluidic large-scale integration. *Science (New York, N.Y.)*, 298 (5593):580–4, October 2002. ISSN 1095-9203. doi: 10.1126/science.1076996. URL http://www.ncbi.nlm.nih.gov/pubmed/12351675.

[86] Peter J Turnbaugh, Ruth E Ley, Micah Hamady, Claire Fraser-liggett, Rob Knight, and Jeffrey I Gordon. The human microbiome project: exploring the microbial part of ourselves in a changing world. *Nature*, 449(7164):804–810, 2007. ISSN 1476-4687. doi: 10.1038/nature06244.The.

[87] Ernst Weber, Carola Engler, Ramona Gruetzner, Stefan Werner, and Sylvestre Marillonnet. A modular cloning system for standardized assembly of multigene constructs. *PLoS ONE*, 6, 2011. ISSN 19326203. doi: 10.1371/journal.pone.0016765.

[88] Wilfried Weber and Martin Fussenegger. Emerging biomedical applications of synthetic biology. *Nature reviews. Genetics*, 13(1): 21–35, January 2012. ISSN 1471-0064. doi: 10.1038/nrg3094. URL http://www.ncbi.nlm.nih.gov/pubmed/22124480.

[89] Jennifer J Wernegreen. Genome evolution in bacterial endosymbionts of insects. *Nature reviews. Genetics*, 3(11):850–61, November 2002. ISSN 1471-0056. doi: 10.1038/nrg931. URL http://www.ncbi.nlm.nih.gov/pubmed/12415315.

[90] George M Whitesides. The origins and the future of microfluidics. *Nature*, 442(7101):368–73, July 2006. ISSN 1476-4687. doi: 10.1038/nature05058. URL http://www.ncbi.nlm.nih.gov/pubmed/16871203.

[91] Daniel M Widmaier, Danielle Tullman-Ercek, Ethan a Mirsky, Rena Hill, Sridhar Govindarajan, Jeremy Minshull, and Christopher a Voigt. Engineering the Salmonella type III secretion system to export spider silk monomers. *Molecular systems biology*, 5 (309):309, January 2009. ISSN 1744-4292. doi: 10.1038/msb.2009.

62. URL http://www.pubmedcentral.nih.gov/articlerender.fcgi?artid=2758716&tool=pmcentrez&rendertype=abstract.

[92] René H Wijffels, Olaf Kruse, and Klaas J Hellingwerf. Potential of industrial biotechnology with cyanobacteria and eukaryotic microalgae. *Current opinion in biotechnology*, 24(3):405–13, June 2013. ISSN 1879-0429. doi: 10.1016/j.copbio.2013.04.004. URL http://www.ncbi.nlm.nih.gov/pubmed/23647970.

[93] Bas Wijnen, Emily J Hunt, Gerald C Anzalone, and Joshua M Pearce. Open-source syringe pump library. *PloS one*, 9(9):e107216, January 2014. ISSN 1932-6203. doi: 10.1371/journal.pone.0107216. URL http://www.pubmedcentral.nih.gov/articlerender.fcgi?artid=4167991&tool=pmcentrez&rendertype=abstract.

[94] Chenlong Zhang, Nicholas C Anzalone, Rodrigo P Faria, and Joshua M Pearce. Open-source 3D-printable optics equipment. *PloS one*, 8(3):e59840, January 2013. ISSN 1932-6203. doi: 10.1371/journal.pone.0059840. URL http://www.pubmedcentral.nih.gov/articlerender.fcgi?artid=3609802&tool=pmcentrez&rendertype=abstract.

[95] Feng Zhang, Le Cong, Simona Lodato, Sriram Kosuri, George M Church, and Paola Arlotta. Efficient construction of sequence-specific TAL effectors for modulating mammalian transcription. *Nature*, 29(2):149–154, 2011. doi: 10.1038/nbt1775.